POLITECNICO DI MILANO

SCHOOL OF INDUSTRIAL AND INFORMATION ENGINEERING

Master of Science – Materials Engineering and Nanotechnology

POLITECNICO
MILANO 1863

Quantum chemical simulations of the interaction of polyynes with silver nanoparticles

Supervisor
Prof. Carlo S. Casari

Co-Supervisors
Dr. Alberto Milani
Dr. Patrick Serafini

Candidate
Alessandro Zalla – 920936

Academic Year 2019 – 2020

Abstract

This thesis focuses on the computational investigation, by means of Density Functional Theory (DFT), of the interaction between metal nanoparticles and polyynes, responsible for the chemical enhancement visible in experimental Surface Enhanced Raman Spectroscopy (SERS) analyses. Different systems have been analyzed, consisting in hydrogen-, methyl- and cyano- terminated polyynes of various lengths, interacting with silver clusters of different sizes, to understand the effect of the dimensions on the obtained results. Such polyynes represent relatively simple molecules, already studied and for which experimental data was available; moreover, the presence of CH_3 and CN terminal groups promised to be an interest feature to investigate.

Firstly, an optimization of the computational setup was carried out, to understand which parameters were more important for an accurate and reliable prediction of the spectra. The effect of different basis-sets (cc-pVTZ, AUG-cc-pVTZ, 6-311++G(d,p), functionals (PBE0 and B3LYP)) and dispersion corrections (Grimme's GD3 corrections) were considered. Then, properties of hydrogen-, methyl and cyano-polyynes interacting with silver clusters of different sizes were investigated, specifically their interaction energies and Raman spectra, which highlighted the peculiar effect of the interaction with the cluster in the modification of such properties. To further understand the characteristics of the spectra, an analysis on the Bond Length Alternation (BLA) and energy band gap was performed, and indicated an increased conjugation on the polyynic chain due to the interaction with the metal cluster. The downshift of the peaks observed in the spectra has been associated to a softening of the force constants of the carbon-carbon bonds, and to the effect of the interaction with the cluster which affect the vibrational motion of the chain with respect to the isolated systems. The nature of the interaction has been assessed by evaluating the lengths of the bonds between the cluster and the chain, and an interaction stronger than a Van der Waals-like one was identified, and considered the main cause of the peculiarities observed for these systems. A model based on a charge transfer between the cluster and the chain was considered for the description of the interaction, but gave only a partial interpretation of the data. Further studies are required to deepen the understanding of this particular phenomenon.

A final comparison between the theoretical and experimental data was performed, with successful results: the strong chemical interaction well described the trends observed in the spectra, and correctly predicted the observed features.

Estratto

Questo lavoro di tesi ha l'obiettivo di analizzare la natura della peculiare interazione che si instaura tra una superficie metallica e una poliina, la quale causa delle particolari modifiche nello spettro Raman e provoca quindi l'insorgenza dell'effetto SERS (Surface Enhanced Raman Spectroscopy). Le analisi svolte sono di tipo teorico-computazionale, e si basano su calcoli che sfruttano i principi della Density Functional Theory (DFT). Per l'analisi di tali sistemi, le specie prese in considerazione sono composte da delle idrogeno-, metil- e ciano-poliine, di diversa lunghezza, interagenti con cluster di argento di varie grandezze, per analizzare l'effetto delle dimensioni. Tali poliine rappresentano dei sistemi relativamente semplici e già analizzati in precedenti studi, con cui è quindi possibile confrontare i risultati ottenuti. Il primo step è stato quello della ottimizzazione del setup computazionale, in particolare riguardante la scelta dei parametri di calcolo DFT, come basis-sets, funzionali di scambio-correlazione, ed eventuali correzioni per l'integrazione delle interazioni di dispersione, fondamentali per una accurata e affidabile descrizione degli spettri. Una volta selezionato il setup computazionale, si è passati allo studio dei sistemi sopra descritti. In particolare si è svolta una analisi riguardante spettri Raman ed energie di interazione. La singolare interazione che si è verificata tra cluster e poliina ha causato delle modifiche strutturali, elettroniche e vibrazionali nella catena. Tali cambiamenti sono stati correlati cone le modifiche nello spettro Raman, e spiegate tramite la valutazione delle energie di interazione. Per spiegare in modo più preciso le caratteristiche degli spettri è stata effettuata una analisi riguardante la Bond Lenght Alternation (BLA) ed il gap elettronico degli orbitali molecolari, che hanno sottolineato una più pronunciata coniugazione della catena poliinica, causata dalla interazione con il cluster. La diminuzione nelle frequenze dei modi normali di vibrazione Raman attivi è stata associata ad un decremento delle costanti di forza dei legami carbonio-carbonio della catena, fenomeno causato dalla interazione tra cluster e poliina, modificando il moto vibrazionale della stessa, rispetto alla situazione antecedente l'interazione. La particolare natura di tale interazione è stata verificata tramite il calcolo delle lunghezze dei legami formatisi tra il cluster di argento e gli atomi di carbonio della poliina. I valori ottenuti hanno evidenziato la presenza di una forte interazione, più intensa di una semplice interazione di tipo Van der Waals, che è stata considerata come la principale causa delle peculiarità osservate. Un secondo modello, basato sul fenomeno del trasferimento di carica è stato valutato, risultando però in una parziale interpretazione dei dati: di conseguenza, una analisi più approfondita risulta necessaria per appurare se effettivamente ciò si verifica e sia in grado di spiegare le particolarità dell'interazione tra le due specie. Per validare la accuratezza del modello basato sulla interazione tra cluster e poliina, è stato eseguito un confronto tra gli spettri SERS ottenuti sperimentalmente e quelli teorici ricavati dall'analisi precedentemente descritta: la

forte interazione chimica sopra citata si è dimostrata molto precisa e ha descritto accuratamente l'andamento degli spettri sperimentali.

Contents

Introduction and scope of the work

In recent years, discoveries related to the various allotropic forms of carbon got great importance in the global research landscape, especially in the field of nanoscience and nanotechnology. Nanomaterials such as graphene, fullerenes, nanotubes, have unique and exotic properties, directly related to their characteristic quantum confinement effects. The above mentioned carbon structures are the most representative examples of the sp^2 hybridization of carbon and have been intensively studied in the last decades. More recently, the attention has been shifted towards the study of the most exotic allotropic form of carbon, carbyne, which represents the *true* one-dimensional material, thanks to its *sp* hybridization. This form of carbon consists in a linear chain of atoms of approximate infinite length. Its predicted properties are even better than those of the other carbon nanostructures already discovered. In particular, the transport, mechanical and optical properties are quite exceptional. Furthermore, as shown by several studies, there is a strong correlation between the structural, electronic and vibrational properties of these systems. However, the production and synthesis of carbyne proved to be very difficult, mainly due to its characteristic instability. Instead, it has been possible to synthesize linear structures of *sp* hybridized carbon with finite lengths called carbon atom wires (CAWs).

Two different configuration of CAWs have been isolated and investigated, i.e. polyynes and cumulenes. The former type of CAW is characterized by an alternated *quasi*-single-*quasi*-triple bond structure, while the latter has an equalized double bond one. Due to their finite length, carbon atom wires are also characterized by the presence of end groups, that have the important effect of inducing a particular configuration to the chain, i.e. polyynic or cumulenic one, depending on the nature of the end group itself. Moreover, end groups can be exploited to improve significantly the stability of the systems, which is a critical issue for the employment of CAWs in technological applications.

A useful and diffused technique used in the characterization of CAWs is Raman spectroscopy, in the past widely used to study other carbon nanostructures. Experimentally, Raman spectroscopy is performed on the solutions that contain CAWs, but due to the poor concentrations obtainable for the samples, the signals are sometimes weak and of difficult interpretation. To tackle this problem, Surface Enhanced Raman Spectroscopy (SERS) is used: in the case considered, when a linear carbon chain interacts with a metal nanoparticle (e.g. Au or Ag), the Raman signal is greatly enhanced thanks to a dual effect: a chemical effect, due to the interaction between the monomers, and a physical effect, related to the surface plasmon resonance of the metallic substrate.

To support the hypotheses based on the experimental results, theoretical models are built and studied by means of numerical simulations. Indeed, the data obtained with the computations are exploited to study in detail the different properties of CAWs, for example their Raman spectra, interaction energies, electronic structure and so on. Nonetheless, the number of studies found in the literature that try to give an interpretation of the SERS effect observed for polyynes is very limited. The reason is that to perform a detailed and accurate numerical simulation of a complex phenomenon like the SERS effect is no simple task, due to the difficulty to model the the interaction between the metallic surface and the carbon chain. Indeed ad-hoc models and tailored theoretical frameworks are necessary to accurately represent such systems and the phenomena taking place in the interaction. In this context, the aim of this work is to employ quantum chemical computations, based on Density Functional Theory (DFT), to model and study the peculiar SERS spectra observed for systems formed by CAWs and silver nanoparticles.
CAWs that have been considered in this work are polyynes terminated with H, CH_3, CN groups, for which experimentally obtained SERS spectra were available for comparisons. The first step was the optimization of the computational setup, performed with the analysis of the interaction energies and of the Raman spectra of hydrogen-terminated polyynes of different length interacting with silver clusters of different size; the choice of hydrogen-polyynes is mainly due to the fact that these carbon atom wires are the most studied from both the computational and experimental point of view, and represent the simplest case of an experimentally available CAW. For this analysis, different computational parameters (basis sets, exchange-correlation functional and Van der Waals corrections) have been used to investigate how they influence the description of the interaction and its effect on the molecular properties. Once the configuration of the computational setups was assessed, the first analysis was performed on hydrogen-terminated polyynes interacting with silver clusters. The considered systems were again chains of different length and clusters of different sizes to address the effect of the dimensions of the cluster on the calculated properties. The study of the peculiar interaction taking place between the polyyne and Ag cluster was based on the analysis of the interaction energies,which indicate the degree of stability of the complexes; SERS spectra, were studied to verify the influence of the structural and dimensional characteristics of the dimers on the vibrational properties of the carbon chain; bond lengths and related force constants were calculated to precisely understand the impact of the interaction with the metallic cluster on the polyyne. In the literature a model based on a charge transfer between the cluster and the chain has been proposed to explain the features of the SERS spectra observed for these systems, thus, in order to further investigate this theory, a study on the charges of the dimers was also carried out. A comparison of the predicted data and the experimentally obtained results was done to assess the quality of the theoretical analyses. The same procedures were also applied to differently terminated polyynes, specifically cyano- and methyl-terminated ones. In this case the length of the chain and size of the cluster were fixed. However, the presence of a different end group introduced a new parameter to be taken into account, that is the availability of different possible sites for the polyyne-metal interaction. For this reason the effect of the relative positions of cluster and terminal group was investigated. Interaction energies and SERS spectra were again employed to understand and model the peculiar interaction between the cluster and the chain, and the analysis of the charges was performed to verify whether the charge transfer model was in agreement with the predicted results. At last, a comparison to check the accordance with experimentally obtained data was carried out in this case, to give an interpretation to the features observed in the SERS spectra recorded in the laboratory for these systems.

Chapter 1

Carbon Atom Wires

1.1 Carbon and its allotropes

The outstanding properties, both physical and chemical, of carbon are due to the peculiar electronic configuration of its orbitals, which may assume different *hybridization* configurations, each characterized by its set of properties.
Probably, the most known carbon allotrope is diamond. In this form, carbon atoms form four different covalent bonds with other neighboring carbons and its hybridization state is sp^3. The electronic structure makes it an insulator, as the energy gap between valence and conduction band is of about 5 eV. Direct consequences of the strong covalent bonds are hardness and high thermal conductivity. In case of sp^2 hybridization, the most common material is graphite. This mineral is formed by a stack of planes of carbon atoms. The hybridization induces the formation of σ and π bonds for carbon atoms of the same plane, and an induced dipole-dipole Van der Waals interaction takes place between different planes along the transverse direction.
In the past decades, the scientific research on carbon-based materials got a huge development. The discovery of *Fullerenes*, awarded with the Nobel prize, opened the path toward "the era of carbon allotropes" [1]. In 2004 followed the discovery of graphene, and A. Geim and K. Novoselov were honored with the Nobel prize "for groundbreaking experiments" regarding this material [2]. Graphene is the first isolated *true* $2D$ material, made solely of carbon atoms, arranged in space in a honeycomb lattice, as shown in Fig. 1.1. Among the reasons of interest in this material there are certainly its chemical and physical properties. Each atom forms a σ bond with its three closest neighbors, and a fourth π bond along the normal direction with respect to the plane. Covalent σ bonds are responsible for the excellent structural properties of graphene. On the other hand, π bonds are related to electronic and transport properties. Indeed, the orbital related to the π bond interacts with the other π orbitals to form what are referred to as the π-band and π^*-band, forming a conjugated system in which electrons are delocalized and free to move. [3]. Graphene can also be considered as the starting point for the formation of all the other carbon nanostructures: nanotubes can be mathematically "built" as a rolled sheet of graphene; fullerenes, on the other

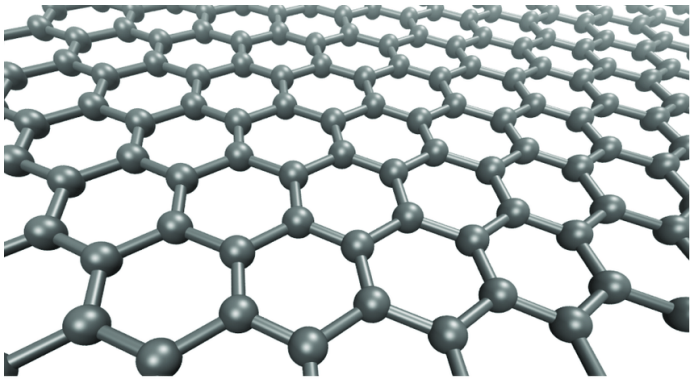

Figure 1.1. Exemplative ball and stick model of a portion of graphene sheet where carbons atoms are arranged in an hexagonal lattice [4].

hand, are obtained by ideally inserting pentagons in the lattice, to obtain a curvature and thus the famous spherical shape of this allotrope.
Another family of exotic and widely investigated carbon-based materials are nanotubes: the first specimens were discovered in 1993 in carbon arc-discharge chambers, similar to those that are used for the production of fullerenes [5]. Although they are not produced directly from a sheet of graphene (as mentioned above), they can be idealized as a portion of graphene which is rolled up (Fig. 1.2) on itself along one of the vectors of the Bravais lattice, forming a hollow cylinder.

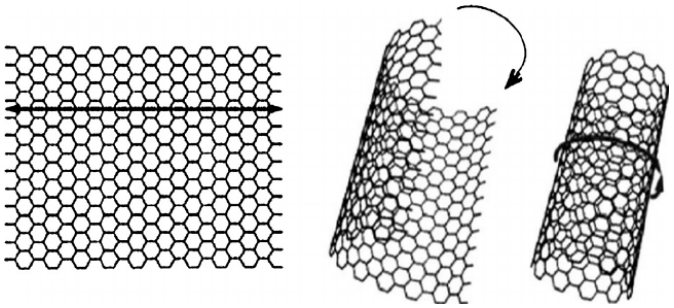

Figure 1.2. Rolling up of graphene sheet to form carbon nanotubes [6].

Nanotubes are usually distinguished by the number of walls they have: a Single Wall Carbon NanoTube (SWCNT) is a single nanotube, while a MWCNT is a structure formed by several concentrically arranged nanotubes. These structures are considered true one-dimensional structures, as their diameters, which vary according to the way they are "built", are much smaller than the length, often approximated as infinite. Indeed, the smallest diameter reached experimentally is 3 Å [7], in a Multi-Wall Carbon NanoTube (MWCNT), 4.3 Å for a SWCNT instead. As for the length, the record is about 0.5 m [8]. Carbon nanotubes are the strongest and stiffest materials that have so far been discovered, in terms of tensile strength and elastic modulus. Experimentally, one MWCNT reached a value of 63 GPa in a tensile test. Further studies have shown that the limit can be shifted towards values of 100 GPa [9]; the specific strength of a nanotube is therefore 300 times greater than steel. As for the electronic properties, different types of behavior can be obtained: metallic, insulating and semiconductive; concerning transport properties, nanotubes feature a single electron tunneling behavior, due to Coulomb blockade [10].
As for fullerenes, they can be defined as a set of carbon atoms linked by single or double bonds, to give rings, which form a closed cage in space, as shown in Fig. 1.3. The rings that form this

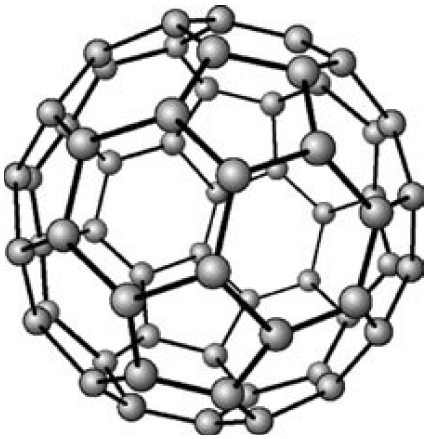

Figure 1.3. Structure of fullerene C_{60} [11]

structure have 5 to 7 carbon atoms. They can be considered confined in all directions, which is why they are also referred to as 0D structures. The character of the hybridization of these allotropic forms is mixed: most of the bonds that hold together the carbon atoms are double (sp^2), while the rest are single bonds, and therefore characterized by hybridization sp^3. The properties of fullerenes are peculiar and strongly depend on their morphology. The famous experiments that unveiled the existence of fullerenes were performed in 1985, by *Kroto et al.*, who were actually trying to find a way to prove the existence of the most elusive species of the family of carbon allotropes: *sp* carbon. This exotic material has aroused the attention of the scientific community, as the so-called carbyne represents the missing step in the scale of *N-dimensional* structures based on carbon (see Fig. 1.4).

1.2 Carbyne, the infinite linear carbon chain

Carbyne represents the ultimate one-dimensional material. We can describe it as a chain of carbon atoms having an infinite length. It represents a physical model, useful to understand and study from a theoretical point of view the properties of *sp* carbon chains. Promising results have been obtained: linear carbon chains have a Young's modulus of approximately $32TPa$ [12, 13] and a stiffness of approximately $10^9 Nm/kg$, much higher than any other material, including carbon nanotubes and graphene. Thermal and electronic properties are also remarkable: the thermal conductivity is between $80 - 200 kW/mK$ at room temperature, while electrical conductivity reaches high values due to the fact that charges are conducted by ballistic transport along the chain. Finally, among the properties that deserve attention, especially in the field of nanotechnologies, *sp* carbon chains have a specific surface area estimated to be approximately $13000 m^2/g$, four times greater than graphene. This peculiarity can be exploited in the field of materials engineering, especially for nanocomposites. It is also possible to combine *sp* chains with other allotropes to obtain *hybrid* structures (see 1.4). Among these, graphydine ($sp^2 - sp$) and yne-diamond ($sp^3 - sp$), are currently being studied, after being hypothesized as possible hybrid systems in the recent past [1].

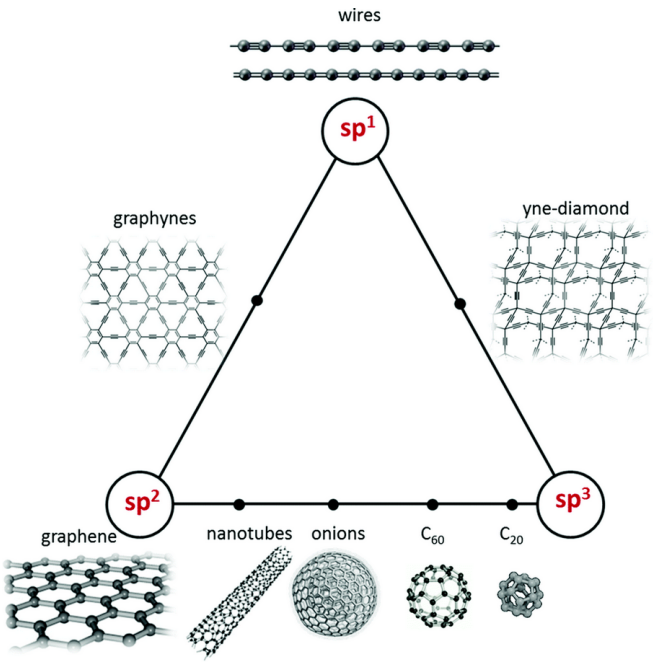

Figure 1.4. Illustration of the carbon nanostructure based on their hybridization state. In vertexes, *pure* hybridization: diamond, graphite (sp^3); graphene (sp^2); carbon atom wires (sp). In between vertexes, mixed hybridization structures: fullerenes, graphynes, yne-diamond [14]

1.2.1 Structural properties

The geometry of carbyne is linear, due to the *sp* hybridization that affects the chemical bonds between the various atoms. There are, from a theoretical point of view, two possible equilibrium configurations for this system, depending on the bonding of the carbon atoms in the chain, as visible in Fig. 1.5. In the first case, we have a series of alternating *quasi*-single and *quasi*-triple bonds, which are respectively shorter and longer than single and triple carbon-carbon bonds due to the effect of the conjugation of the chain. In the second case, the bonds are equivalent. We use the terms polyyne and cumulene, respectively. It is possible to refer to cumulenic carbyne as to a

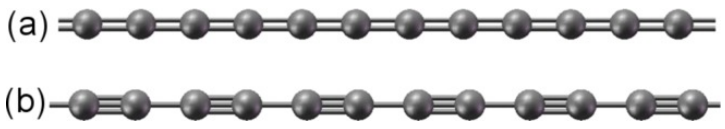

Figure 1.5. The two possible configurations of carbyne: (a) cumulenic; (b) polyyinc.

one-dimensional crystal, having a crystalline unit cell featuring a single atom. On the other hand the unit cell of polyynic structures has two atoms. In order to take into account the structural difference between these two forms we introduce a parameter: the Bond Length Alternation (BLA). Mathematically, it can be defined in different ways, the simplest being the difference between the lengths of two adjacent bonds (see Fig. 1.6):

$$BLA = |r_1 - r_2| \tag{1.1}$$

The consequence is that cumulenes and polyynes will have $BLA = 0$ and $BLA \neq 0$ respectively.

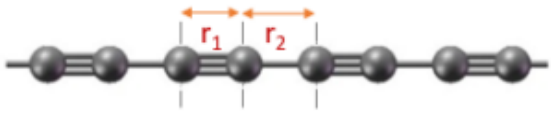

Figure 1.6. Bond length alternation in polyynic carbyne [15]

An important physical effect related to the type of chain structure is the *Peierls distortions*. Peierls theory, which always applies for a $1D$ crystal, states that a one-dimensional chain with equalized bonds, having one electron per ion, is unstable and tends to form dimers. This has a very important consequence: for linear chains of several tens of atoms in length, as carbyne, the stable equilibrium configuration is the polyynic one (see Fig 1.7) [16]. The electronic behavior of the chains is directly

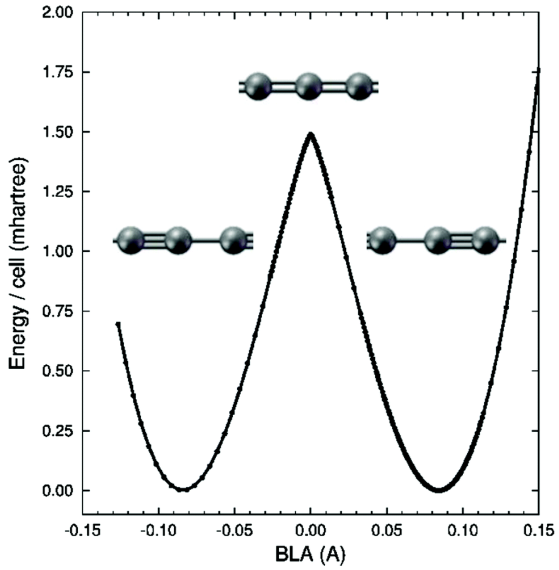

Figure 1.7. Potential energy surface of an isolated infinite linear carbon chain as a function of BLA showing the occurrence of Peierls distortion and the stabilization of the two possible (and equivalent) bond alternated structures [14]

related to the structural configuration: due to the different nature that exists in the chemical bonds that affect the chain, the two possible forms have profoundly diverse properties: cumulenes, for example, behave like a metal, while polyynes tends to be semiconductors. Therefore, BLA and electronic behavior are strictly related: with BLA tending toward zero, carbyne behave as a metal, while on the other hand as BLA increases the energy gap between the bands increases. This peculiar behavior, as will be discussed in the following sections, is due to the delocalization of π electrons, which influences the structural properties in conjugated materials. It is important to underline that these considerations are valid for systems such as carbyne, i.e. with a length that is considered infinite.

1.2.2 Electronic properties

Using a solid state physics approach, it is possible to correlate structural configuration of carbyne with its electronic properties. In figure 1.8 it is showed a representation of the conduction and valence bands in the case of cumulenic and polyynic structures. The modulation of the BLA, as hinted above, for these polyconjugated molecules is caused by the delocalization of π orbitals. Indeed, in the case of all equalized bonds the value of BLA is zero, and thus the system has a truly metallic behavior, instead in the case of the chain with alternating conjugated quasi-single and quasi-triple bonds a insulating/semiconducting behavior is observed. The band structure highlights the opening of an energy gap for the latter. At the edges of the Brillouin zone there is the separation between the conduction and valence band, that are completely full and empty, respectively.

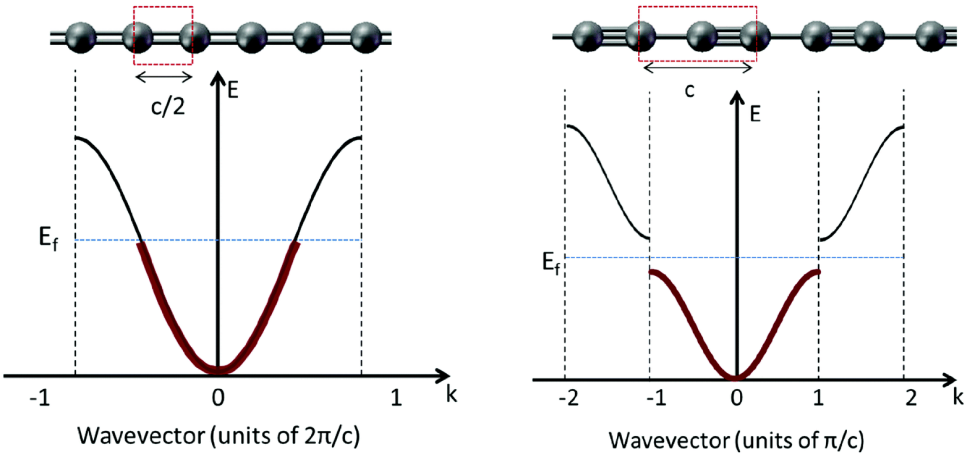

Figure 1.8. Dispersion relation (theoretical) for the infinite carbon chain in its two possible configurations [14]

It is possible to prove this by considering the electronic contribution given by the atoms in the two different chain configurations. In the case of the cumulenic chain, the unit cell is composed of a single atom, all the chain bonds being equivalent to each other. For this, each carbon atom contributes with one electron to each of the two π orbitals, having one electron each. This results in a half-filled conduction band, which is the reason for the metallic behavior.
Conversely, in the case of a polyynic chain, there are two carbon atoms in the base cell, thus two electrons per orbital, and the result is a filled valence band and an empty conduction band. This leads to the opening of an energy gap between the conduction band and the valence band, with consequent semiconducting behavior. Specifically, as can be seen in 1.9 for increasing BLA there is an intensification of the semiconducting behavior, with the energy gap increasing; for a decreasing BLA, on the other hand, the gap tends to zero showing a metallic behavior. An important consideration has to be made on the strong π conjugation that affects these systems, which is typical of polyconjugated systems, and has peculiar interplays with the structural parameters and the electronic structure: a strong conjugation on the chain, reduces the value of the BLA, and at the same time decreases the band gap. One effect is thus linked to the other. This however is in contrast with Peierls distortion that foresees a polyynic behavior increasing the length of the chain. However, this last effect is predominant only for very long chains, approximable to the infinite case.

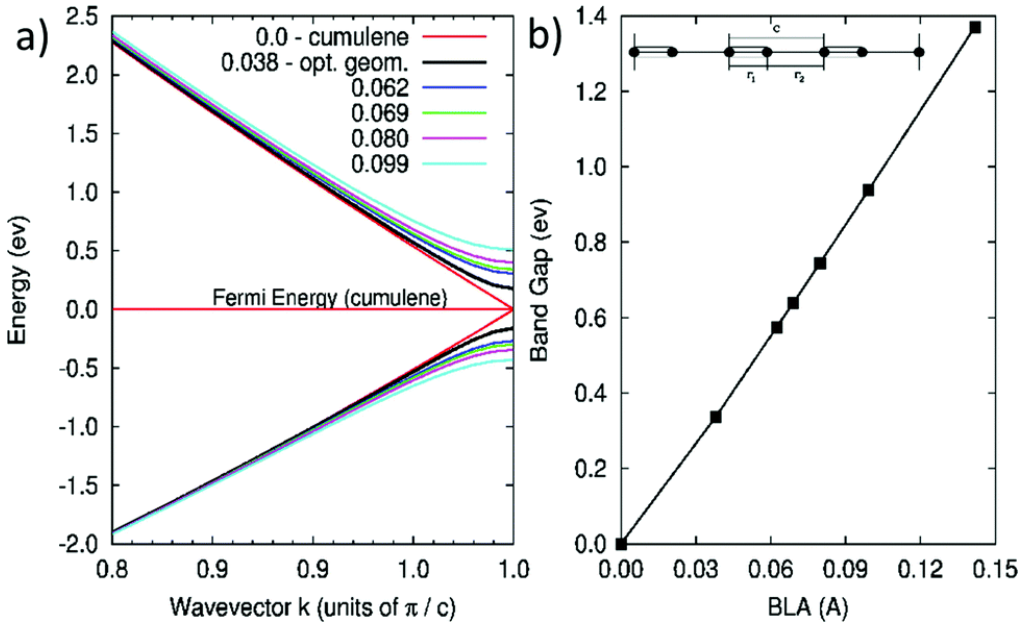

Figure 1.9. Correlation between structural and electronic properties of carbyne. (a) Band structure of different systems, increasing for increasing values of BLA; (b) Band gap as a function of BLA [14]

This is not completely true for finite length linear carbon chains, also because the presence of end groups has a significant effect on the structural properties of the linear chain.

1.2.3 Vibrational properties of carbyne

Vibrational properties, as said, are strongly influenced by structural (BLA) and electronic properties. In fact, electron-phonon coupling is typical of π conjugated systems. Taking into account the two different configurations, it is possible to think about the cumulene-like carbyne as a one-dimensional crystal with a basis equal to one. Consequently, as described in solid state physics theory, only the acoustic branch exists in the phonon dispersion relation. In particular, the modes that can be distinguished are one in the longitudinal direction, and two in the transverse direction. In the second case, the lattice base cell of the polyynic chain has two atoms, due to the fact that two adjacent atoms are non-equivalent. For this reason in the dispersion relation is also present an optical branch, and therefore we will have three acoustic and three optical components.
The effect of BLA on the phonon dispersion relation is certainly interesting: it has been shown that the longitudinal optical branch can assume values ranging from 1200 to more than 2000 $cm^{-}1$ for BLA values belonging to the range $0.038 - 0.142$ Å [17]. The behavior observed in the right panel of Fig. 1.10 as $qc/\pi \to 0$ is due to long-range vibrational interactions along the chain [18,19]. Such long-range interactions become stronger when the chain approaches the cumulenic configuration, i.e. for a decreasing value of the BLA or an increased conjugation of the chain. Furthermore, as demonstrated by Tommasini et al. [20], the effect of conjugation is to increase the frequency for the optical mode in correspondence with phonon wavevector $q = 0$, because conjugation itself has the effect of increase the range of vibrational interactions. On the other hand, the value of the

acoustic branch remains almost unchanged (see Fig. 1.10). Moreover, since polyynes and cumulenes are π conjugated materials, it is possible to model the longitudinal optical phonon at $q = 0$ as a stationary wave in which the bonds of the chain, $r_1,\ r_2$ simultaneously oscillate out of phase. Therefore the nuclear displacements that are related to such longitudinal optical phonon can be considered as a collective BLA oscillation. It is possible to estimate the frequency of oscillation of such phonon in terms of bond stretching force constants [17]:

$$\omega^2 = \frac{4F_R}{m}; \quad F_R = \frac{k_1 + k_2}{2} + \sum_{n \geq 1} [f_1^n + f_2^n - 2f_{12}^n] \tag{1.2}$$

where k_1 and k_2 are the diagonal stretching force constant related to the two bonds of the cell, i.e. r_1, r_2, and the various f_i^n terms describe the force constants of the various interactions along the chain as its length increases. This equation relates the behavior of cumulenes or polyynes with other polyconjugated materials. Moreover, it has been demonstrated that the sequence of interaction force constants considered for a carbon-carbon bond and a sequence of bonds found along a path of other carbon-carbon bonds have alternated values in polyynes [18–20]. For this reason, the sum in the above equation has a negative value, and decreases for an increasing π conjugation, meaning that the frequency of the phonon, which is related to the force constants, is dependent on the conjugation. The physical origin of this behavior is the already mentioned electron-phonon coupling.

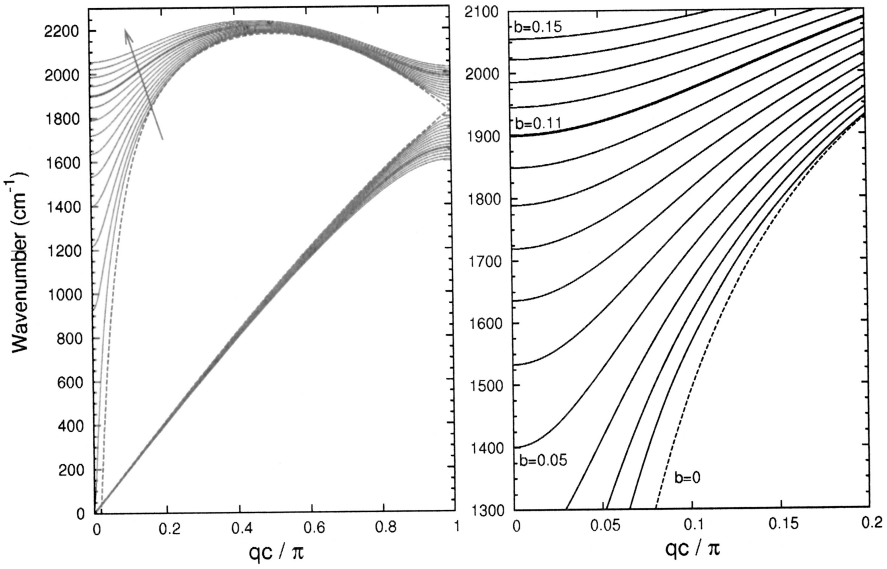

Figure 1.10. Longitudinal phonon dispersion relation for a dimerized infinite carbon chain. Right: the optical branches in the interval $1300 - 2100\ cm^{-1}$

1.3 Finite length linear carbon chains: Carbon Atom Wires

Linear carbon chains having a finite length are different systems with respect to carbyne, but the properties related to finite length chains can be derived from the investigation of the infinite chain, with all the necessary adjustments. For example, finite length chains can be modeled with an infinite chain having a specific BLA. Experimental data suggest that the polyynic configuration is the most common one for synthesized Carbon Atom Wires (CAWs), and the relationship between structural parameters and electronic properties is the same: as the π conjugation increases with increasing length of the chain, the BLA decreases. Therefore the systems tend toward a cumulenic configuration. The main difference that exists between finite length carbon atom wires and carbyne is the presence of end groups in the chain. These have an important effect on the properties of the wires, probably causing the predominance of the polyynic configuration in synthesized samples.
Indeed, end groups induce a particular configuration of the chain. For instance, CH_2 will favor a cumulenic structure, as the first atom of the chain is forced to share a double bond with the end group. On the other hand, a CH may help to obtain a polyynic configuration, as the bond shared with the first atom of the chain would be triple. In CAWs, the effect of the end groups is predominant with respect to Peierls distortion, which can be rigorously defined only in the ideal case of the infinite chain. The configuration of finite length systems depends instead on a trade off between the length of the chain and the properties of the end groups.
The presence of end groups may also be exploited to tailor the properties of the synthesized samples as their presence influences structural and electronic properties of the wires. Therefore, by proper choice of end groups, it would be possible to produce carbon atom wires (CAWs) with specific properties.

1.4 Raman of carbon nanostructures

Among the techniques that are used to study carbon structures, Raman spectroscopy certainly stands out. One of its greatest advantages is its effectiveness in the analysis of systems with a pronounced π conjugation. It is a non-destructive technique, and has a high sensitivity to the type of chemical bonding characterizing the observed sample. The ability of Raman spectroscopy in the identification of the analyzed sample rely on the interaction of the vibrational features of the sample itself with the incident electromagnetic radiation. The quanta of vibration, phonons, are characteristic of the substance, as directly related to the structure. Therefore different spectra will be obtained for different samples. Specifically, this is of interest in the analysis of carbon based nanomaterials, because of the different hybridization states involved in C−C bonds in different structures (see Fig. 1.11).

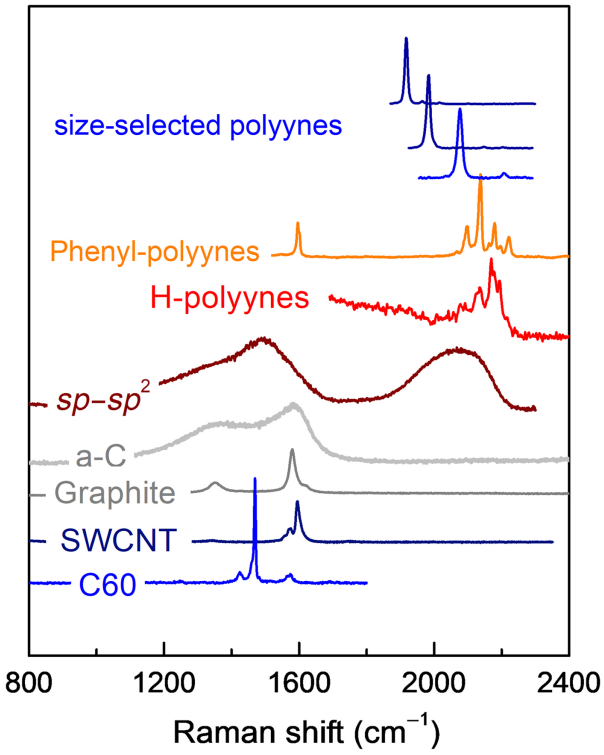

Figure 1.11. Raman spectra of carbon atom wires compared with other carbon based nanostructures [15].

1.4.1 Raman investigation of Carbon Atom Wires

The study of CAWs by Raman spectroscopy has extensively been applied in the past two decades. In principle a Raman investigation on infinite length chains would be effective only for the polyynic configuration. Indeed, as explained by solid state theory, the total number of optical phonons is $3N - 3$, where N is the number of atoms in the primitive cell. Therefore for the monoatomic ideal cumulene no optical phonon is detected. However, as mentioned in section 1.3 this does not occur in the case of chains of finite length i.e. CAWs, since the effect of boundary conditions take place, forcing a relaxation of the hypotheses suggested for the study of the infinite ideal chain [21]. Moreover, the presence of terminal groups has an important role: the interaction that occurs between such end groups and the chain leads to the activation of peculiar normal modes, that are detectable with Raman spectroscopy.
Moreover, it must be taken into account that the support of computational data is often necessary, as it allows to assign all the features that are detected by the spectroscopic analysis.
As for other carbon-based systems, such as polyconjugated polymers, the spectrum highlights features that are clearly visible and delineated. Multiple studies found out that the signature of *sp* carbon relies in the range $1800 - 2300\ cm^{-1}$ [22]; in the same area two clear peaks emerge in the simulations of hydrogen terminated polyynes [23]. This is a range of the spectrum where no other signal of carbon structures is present.
The presence of such intense peaks (see Fig. 1.12) is linked to the oscillation of the BLA, as already hypothesized in the study of similar systems such as polymers having intense π conjugation [24].
The analysis of the spectra of hydrogen terminated CAWs, having different chain lengths, has shown how the exact position of these two peaks is closely related to the length of the chain and to the

BLA [23, 25]. To explain such behavior we may refer to the theory of the *Effective Conjugation Coordinate* (ECC) model [20, 26–28], successfully applied in the study of other oligomers and polymers having a pronounced π conjugation. Indeed, we may associate the most intense line (i.e. α line or *ECC mode*) of the spectrum with a collective stretching of the triple bonds and a simultaneous compression of the single bonds due to nuclear movements. Therefore, this vibrational mode describes an out-of-phase oscillation of the BLA. In this context, the redshift of the peaks can also be explained: the longer the chain, the more the conjugation, which is related to a decrease in the force constant of the carbon-carbon bonds, causing a downshift of the frequencies (as discussed in 1.2.3).
The nature of the second peak (i.e. β line), is instead related to a second carbon-carbon stretching active mode.

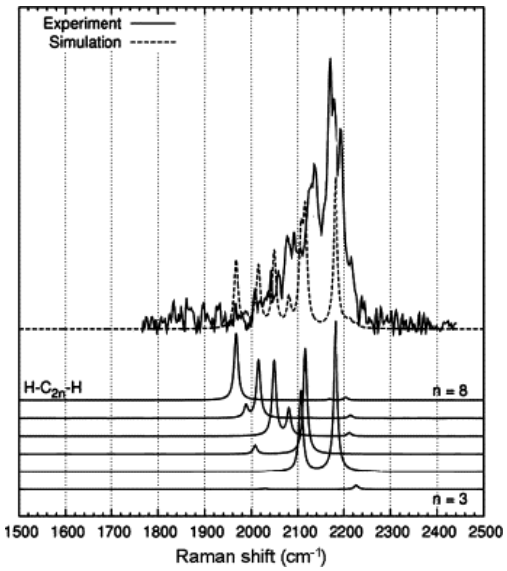

Figure 1.12. Comparison between experimental Raman spectrum of hydrogen terminated polyynes and Density Functional Theory (DFT) calculation of Raman active modes [23].

1.4.2 SERS investigation of Carbon Atom Wires

A particular effect is obtained when a generic molecule interacts with a metallic substrate (for example, Au or Ag). This results in a considerable intensification of the measured signal, with sensitivity increased up to few orders of magnitude. The detection of single molecules or single atoms of the sample is possible. This effect has been renamed surface enhanced Raman scattering (SERS), and has proven effective in the analysis of CAWs.
The increase in the sensitivity of the measurement can be explained by considering two contributions: electromagnetic and chemical. In the first case there is an intensification of the electromagnetic field experienced by the sample, while in the second case we have a contribution arising from the chemical interaction, i.e. formation of a bond or Van der Waals interaction, between the substrate and the sample (see 2.5).
The first experimental works highlighting the peculiarities of the Surface Enhanced Raman Spectroscopy (SERS) effect in the study of *sp* chain systems are those of Lucotti et al. and Tabata

et al. [23, 29]. These show the existence of a shift between the features measured with the two different techniques, i.e. Raman and SERS, and an enhancement of approximately 10^6 of SERS with respect to Raman. Both studies focused on hydrogen-polyynes interacting in different ways with silver nanoparticles. Furthermore, Lucotti et al. [23] showed that there is a change in the number and shape of the peaks in the SERS spectra: the more intense line is redshifted and new features appear below 2000 cm^{-1}. The causes of these behaviors, as suggested by the authors, are different experimental parameters, such as acidity of the solution, formation of cumulenic chains, rearrangement of the species due to the presence of silver.
Moreover, parameters related to the solution influence the measured spectrum. In fact, it can be seen that higher concentrations of hydrogen-terminated CAWs can increase the intensity of the peaks and shift them to longer wavelengths. A possible explanation could be the formation of aggregates [30].
This peculiar behavior of hydrogen-polyynes interacting with Ag nanoparticles has also been assessed by Milani et al., where a charge transfer between the chain and the metal cluster is hypothesized to justify these changes in the SERS spectrum with respect to the Raman one. This behavior is caused by a chemical interaction involved in the formation of the complex [31].
The effect of end groups has been studied by Milani et al. in diphenyl-polyynes. The analysis of the Raman spectrum showed a redshift of the peaks with respect to those of the hydrogen-polyynes, due to a more pronounced π conjugation. SERS experiments performed on the same samples interacting with silver clusters in colloidal solution highlighted peaks that were instead not detected by Raman spectroscopy, both in the typical range of the *ECC mode*, and below 2000 cm^{-1} [32]. The explanation for this phenomenon cannot take into account the acidity of the solution as hydrogen groups are not present. Therefore, in-depth investigations using DFT calculations were performed on the same diphenyl-polyynes having a non-neutral charge. The theoretical spectra obtained showed a very pronounced shift and an increase in intensities in the typical region of *sp* hybridized structures. These results are justified on the basis of the chemical enhancement theory. Furthermore, the charge transfer induced an even more effective π conjugation in diphenyl-polyynes, implying a decrease of the BLA and the stabilization of a more cumulenic-like electronic configuration, as shown in Fig. 1.13. Recently, Milani et al. investigated other systems consisting of chains of different lengths terminated with dimethylanilines deposited in the form of films on silver nano-islands. As seen in Fig. 1.14, in the case of C_8, there are several features that appear only in the SERS spectrum. The origin of this specific peak in the range $1900 - 2000$ cm^{-1} is associated with a charge transfer between the chain and the cluster, in accordance with what has already been stated in [31]. In fact, the presence of charge transfer involves a change in the electronic structure of the system, making the conjugation more pronounced, and therefore decreasing the BLA. The measured features are therefore located in an area that is typical of cumulene-like systems. In the case of the $C2$ sample, the strength of the electron acceptor is low, due to the limited number of electronegative carbon atoms. The results of DFT calculations were exploited to verify the preferential direction of the charge transfer phenomenon, interpreting SERS spectra considering charged molecules as model. Similarities in the spectra of the charged species and those of the nanoparticles and sp chain system are a further indication of the direction of the charge transfer. Moreover, the calculation of the ionization energy provides some insights on the energetically favored behavior: as visible in Fig. 1.15, a system featuring a positively charged CAW interacting with a negatively charged cluster has the lower energy [33].

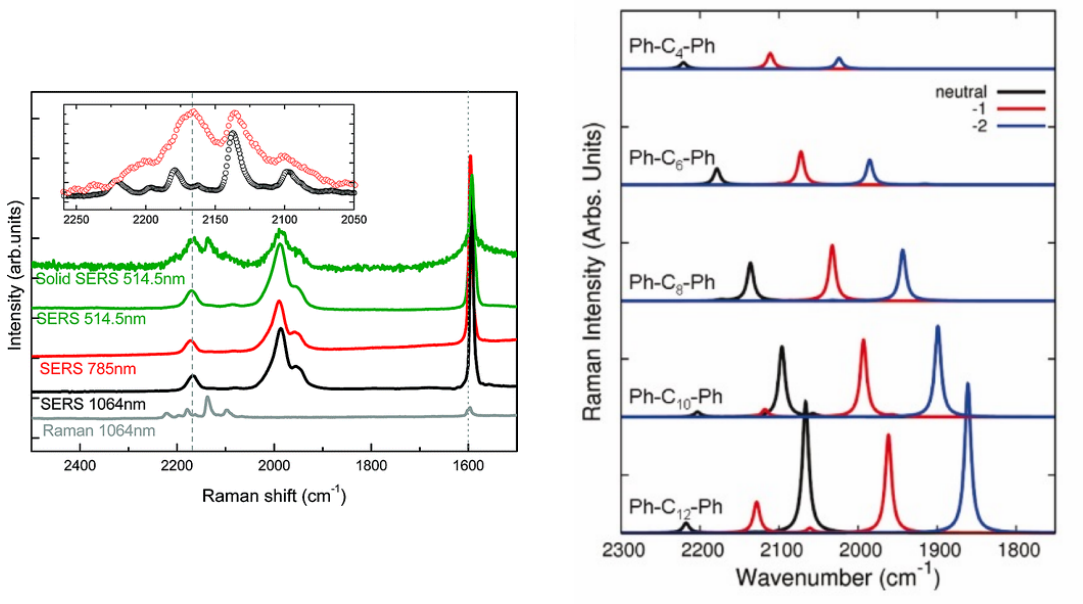

Figure 1.13. Comparison between normal Raman and SERS spectra of diphenyl-polyynes collected at different excitation wavelength (inset: zoom on the sp carbon region); b) Raman spectra DFT simulation for neutral and negatively charged diphenyl-polyyne [31]

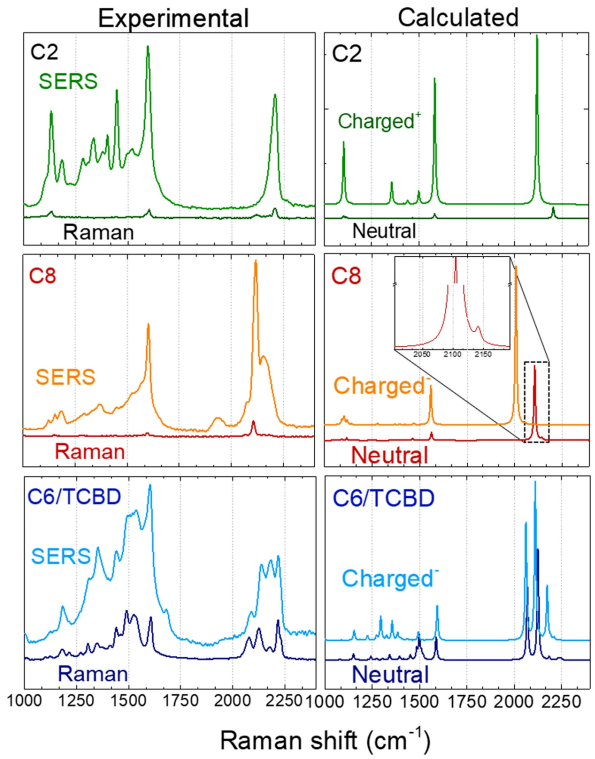

Figure 1.14. Comparison between different spectra obtained for different samples. On the left experimental solid-state SERS spectra of C2, C8, and C6/TCBD deposited on SERS-active substrate. On the right, comparison of DFT computed Raman spectra of neutral, positively charged C2 and negatively C8, and C6/TCBD [33]

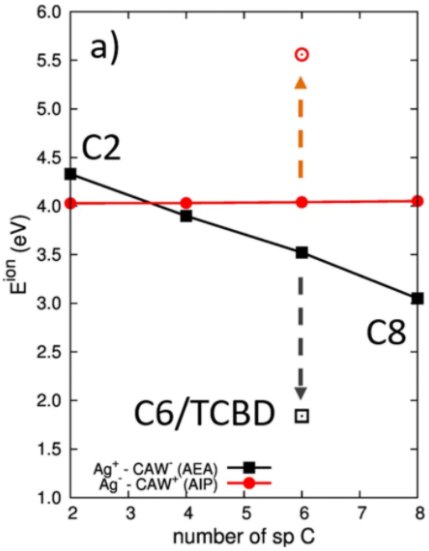

Figure 1.15. Plot of the DFT computed values of E_{ion} for the systems investigated [33]

1.5 Synthesis of CAWs

In recent years, due to the progress made in the study of nanostructures, it has been possible to produce real carbon atom wire (CAW)s in laboratory. At the moment, these compounds can only be synthesized in a carefully tailored condition, and for this reason the studies on the subject are mostly carried out in an academic environments. The main issue is the instability of CAWs. These systems degrade very easily, either by oxidation reactions or by cross linking with other elements to reach a more stable energy configuration (mostly the sp^2 one) [34, 35]. Synthesis of CAWs with specifically tailored end groups demonstrated that it is possible to address this issue. Specifically, the choice of bulky end groups, with an important steric hindrance, helps preventing cross linking reactions. In this context, the work by Tykwinski and Chalifoux is very promising, since it was possible to obtain structures more than 40 atoms long [36]. Possible other solutions to the stability related problems are the synthesis of CAWs in protected environments, for example in solution or inside multi-walled carbon nanotubes [37], or by encapsulation in cages formed by rotaxane macrocyles, in which end groups are no longer required [38].

1.5.1 Physical methods

Physical techniques are probably the most suitable for the synthesis of CAWs. These are usually based on physical vapor deposition, in which a carbon vapor or plasma is formed, then rapidly cooled to induce the growth of carbon clusters in non-equilibrium conditions.
One of the most notable result is that of Ravagnan et al., in which a nanostructured carbon film was produced by exploiting a supersonic deposition of a low-energy cluster beam, obtaining both cumulenes and polyynes.
A similar technique, which allows development of thin films on substrates, is the femtosecond laser ablation of graphite targets. The synthesized species are characterized by a certain amount of

moieties in which *sp* chains are embedded in an amorphous carbon sp^2 matrix [39, 40].
A simple technique which is not very expensive in terms of resources is the arc-discharge in liquids of graphite targets, developed by Cataldo [41]. In this context, a recent study developed by Peggiani et al. was focused on exploiting water as a cheap and non-toxic solvent in the synthesis of polyynes. Hydrogen capped polyynes of a length up to 16 carbon atoms were obtained, comparable to the ones obtained with organic solvents. The experimental setup featured high quality graphite electrodes as a carbon source, and the process was carried out in a reactor filled with deionised water. Identification of polyynes of different lengths was possible using high-performance liquid chromatography [42].
Pulsed laser ablation in liquids (PLAL) is another successful technique used in recent years. One of the advantages is the possibility to obtain polyynes with extremely low fraction of by-products. PLAL allowed the synthesis of diverse kind of polyynes, from the common hydrogen-capped, to cyanopolyynes, i.e. featuring a cyano end-group, and methyl-capped polyynes, i.e. featuring a CH_2 end group. Peggiani et al. exploited this technique in a recent work, to assess the role of the solvent in the termination of the carbon chain, in the stability of the samples and on the selection of their length. Second harmonic pulses of a Nd:YAG laser with a duration of 6 *ns* were used on a pure graphite target, submerged in different solvents, such as deionised water, acetonitrile, isopropanol, methanol and ethanol (see Fig.1.16) [43].

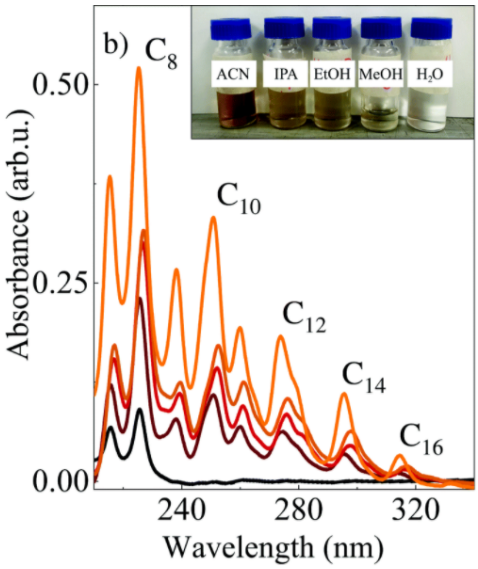

Figure 1.16. UV-vis spectra of filtered solutions of polyynes in acetonitrile, isopropanol, methanol, ethanol and water after laser ablation. Different size obtained are highlighted in the spectrum. Pictures of the solutions obtained in the inset [43]

Carbon atom wires of considerable length, over one hundred units and up to 6000 have been synthesized inside carbon nanotubes. The techniques used in this case consist in the direct arc discharge, or by indirect growth through post-treatment [37].

1.5.2 Chemical methods

A different way to obtain polyynes is by means of organic chemical reactions. The process can exploit the presence of end groups that are able to stabilize the chain [44]. For example, polyynes have been produced having as end caps heteroatoms such as hydrogen [45,46], or alkyl [47], aryl [48] and some metals groups [49,50].
The first attempts date back two centuries ago, when Glaser proposed a methodology based on the oxidative dimerization reaction of copper(I)-phenylacetylide [51].
In general, chemical methods are often used to synthesize systems in solution. In this context, two particular categories can be highlighted: polymerization and dimerization of etynyl groups. In the first approach, explored by Kudryavtsev different process are possible: dehydropolycondensation of acetylene, polycondensation of halides and dehydrohalogenation of polymers (chemical carbonization of polyvinylidene halides). An advantage of these type of processes is the possibility to synthesize carbon wires in a single step, but with the drawback of polydispersion of the products [52,53]. The second approach is used for the synthesis of molecules with a defined length and end group, by dimerization reaction of ethynyl group, via a *Glaser*-like reaction [51,54].
A successful technique has been employed for the synthesis of polyynes of 40 atoms in length [36]. Specifically, the use of very bulky terminal groups allows the stabilization of the electronic effects, protecting the very delicate triple bonds of the structure.

1.6 Possible application of CAWs

The range of the fields of application for polyynes are potentially many, due to the broad set of properties displayed by these systems. The bottlenecks that prevent the use linear carbon chains at an industrial scale are the poor stability and the complex synthesis process. Nonetheless, advantages would greatly overcome costs and production difficulties, as carbyne has proven to be a potential *champion* material with mechanical, thermal, electronic and optical properties that outperform any other known existent material [15]. On the other hand, finite length CAWs have also shown interesting behaviors, mainly related to the possibility to tune their properties.
The mechanical properties shown by polyynes make them feasible as structural elements for molecular mechanics, and the high tensile strength derived from the characteristic *sp* hybridization makes them appealing for the nanocomposites material industry. On the other hand, structural parameters of CAWs influence their electronic behavior, resulting in a wide range of possibilities in the nanoelectronics field. The geometry of linear carbon chains may be of interest for their application as molecular wires, due to the cylindrical charge distribution and high carrier mobility. Moreover, different types of transport regimes have been identified and correlated with effects of strain and doping of the chain, as for example negative differential resistance (see Fig. 1.17) [55] and quantum ballistic transport [56,57]. In this context, a recent work from Scaccabarozzi et al. resulted in the production of a field effect transistor (FET) exploiting cumulenic wires as active material. Specifically, tetraphenylbutatriene ([3]Ph) has been chosen as the molecular semiconductor, consisting of a four atom long carbon wire, with three cumulated double bonds, terminated at each end by two phenyl moieties (Fig. 1.18) [58]. A further property that may be

exploited in this field is the variable electronic structure depending on the mechanical strain applied: a transition from metallic to insulator behavior has been highlighted [59, 60]. The extremely high surface area is suitable for applications in the energy storage field, where the chains are used as a host material. The possibility to engineer the conjugation length is interesting for applications in imaging, screening, and biomedicine [61]. Finally, combination of linear carbon chains with other nanostructures with different hybridization could provide different materials and properties [62].

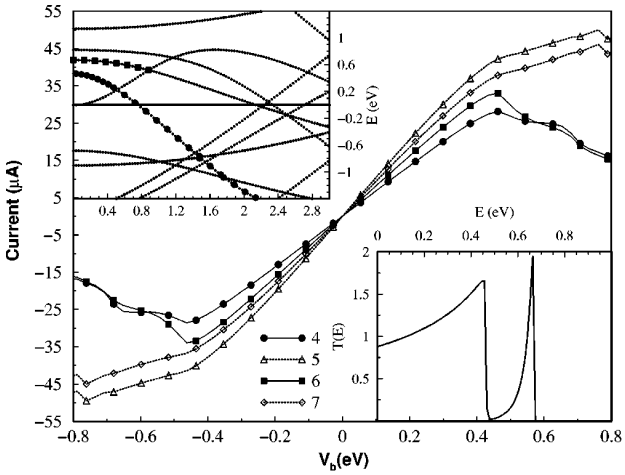

Figure 1.17. Current-voltage characteristic of Al−C_N−Al CAWs. Upper inset: band structure of the atomic electrodes along the wire direction. Lower inset: transmission coefficient $T(E)$ versus electron energy E for Al−C_4−Al at zero bias. It is possible to observe a negative differential resistance at $\pm 0.46\ V$ where the current decreases with increasing bias voltage [55].

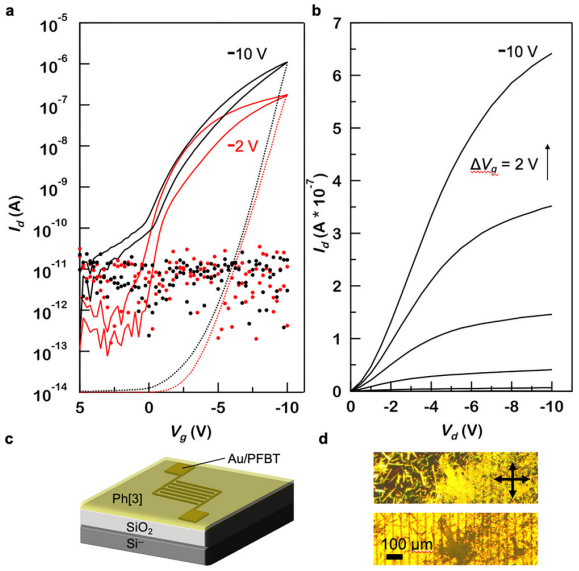

Figure 1.18. a) Representative transfer characteristic of a [3]Ph microcrystal bottom-gate bottom-contact field effect transistor (dimensions: $L = 5\mu m$; $W = 1cm$). Drain voltages in linear (red curve) and saturation (black curve) regimes are indicated with a solid line. b) Output characteristic. c) Device architecture. d) Optical micrographs of the FET in bright field (bottom) and polarized light (top) [58].

Chapter 2

Theoretical background

In this chapter the main theories exploited for research analysis and in results study will be presented.
Density Functional Theory, (DFT) is introduced in section 2.1 as a powerful tool in the analysis of many-body systems [63–68]. Density functional theory is a quantum mechanical modelling method used in physics and chemistry. It provides an acceptable solution to the Schrödinger equation for a many electron system exploiting functionals of the electronic density. In the first part of this section the focus will be on the basics of quantum mechanics, starting from the definition of the Schrödinger equation towards the description of the Hartree-Fock theory. After the introduction of the fundamental concepts about DFT, such as Kohn-Sham theory, the formalization and analysis of the application of the different functionals will be discussed.
In section 2.4 the fundamentals of Raman and SERS theory are presented. The focus will be on the explanation of the classic and quantum treatment of the phenomenon. A brief introduction on vibrational properties is also reported.

2.1 From Schrödinger equation to Hartree-Fock Theory

2.1.1 The Schrödinger equation

One of the most important postulates of quantum mechanics is that every non-relativistic system is explainable on the basis of its *state*, a physical concept that is described by a *wavefunction*.
The Schrödinger equation is an important relation that is used to calculate the wavefunction of a many particle system. It is a linear partial differential equation having terms depending on space and time variables:

$$i\hbar\frac{\partial\Psi}{\partial t} = \hat{H}\Psi \tag{2.1}$$

where $\hat{H}$ is the *Hamiltonian* operator, that expresses the total energy of the system and Ψ is the wavefunction. Generally, Ψ is a many body function containing the coordinates for all the degrees of freedom in a system, as well as time. As such, no solution can be find for non-trivial cases, and the only analytical solutions are computable for the two-body problem (e.g. hydrogen atom and its only electron).
The standard method to solve this type of equations is the separation of variables, i.e. trying to find a solution that is the product of of two different functions, each of them dependent on a single variable:

$$\Psi(x,t) = \psi(x)\phi(t) \tag{2.2}$$

It is possible to obtain a solution for the space-dependent part of the problem, which is the time-independent Schrödinger equation:

$$\hat{H}\psi = E\psi \tag{2.3}$$

Time-independent Schrödinger equation is used to calculate the time-independent part of the total wavefunction, i.e. ψ whose probability density is also independent on time. For this reason this condition represent a stationary state. The time-dependent equation is instead used whence the studied system is subjected to time varying perturbations.
Usually the goal is to calculate the ground state of the system, by minimizing the total energy with respect to the degrees of freedom of Ψ, with constraints such as normalization and particle symmetry. For an eigenstate, the time-independent value of energy is the *expectation value* of the Hamiltonian:

$$E = \frac{\langle\Psi|\,\hat{H}\,|\Psi\rangle}{\langle\Psi|\Psi\rangle} \tag{2.4}$$

As said, the Hamiltonian operator takes into account the total energy of the system, that in general is given by the sum of kinetic energy and potential energy:

$$\hat{H} = \sum -\left(\frac{\hbar^2}{2m_i}\nabla_i^2\right) + \hat{V} \tag{2.5}$$

where $\hat{V}$ is the potential energy operator.

2.1.2 The many body problem

The Hamiltonian described in (2.5) does not take into account spin-spin interactions nor spin-orbit coupling events since is not taking into consideration any external magnetic field contribution.
The sum considers all the particles of the system, while the potential energy operator includes the possible electrostatic interaction between them.
In order to analyze a generic system we need to consider the contributions given by different types of particles that are present, i.e. M nuclei and N electrons. We define the positions $\boldsymbol{R}_A$ and $\boldsymbol{r}_i$ of the generic nucleus and electron respectively; the distance between nuclei A and B is $\boldsymbol{R}_{AB}$; the distance between electrons i and j is $\boldsymbol{r}_{ij}$. The overall Hamiltonian can be now written:

$$\hat{H} = -\sum_{i=1}^{N}\frac{1}{2}\nabla_i^2 - \sum_{A=1}^{M}\frac{1}{2M_A}\nabla_A^2 - \sum_{i=1}^{N}\sum_{A=1}^{M}\frac{Z_A}{\boldsymbol{r}_{iA}} + \sum_{i=1}^{N}\sum_{j>1}^{N}\frac{1}{\boldsymbol{r}_{ij}} + \sum_{A=1}^{M}\sum_{B>A}^{M}\frac{Z_A Z_B}{\boldsymbol{R}_{AB}} \tag{2.6}$$

in which M_A represents the ratio between the mass of nucleus A and electron, and Z_A is the atomic number of nucleus A. In (2.6) we have the appearance, from left to right, of the kinetic energies of electrons and nuclei, the attraction the two different particles, and the electron-electron and nucleus-nucleus repulsive contributions.
It is useful to highlight the components of the Hamiltonian operator, considering the electronic point of view (i.e. potential of nuclei is seen as *external*):

$$\hat{H} = \hat{T}_e + \hat{T}_N + \hat{V}_{ext} + \hat{V}_{int} + \hat{V}_{N-N} \tag{2.7}$$

in which the components are the same as (2.6).
As stated above, the Schrödinger equation with this Hamiltonian cannot be solved analytically for more than two bodies (i.e. the hydrogen atom). Even numerically, this Hamiltonian leads to a system which is practically impossible to solve with reasonable accuracy for all but trivial systems. In the coming sections we detail the approximations used to turn this fully-interacting, multi-body Schrödinger equation into a solvable problem.

2.1.3 Born-Oppenheimer approximation

The elevated complexity of the problem we are trying to solve prevent us to analytically compute its exact solution, hence approximations are needed. The first and simplest one is the *Born-Oppenheimer approximation* (or identically, *adiabatic approximation*). Its exploits the large asymmetry in the kinetic energy of electrons versus ions due to the latter much larger mass (i.e. $M_I \gg m_e$). This results in very different time-scales for electronic and nuclear motion, as nuclei have a much lower velocity than electrons.
Therefore, considering nuclei as frozen, we can neglect their kinetic energy contribution, and the interaction between two of them constant. This means that the electronic problem can be treated separately, i.e. electrons interact within a fixed nuclear potential. Specifically, we can rewrite the total wavefunction as:

$$\Psi_{tot} = \Psi_{elec} \times \Psi_{nuc} \tag{2.8}$$

The Hamiltonian instead becomes:

$$\hat{H}_{elec} = -\sum_{i=1}^{N} \frac{1}{2}\nabla_i^2 - \sum_{i=1}^{N}\sum_{A=1}^{M} \frac{Z_A}{\boldsymbol{r}_{iA}} + \sum_{i=1}^{N}\sum_{j>1}^{N} \frac{1}{\boldsymbol{r}_{ij}} \tag{2.9}$$

The resulting stationary state Schrödinger equation for the electrons will be written as:

$$\hat{H}_{elec}\Psi_{elec}(\boldsymbol{r}_i|\boldsymbol{R}_A) = \varepsilon_{elec}(\boldsymbol{R}_A)\Psi_{elec}(\boldsymbol{r}_i|\boldsymbol{R}_A) \tag{2.10}$$

in which the parametric contribution of nuclei is highlighted. For each set of nuclear coordinates we have a different equation that allow us to calculate the wavefunction with respect to electronic coordinates. As Ψ_{elec} is solved for, the corresponding nuclear problem can be considered. Formally, this means to solve:

$$\left[\hat{T}_N + \varepsilon_{elec}(R)\right]\Psi_{nuc} = E(R)\Psi_{nuc} \tag{2.11}$$

in which E is the energy eigenvalue for the entire system. This is an iterative process, in which nuclear position are updates in small increments, and electronic wavefunction completely recomputed at each step.

2.1.4 Hartree approximation

Born-Oppenheimer approximation is a powerful tool that simplifies the initial complete Schrödinger equation. Nonetheless, it is still not sufficient to allow the computation of the solution. Other approximations are thus necessary.
The focus will be now on the electronic problem only (i.e. (2.10)), thus the subscript *elec* will be omitted.
One of the first approximations developed to further simplify the electronic problem is the Hartree approximation. It is valid for a system of non-interacting particles. The electron-electron interaction is considered by means of a *mean potential* caused by all the electrons of the system. This means that we can now express the overall Hamiltonian as sum of single particle Hamiltonians:

$$\hat{H} = \sum_{i=1}^{N} h(i) \tag{2.12}$$

where $h(i)$ takes into account kinetic and potential energy of the single electron.
In this context is possible to rewrite also the wavefunction as the product of the wavefunctions of the electrons. Accordingly, it is possible to write the total Schrödinger equation for the only electronic problem as:

$$\hat{H}\Psi_{HP} = E\Psi_{HP} \tag{2.13}$$

And in this context the total energy E can be written as sum of single electron energies. The approximation for the wavefunction introduced with the Hartree product does not allow us to consider the interaction between two different electrons, as Ψ is now a non-correlated wavefunction. In other terms, since it is the product of single wavefunctions then its probability density is the product of single probability densities, which means that the probability of finding an electron in a point in space is not related to positions of any other electron, irrespective of the Coulomb repulsion.
A big drawback of the Hartree approximation is that the information related to the antisymmetry principle is completely lost. Since electrons are indistinguishable fermions, the total wavefunction of the system must be antisymmetric. In practical terms, the switching of coordinates between two particles has to be accounted for by a negative sign of the wavefunction obtained after the process. A solution to this issue, is to write the total wavefunction of a system with N electrons as a Slater determinant:

$$\Psi(1, 2, \ \ldots, \ N) = \frac{1}{\sqrt{N!}} \begin{vmatrix} \psi_1(1) & \psi_2(1) & \ldots & \psi_N(1) \\ \psi_1(2) & \psi_2(2) & \ldots & \psi_N(2) \\ \vdots & \vdots & \ldots & \vdots \\ \psi_1(N) & \psi_2(N) & \ldots & \psi_N(N) \end{vmatrix} \tag{2.14}$$

In this way we can correctly interpret the antisymmetry principle, since exchange of coordinates of electrons in the wavefunction corresponds to an exchange in the rows of the determinant,that implies a change in sign. In this way we can also correctly satisfy the conditions imposed by Pauli's exclusion principle, because two equals columns of the determinant cause the wavefunction to be zero (i.e. we would have two identical electrons).
Finally, applying Slater determinant allows to take into consideration the correlation of the motion of two electrons having the same spin. It doesn't however account for the motion of electrons

with anti-parallel spin. For this reason theories based on Slater determinant neglect the so-called electronic correlation.

2.1.5 Hartree-Fock approximation

Hartree-Fock theory is used to find a solution to the electronic problem in which the wavefunction is defined by (2.14).
The method exploited is the variational method, which consists in finding the wavefunction that minimizes the overall energy of the system of electrons:

$$E_0 = \langle \Psi_0 | \hat{H} | \Psi_0 \rangle \tag{2.15}$$

From this relation we obtain the Hartree-Fock equation, that corresponds to the equation for the optimized orbitals. In case of double occupied orbitals (i.e. closed-shell configuration) we can write such equation:

$$f(i)\psi_i = \varepsilon\psi_i \tag{2.16}$$

in which $f(i)$ is the Fock operator, defined as:

$$f(i) = -\frac{1}{2}\nabla_i^2 - \sum_{A=1}^{M} \frac{Z_A}{\boldsymbol{r}_{iA}} + \nu^{HF}(i) \tag{2.17}$$

where $\nu_{HF}(i)$ is the mean potential that is experienced by the i^{th} electron, due to the presence of other electrons. This approximation changes the nature of the problem, since it is now a single-body problem, from the moment that electron-electron repulsion is treated as a mean effect.
A problem that is still to be faced, though, is that the mean field itself depends on the wavefunctions. The solution to this problem is to use an iterative method called Self-Consistent-Field (SCF) method. The first step is the choice of suitable trial functions to evaluate for the first time the initial mean field. Then such field is used to solve the Schrödinger equation, finding new wavefunctions. At this point the procedure is repeated until convergence is reached for the value of the mean field: the next calculated mean field is equal to the previous and the orbitals used to build the Fock operator are equal to its wavefunctions. This system is said to now be self-consistent.
The fundamental state is the corresponding wavefunction calculated on the basis of Slater determinant, in which the element of the determinant itself are the computed orbitals. The spare orbitals are empty and are defined as *virtual* orbitals.
The standard Hartree-Fock equation can be obtained by means of Lagrange's multiplier method, in order to minimize Slater's single-determinant energy. The solution of the Hartree-Fock equation yields the minimum energy wavefunctions. It is an integral-differential equation, and takes the form:

$$h(1)\psi_a(1) + \sum_{b\neq a}\left[\int \frac{dx_2|\phi_b(2)|^2}{\boldsymbol{r}_{12}}\right]\phi_a(1) - \sum_{b\neq a}\left[\int \frac{dx_2\phi_b^*(2)\phi_a(2)}{\boldsymbol{r}_{12}}\right]\phi_b(1) = \varepsilon_a\phi_a(1) \tag{2.18}$$

where:

$$h(1) = -\frac{1}{2}\nabla_1^2 - \sum_A \frac{Z_A}{\boldsymbol{r}_{1A}} \tag{2.19}$$

represents the sum between the kinetic and potential energy related to the single electron nucleus

interaction. The other two terms are related to ν^{HF}. The first sum in (2.18) is the classical Coulomb repulsion involving electrons, also featured in Hartree's approximation. The second sum instead is an exchange term, required to satisfy anti-symmetric properties. We can introduce a suitable operator for the both of them. For the first term:

$$\hat{F}_b(1) = \int \frac{dx_2 \psi_b(2)^2}{\boldsymbol{r}_{12}} \tag{2.20}$$

we use the Coulomb operator, which represents the mean potential in x_1 caused by an electron in the ϕ_b state.
As for the second term, we introduce the exchange operator, defined for its action on orbital ψ_a :

$$\hat{K}_b(1)\psi_a(1) = \left[\int \frac{dx_2 \psi_b^*(2)\phi_a(2)}{\boldsymbol{r}_{12}}\right] \psi_b(1) \tag{2.21}$$

The exchange operator is defined as non-local, unlike the Coulomb operator, since it doesn't exist a potential $\hat{K}_b(x_1)$ uniquely defined in a point x_1. This means that when we apply this operator on ψ_a we have to consider the overall value of ψ_a in all points in space.
Therefore, considering equations (2.19), (2.20), and (2.21), we can write in a more compact form equation (2.18):

$$\left[h(1) + \sum_{b \neq a} \hat{F}_b(1) - \sum_{b \neq a} \hat{K}_b(1)\right] \psi_a(1) = \varepsilon_a \psi_a(1) \tag{2.22}$$

Similarly, the same can be done for the Hartree-Fock operator:

$$\nu^{HF}(1) = \sum_b \left[\hat{F}_b(1) - \hat{K}_b(1)\right] \tag{2.23}$$

where the condition $b \neq a$ has been suppressed, since:

$$\left[\hat{F}_a(1) - \hat{K}_a(1)\right] \psi_a(1) = 0 \tag{2.24}$$

In this way, Fock operator now is the sum of the single electron Hamiltonian and the Hartree-Fock operator:

$$f(1) = h(1) + \nu^{HF}(1) \tag{2.25}$$

2.1.6 Spin orbitals and Hartree-Fock restricted method

In the previous sections the term orbital was used. It is nothing more than the representation of the wavefunction of an electron. Since we are dealing with molecules, we have to consider that a molecular orbital (MO) is required for the analysis. A MO represents the wavefunction of an electron of the molecule.
It is possible to describe a wavefunction (i.e. an orbital) defining its spatial part and its spin property. Indeed, a *spatial orbital* is a wavefunction depending on the position only. Using $\boldsymbol{r}$ as usual, we indicate $\varphi_i(\boldsymbol{r})$ the spatial orbital whose square modulus, $|\varphi_i|^2\ d\boldsymbol{r}$ represents the probability to find the related electron in a volume element $d\boldsymbol{r}$ around $\boldsymbol{r}$.
To take into account the spin of the electron we use two functions, $\alpha(\omega)$ and $\beta(\omega)$ indicating spin-up and spin-down respectively.
The total wavefunction that considers both space and spin is the *spin orbital*, i.e. $\phi(\boldsymbol{x})$. For each

space orbital there exists two possible spin configurations, and thus two possible forms for the spin orbital:

$$\psi(\boldsymbol{x}) = \begin{cases} \varphi(\boldsymbol{r})\alpha(\omega) \\ \quad \text{or} \\ \varphi(\boldsymbol{r})\beta(\omega) \end{cases} \tag{2.26}$$

This considerations are significant in the theory of the implementation of the different Hartree-Fock methods based on the approximation described in 2.1.5. One of them is the restricted Hartree-Fock (RHF). The term restricted refers to the fact that the considered spin orbitals are all characterized by the same spatial part. Moreover, the determinant is in a *closed-shell* configuration, meaning that each orbital is occupied by a pair of electrons.

2.1.7 Roothan-Hall equations

The solution of the integral-differential equation proposed by Hartree-Fock approximation is difficult to solve by means of numerical algorithms. An efficient implementation may be otherwise possible exploiting the results obtained by Roothan and Hall.
The basic idea is to use a set of *known* functions to build the wavefunctions (i.e. the molecular orbitals). The advantage would be the possibility to express MOs as linear combination of atomic orbitals, approximated themselves by means of gaussian contractions.
Therefore with a suitable set of K known functions, i.e. a *basis set*, it is possible to define such orbitals as:

$$\varphi_i = \sum_{\mu=1}^{K} C_{\mu i}\phi_\mu, \quad i = 1, 2, \ \ldots, \ K \tag{2.27}$$

In the case of a complete set ϕ_μ the expansion above would turn out to be exact. Computational constraints prevent the usage of a complete set. Nonetheless, the larger the set, the more precise the approximation.
The first step would be to consider the closed-shell Hartree-Fock equation, obtained from (2.16) taking into account the spatial part only, that has the form:

$$f(\boldsymbol{r}_1)\varphi_j(\boldsymbol{r}_1) = \varepsilon_j\varphi_j(\boldsymbol{r}_1) \tag{2.28}$$

Then, a matrix expression for (2.28) is obtained by multiplying the left side by $\phi^*_\mu(1)$, substituting the wavefunction ψ with its expansion (i.e. (2.27)), and integrating over $\boldsymbol{r}_1$:

$$\sum_\nu F_{\mu\nu}C_{\nu i} = \varepsilon_i \sum_\nu S_{\nu\mu}C_{\nu i} \quad i = 1, 2, \ldots, \ K \tag{2.29}$$

In which we can distinguish the overlap matrix:

$$S_{\mu\nu} = \int \phi^*_\mu(1)\phi_\nu(1)d\boldsymbol{r}_1 \tag{2.30}$$

and the Fock matrix:

$$F_{\mu\nu} = \int \phi^*_\mu f(1)\phi_\nu(1)d\boldsymbol{r}_1 \tag{2.31}$$

The final form for the Roothan-Hall equation is therefore:

$$\mathbf{FC} = \mathbf{SC}\boldsymbol{\varepsilon} \tag{2.32}$$

in which C is the $K \times K$ square matrix of the expansion coefficient $C_{\mu\nu}$ while ε is the diagonal matrix of the single orbital energies ε_i. At this level, it is necessary to evaluate the value of the Fock matrix:

$$F_{\mu\nu} = H_{\mu\nu}^{core} + G_{\mu\nu} \tag{2.33}$$

the first term is the core Hamiltonian matrix, while the second is the two-electrons contribution to the Fock matrix. The latter may be represented by means of double integrals; these contributions are defined as:

$$H_{\mu\nu}^{core} = \int \phi_\mu^*(1) h(1\psi_\nu) d\boldsymbol{r}_1 \tag{2.34}$$

$$P_{\mu\nu} = 2 \sum_a^{N/2} C_{\mu a} C_{\nu a}^a \tag{2.35}$$

Finally, in order to carry out a solution for Roothan equations an iterative process must be used, since such equations are nonlinear. Indeed, the Fock matrix $\boldsymbol{F}$ depends on the density matrix, which in turns depend on the expansion coefficient, i.e. $\boldsymbol{F=F(C)}$. It is possible to turn the problem of (2.32) into a simple eigenvalue problem exploiting ortho normalization, by loosing the dependence on the overlap matrix. The final form of the problem is then:

$$\mathbf{F'C'} = \mathbf{C'}\boldsymbol{\varepsilon} \tag{2.36}$$

Thereafter, diagonalizing $\boldsymbol{F'}$ we obtain $\boldsymbol{C}$, and finally we can solve (2.32) for $\boldsymbol{C}$ and $\boldsymbol{\varepsilon}$.

2.1.8 SCF method

It is possible to enumerate the various steps required by the SCF iterative procedure. These are used to solve the Roothan equations expressed in their matrix form. Specifically, it consists of the following passages:

1. Identification of the molecule and its most important properties: nuclear coordinates, atomic number, number of electrons, initial guess of wavefunctions to be used in the computations.
2. Calculation of the required integrals: $S_{\mu\nu}$, $H_{\mu\nu}^{core}$, $(\mu\nu|\lambda\sigma)$.
3. Diagonalization of the overlap matrix $\boldsymbol{S}_{\mu\nu}$ and evaluation of the transformation matrix.
4. Guess of the density matrix $\boldsymbol{P}$.
5. Computation of the $\boldsymbol{G}$ matrix from density matrix and double integrals $(\mu\nu|\lambda\sigma)$
6. Addition of $\boldsymbol{G}$ matrix to $H_{\mu\nu}^{core}$ to obtain the Fock matrix.
7. Calculation of the transformed Fock matrix $\boldsymbol{F'}$.
8. Diagonalization of $\boldsymbol{F'}$ to obtain $\boldsymbol{C'}$ and $\boldsymbol{\varepsilon}$.
9. Evaluation of $\boldsymbol{C}$ from $\boldsymbol{C'}$.
10. Calculation of a new matrix density from $\boldsymbol{C}$.

11. If the newly calculated matrix is equal to the previous, then the problem is solved. If it is not, the procedure is repeated from point 5 with the new density matrix.

12. If the procedure reached convergence, then $\boldsymbol{C}, \boldsymbol{P}, \boldsymbol{F}$ are used to calculate the quantities of interest.

2.2 Basis sets

The possibility to exploit Hartree-Fock theory in computations, by means of the iterative procedure, relies on the theories of linear combination of atomic orbitals and molecular orbitals, as expressed in (2.27). A correct expression for the atomic orbitals ϕ_μ is given by slater functions or Slater-type orbitals (STO) functions:

$$\phi_i(\zeta, n, l, m;\ \boldsymbol{r}, \vartheta, phi) = N r^{n-1} e^{-\zeta \boldsymbol{r}}\ Y_{ln}(\vartheta, \phi) \tag{2.37}$$

here represented in spherical coordinates. The variables n, l, m are a set of quantum numbers, N is a normalization constant and ζ is the exponent for the STO function, Y_{lm} is the angular part.
Due to the fact that they are computationally heavy because of the double integrals calculation, they are replaced by Gaussian-type orbitals (GTO), in which we have gaussian functions instead of Slaters':

$$g(\alpha, l, m, n;\ x, y, z) = N e^{-\alpha \boldsymbol{r}^2}\ x^l y^m z^n \tag{2.38}$$

in which N is still a normalization constant, α is the exponent, x, y, z the coordinates and l, m, n are no more quantum numbers but instead simple exponents.
These functions are much simpler to integrate with respect to those related to STO. Nonetheless the combination time associated with the integrals calculation is $O(m^4)$, where m is the number of the so called *gaussian primitives*, i.e. the GTO functions. A solution to lower the computational effort is to replace these gaussian primitives with *contractions* of gaussian functions to represent the single atomic orbital. This is equal to write atomic orbitals as linear combinations of simple gaussian functions:

$$\phi_\mu = \sum_{p=1}^{L} d_{p\mu} g_p(\alpha_{p\mu}, \boldsymbol{r}) \tag{2.39}$$

where both coefficients and exponents are determined at the beginning of the process and remain the same until the end of the SCF procedure. The basis set in which each ground-state orbital is described by a single contraction is referred to as *minimal*. A more complex form is the *split-valence* basis set, in which a distinction between valence and core orbitals is introduced. Indeed the latter are described by one contraction, while the former by more than one contractions. One of the most notable mentions is the *6-31G*, in which core orbitals are described by six primitives and two contractions, of three and one primitives respectively, to describe outer shell orbitals. To increase the accuracy of the description of the chemical bond, it is possible to introduce *polarization functions* in which d orbitals on heavy atoms and p orbitals for hydrogen are considered. These forms are denoted as *6-31** or *6-31*** or *6-31G(d,p)*. Since these functions are calculated as non contracted primitives the cost for the computation is increased. A common technique employed to better set up the basis sets is the addition of the so-called *diffuse* functions. Denoted with a

plus sign or "aug" prefix, these functions are shallow basis functions, which represent with a higher accuracy the *tails* of atomic orbitals, distant from nuclei. Diffuse functions are important when considering anions and other large molecular systems.

2.3 Density Functional theory

Density functional theory (DFT), is very different from Hartree-Fock theory, since the description of the system is now based on the electronic density instead of the wavefunctions. This has an important consequence on the number of variable involved in the computations. Indeed, for a system of N electrons, there is a set of $3N$ spatial coordinates plus N spin coordinates for the wavefunctions approach. On the other hand, the electronic density depends only on three spatial coordinates. The advantages of a method based on the electronic density is evident. The theory consists in writing all the quantities of the fundamental state of a system as functionals of the electronic density, i.e. $\rho(\boldsymbol{r})$. In particular, it is possible to express the energy of the ground state as a functional of the density and it is the minimum energy if the density is exact. This theory is exact: indeed, an exact result can be obtained if the correct value of the exchange-correlation potential is known. However, approximation are necessary, since no clues on how to properly build the functional is known.

2.3.1 Hohenberg-Kohn theorems

DFT is based on the Hohenberg-Kohn theorems, which allowed for a correct and rigorous formalization of the Thomas-Fermi theory. Thomas-Fermi was the first theory that exploited the electronic density to describe a physical system. The contribution of the electron-electron repulsion is substituted by Coulomb repulsion, while kinetic energy functional is approximated on the basis of the uniform gas of non-interacting electrons. No evaluation for exchange and correlation effects is provided.
The physical-mathematical theory based on electronic density relies on the following:

Theorem 1. *The external potential $\nu(\boldsymbol{r})$ is uniquely determined by the electronic density, $\rho(\boldsymbol{r})$, apart from an additive constant.*

To this theorem is linked also an important corollary:

Corollary 1.1. *Since the electronic density $\rho(\boldsymbol{r})$ uniquely determines $\nu(\boldsymbol{r})$, then it also determines the wavefunction Ψ of the ground state.*

To better highlight the importance of these observations, it is possible to rephrase the 1: each observable of a stationary quantum-mechanical system (i.e. energy included), may be calculated as a function of electronic density, i.e. it may be written in terms of a functional of said density.
The second theorem states that:

Theorem 2. *Let $\tilde{\rho}(\boldsymbol{r})$ be a non negative density normalized by N. Then, $E_0 < E_\nu[\tilde{\rho}]$, where $E_\nu[\tilde{\rho}]$ is the functional of a state whose external potential is determined by a density of the ground state $\tilde{\rho}(\boldsymbol{r})$. The ground-state density can be evaluated using a variational method based on the density only.*

It is possible to rewrite the electronic Hamiltonian as:

$$\hat{H}_{elec} = \hat{T}_e + \hat{V}_{ext} + \hat{U}_{ee} \tag{2.40}$$

being the first term the kinetic energy of electrons, the second the external potential arising from the electrons-nuclei interaction, and the last one the interaction term for electron-electron repulsion. Once the external potential is set, then the electronic density changes to reach the minimum energy configuration. Theorem 1 and theorem 2 prove that it is in fact true also the opposite, i.e. the external potential is uniquely determined by the electronic density, meaning that nuclear configuration is itself dependent on the density ρ:

$$E[\rho] = T_e[\rho] + V_{ext}[\rho] + U_{ee}[\rho] \tag{2.41}$$

Here we used expectation values of (2.40). If the terms that are not dependent on the external potential are regrouped, it is possible to provide an exact representation of the system:

$$E[\rho] = V_{ext}[\rho] + F_{HK}[\rho] = \int \rho(\boldsymbol{r})\nu(\boldsymbol{r})dr + F_{HK}[\rho] \tag{2.42}$$

in which we have that:

$$F_{HK} = \langle \Psi[\rho] | \, \hat{T}_e + \hat{U}_{ee} \, | \Psi[\rho] \rangle \tag{2.43}$$

where Ψ is the ground state wavefunction having electronic density ρ, while F_{HK} is a *universal* functional that depends only on electronic density. Thus, equation (2.42) is an exact representation of the system. Moreover, knowing the exact expression for F_{HK} would allow for the correct computation of all of the properties of such system. Another consequence given by the second theorem is that it makes the used method variational: let ρ' be the electronic density of a system with N electrons, then, the total energy calculated using ρ' must be larger than the real energy. Unfortunately, the main flaw in this theory is that no exact expression for F_{HK} functional is known, as it is an extremely complex physical quantity.

2.3.2 Kohn-Sham equations

The main issue with the DFT is that it is not useful in the description of bounded states, making it useless for theoretical chemistry. The solution to this issue was given by the *Kohn-Sham method*. It is possible to rewrite equation (2.41) in the following way:

$$E[\rho] = T_e[\rho] + V_{ext}[\rho] + \frac{1}{2} \iint \frac{\rho(\boldsymbol{r})\rho(\boldsymbol{r}')}{|\boldsymbol{r} - \boldsymbol{r}'|} d\boldsymbol{r} d\boldsymbol{r}' + E_{xc}[\rho] \tag{2.44}$$

in which U_{ee} is split in two terms, the first being the repulsion energy between electrons, the second is the exchange correlation term, taking into account non classical contributions. Here, the solution provided by the Kohn-Sham method is embedded in the interpretation of the kinetic energy of the

interacting system: it is substituted with the kinetic energy of a system of *non-interacting* electrons, i.e. T_0. The electronic density of the latter is taken to be equal to the density of the former, i.e. $\rho(\boldsymbol{r})_{non-int} = \rho(\boldsymbol{r})_{int}$. The expression for the kinetic energy that accounts for the electron-electron interaction is embedded in the exchange-correlation term. Therefore the total energy functional can be written as:

$$E_{KS}[\rho] = T_0[\rho] + V_{ext}[\rho] + U_{cl}[\rho] + E_{xc}[\rho] \tag{2.45}$$

The exchange-correlation term, E_{xc}, is the only functional of the expression that is not precisely known, thus it is the only approximation performed in DFT. Different forms of this functional have been proposed, but none has been proven accurate for the description of all the chemical systems. As a last step in the treatment of the Kohn-Sham method, a set of equation useful for computational applications has to be defined. The first step is to define, exploiting the Kohn-Sham hypothesis, the Hamiltonian for the non-interacting system:

$$\hat{H}_0 = \sum_{i=1}^{N} \left(-\frac{\nabla_i^2}{2} + \nu_{eff}(\boldsymbol{r}_i) \right) \tag{2.46}$$

The eigenstates can now be expressed in the form of Slater determinant where the Kohn-Sham orbitals $\phi_i^{KS}(\boldsymbol{r}_i)$ are present and consequently define the density and the kinetic energy:

$$\rho(\boldsymbol{r}) = \sum_{i=1}^{N} |\phi_i^{KS}(\boldsymbol{r})|^2 \tag{2.47}$$

$$T_0[\rho] = \sum_{i=1}^{N} \left\langle \phi_i^{KS} \right| - \frac{\nabla_i^2}{2} \left| \phi_i^{KS} \right\rangle \tag{2.48}$$

Applying a variational method on E_{KS} and using (2.45) an equation for $\nu_{eff}(\boldsymbol{r})$ can be derived:

$$\nu_{eff}(\boldsymbol{r}) = \nu(\boldsymbol{r}) + \int \frac{\rho(\boldsymbol{r'})}{|\boldsymbol{r} - \boldsymbol{r'}|} d\boldsymbol{r'} + \mu_{xc}[\rho(\boldsymbol{r})] \tag{2.49}$$

in which we have that:

$$\mu_{xc}[\rho(\boldsymbol{r})] = \frac{\delta E_{xc}[\rho(\boldsymbol{r})]}{\delta \rho(\boldsymbol{r})} \tag{2.50}$$

Finally, it is possible to highlight that Kohn-Sham orbitals satisfy the *Kohn-Sham self-consistent equations*:

$$\left\{ -\frac{\nabla^2}{2} + \nu_{eff}(\boldsymbol{r}) \right\} \phi_i(\boldsymbol{r}) = \varepsilon_i \phi_i(\boldsymbol{r}) \tag{2.51}$$

These equations have the same form of equations (2.16) and (2.18), meaning it is possible to use the same iterative procedure to solve them. Using orbitals energies ε_i, the total energy can be expressed with the following:

$$E_{KS}[\rho] = \sum_{i=1}^{N} \varepsilon_i - \frac{1}{2} \iint \frac{\rho(\boldsymbol{r})\rho(\boldsymbol{r'})}{|\rho(\boldsymbol{r}) - \rho(\boldsymbol{r'})|} d\boldsymbol{r} d\boldsymbol{r'} + \left\{ E_{xc}[\rho] - \int \rho(\boldsymbol{r}) \mu_{xc}[\rho] \; d\boldsymbol{r} \right\} \tag{2.52}$$

These equations have a similar form to Hartree-Fock equations, thus they are useful in computational applications. A major difference with Hartree-Fock equations is that Kohn-Sham equations are computationally lighter since Hartree-Fock considers an exact, non-local exchange term. Moreover, within Kohn-Sham equations the exchange and correlation effects are considered in the ν_{eff} term. Therefore, using a system of N non-interacting electrons having the same electronic density of the correlated system with interacting electrons allows to solve in an exact way the many-body Schrödinger equations. Indeed, the only approximation introduced concerns the $E_{xc}[\rho]$ term. Finally, considering Kohn-Sham orbitals, it is possible to demonstrate that are related to the associated electronic density only.

2.3.3 Exchange-correlation functionals

The different exchange-correlation functionals have some properties. We can write the exchange-correlation functional for the *interacting* system as:

$$E_{xc}[\rho] = \frac{1}{2}\iint \frac{\rho(\boldsymbol{r})\rho(\boldsymbol{r}')}{|\boldsymbol{r}-\boldsymbol{r}'|}\left[\tilde{g}(\boldsymbol{r},\boldsymbol{r}')-1\right]d\boldsymbol{r}d\boldsymbol{r}' \tag{2.53}$$

where $\tilde{g}$ is the *pair correlation function*, and takes into account the electron-electron repulsion. This function is averaged depending in the force of the electronic contribution. Defining the exchange correlation hole we can rewrite equation (2.53):

$$\tilde{\rho}_{xc}(\boldsymbol{r},\boldsymbol{r}') = \rho(\boldsymbol{r})\left[\tilde{g}(\boldsymbol{r},\boldsymbol{r}')-1\right] \tag{2.54}$$

$$E_{xc}[\rho] = \frac{1}{2}\iint \frac{\rho(\boldsymbol{r})\tilde{\rho}_{xc}(\boldsymbol{r},\boldsymbol{r}')}{|\boldsymbol{r}-\boldsymbol{r}'|}d\boldsymbol{r}d\boldsymbol{r}' \tag{2.55}$$

In this expression E_{xc} represents the interaction between the electronic charge distribution and the electronic charge distribution affected by the exchange-correlation effects. Both $\tilde{g}$ and $\tilde{\rho}_{xc}$ must satisfy some requirements, essential for the development of approximated functionals. Specifically, they have to be *symmetrical*:

$$\tilde{g}(\boldsymbol{r},\boldsymbol{r}') = \tilde{g}(\boldsymbol{r}',\boldsymbol{r}) \tag{2.56}$$

they have to satisfy normalization:

$$\int \tilde{g}(\boldsymbol{r},\boldsymbol{r}')\rho(\boldsymbol{r}')d\boldsymbol{r}' = \int \tilde{g}(\boldsymbol{r},\boldsymbol{r}')\rho(\boldsymbol{r})d\boldsymbol{r} \tag{2.57}$$

and lastly it has to be verified that:

$$\int \tilde{\rho}(\boldsymbol{r},\boldsymbol{r}')d\boldsymbol{r}' = \int \tilde{\rho}_{xc}(\boldsymbol{r},\boldsymbol{r}')d\boldsymbol{r} = -1 \tag{2.58}$$

The simplest approximation is the Local Density Approximation (LDA). It considers a general inhomogeneous electronic system as *locally* homogeneous, so that the electronic density is approximated to that of an homogeneous electron gas. In this way, the exchange-correlation functional becomes:

$$E_{xc}^{LDA}[\rho] = \int \rho(\boldsymbol{r})\varepsilon_{xc}^{LDA}[\rho]d\boldsymbol{r} \tag{2.59}$$

with ε_{xc}^{LDA} being the exchange-correlation energy. LDA is a strong approximation, and should be applied only to systems having a slowly varying electronic distribution. Its applicability to molecules is remarkable, since it is based on the evaluation of a real physical system. Moreover, since it doesn't depend on any empirical parameter, is a real *first principle* approximation.
A further extension of LDA is Local Spin Density Approximation (LSDA), in which the spin is taken in consideration too. An evolution of the latter is the Gradient Expansion Approximation (GEA), consisting on a Taylor expansion of the E_{xc} functional. Truncation GEA expansion at first order yields the Generalized Gradient Approximation (GGA), that has the form:

$$E_{xc}[\rho] = \int f[\rho,\nabla\rho]d\boldsymbol{r} \tag{2.60}$$

This approach is commonly used in new and more precise functionals. The strategy is to separate the effects of exchange and correlation, so that:

$$E_{xc} = E_x[\rho] + E_c[\rho] \tag{2.61}$$

The most famous and important exchange functionals are *B88*, *PW86*, *PW91*. As for the correlation ones, notable mentions are *LYP*, *PW86* and *PW91*. These functionals, except PW91, feature contributions from empirical data, and thus make DFT a non *ab-initio* method.

2.3.4 Hybrid functionals

The issue of the dependence of the functionals on empirical parameters has been tackled by Perdew and Wang in their research about PW91, to make DFT a *true ab-initio* method. The procedure adopted to build PW91 was inspired by GEA functional, but a different treatment for the Taylor expansion was used, in order to remove all the terms responsible for the failure of GEA itself. This approach takes the name of *real-space cutoff*, and makes it possible to respect all the requirements for E_{xc} functionals, plus solves the issue related to the dependence on empirical parameters (i.e. it is a theoretical approach). Due to the fact that PW91 is based on GEA, it embeds also LDA, tending to it whence a slowly variable electronic density is involved. On the other hand, other functionals based on GGA (e.g. the LYP one) do not behave in the same way, thus describing an erroneous physical behavior.
With PW91 the issue concerning dependence on empirical parameters is solved, making DFT a true *ab-initio* method, at least for the correlation part. The exchange side of PW91 is in fact derived from B88 functional, that depends on some empirical parameters. Nonetheless, this doesn't cause any problem, since the way PW91 is built eliminates any direct dependence on empirical parameters, and it has been proven that the results obtained wit PW91 and B88 are basically identical.
Starting from this formulation Perdew, Burke and Ehrnzerhof developed the so called PBE functional, nowadays one of the most used in computational chemistry. It is an advanced functional of the GGA type, and covers some conditions not yet satisfied by PW91.
One of the problems that affect GGA functionals is the exchange effects. To be able to correctly account for this feature, hybrid functionals have been developed, in which the exchange part is substituted by the exact exchange. The method is based on the *Adiabatic Connection* formula:

$$E_{xc} = \int_0^1 E_{xc,\lambda}\, d\lambda \tag{2.62}$$

Where the exchange-correlation functional is represented with a single expression, having λ as a variable. When it is $\lambda = 1$ the system is completely correlated, on the other hand if $\lambda = 0$ the correlation is null. In the condition of no correlation, GGA functionals fail to correctly describe the system, thus hybrid functionals have been introduced, and feature an exact contribution regarding the exchange part.
Different schemes have been introduced, the most widely used includes three empirical parameters to take into account both Hartree-Fock exchange part and DFT exchange and correlation:

$$E_{xc}^{ACM3} = E_{xc}^{LSD} + a_1\left(E_x^{HF} - E_x^{LSD}\right) + a_2\Delta E_x^{GGA} + a_3\Delta E_c^{GGA} \tag{2.63}$$

In the family of hybrid functionals based on these three parameters one of the most important is the B3LYP, introduced by Becke. Recently, Becke suggested that a single parameter may be used to consider the Hartree-Fock DFT exchange ratio, with remarkable results. Specifically, the functional can be written as:

$$E_{xc}^{ACM1} = E_{xc}^{GGA} + a_1\left(E_x^{HF} - E_x^{GGA}\right) \tag{2.64}$$

Perdew showed that an optimal value for parameter a_1 can be obtained *a priori* considering fourth-order perturbation theory, obtaining satisfying results also for molecular systems. This

allow to define a family of *adiabatic connection* functionals, i.e. ACM0, having the same number of adjustable parameters of their GGA constituents:

$$E_{xc}^{ACM0} = E_{xc}^{GGA} + \frac{1}{4}\left(E_x^{HF} - E_x^{GGA}\right) \tag{2.65}$$

This particular expression for the functional allows the possibility to use a parameter-free DFT approach, in which are present both PBE functional and Hartree-Fock exchange with specific coefficients. The so built hybrid functional, i.e. PBE0, is probably one of the top functionals currently available, granting good accuracy in the modeling of molecular structures, in compliance with the physical principles.

2.3.5 Grimme's corrections

The possible parameters that can be used in this type of analysis are not only basis-sets and functionals. In fact the accuracy and precision of the description of the analyzed system can be increased by means of specific adjustments. One of this feature is the correction provided by Grimme's functions, which aim to increase the performances regarding the investigation of non local correlation effects and in the estimation in the Van der Waals dispersive interactions [69].
The dispersion energy is a long range electron correlation effect, which is only taken in consideration in the case of short to medium electron-electron interactions. The London components of this type of interactions is not included in the standard DFT based on the Kohn-Sham theory. It can be described as a temporary attractive force taking place when electrons in two adjacent atoms form temporary dipoles. The phenomenon is time-independent, thus regarding stationary electronic states, while the formation of the temporary (instantaneous) dipoles is caused by the motion of electrons. Stronger dispersion forces are related to larger and heavier atoms.
The solution proposed by Grimme et al. is based on empirically obtained parameters, i.e. atom cutoff distances R_0^{AB} and dispersion coefficients C_n^{AB}, related to the A and B atoms considered. In this context, this solution does not provide any influence or dependence on the electronic structure, which may be a problem in some cases. The applicability of these corrections is preferential for functionals as B3LYP, PBE and others, which are considered non optimal for non-covalent interactions, but still having good performances in the description of other properties. In practical terms, a corrected DFT approach, i.e. DFT-D3 (being D3 the most advanced version for these corrections), can be described starting from the overall energy considered:

$$E_{DFT-D3} = E_{KS-DFT} - E_{disp} \tag{2.66}$$

where E_{KS-DFT} is the self-consistent Kohn-Sham energy as obtained from the selected functional and E_{disp} is the dispersion correction, which is itself the sum of two energies related to two-body and three-body interactions:

$$E_{disp} = E^{(2)} + E^{(3)} \tag{2.67}$$

The most important of the two terms is the two-body energy, defined as:

$$E^{(2)} = \sum_{AB} \sum_{n=6,8,10,\ldots} s_n \frac{C_n^{AB}}{r_{AB}^n} f_{d,n}(r_{AB}) \tag{2.68}$$

where the first sum is over all atom pairs in the system, C_n^{AB} is the averaged n^{th}-order dispersion coefficient for the considered atom pair and r_{AB} is the internuclear distance.

2.4 Raman spectroscopy

In this section a brief introduction on vibrational theory of molecules will be presented, fundamental to understand Raman effect and spectroscopy. Then the principles of Raman scattering and SERS will be discussed.

2.4.1 Vibrational theory

Vibrations in molecules affect both electrons and nuclei, and are caused by the non-zero energy that any body possess at temperatures different from the absolute zero. Due to the high complexity of the vibrational problem related to a many-body case, some approximations are needed, as for the electronic problem.
The *Harmonic oscillator* is a simple but effective model used to describe a vibrating system, having the advantage of simplifying the expression of the interatomic potential. Taking into account nuclear vibrations, it is possible to express the potential in the vicinity of such nuclei as a Taylor expansion truncated at the second order, under the approximation of small amplitude vibrations. The expression of the potential is then:

$$V(q) \approx V\left(R_0\right) + \left(\frac{dV}{dq}\right)_{q=q_0} (q - q_0) + \frac{1}{2}\left(\frac{d^2V}{dq^2}\right)_{q=q_0} (q - q_0)^2 \tag{2.69}$$

which is equal, at the equilibrium position, to:

$$V(q) \approx V(q_0) + \frac{1}{2}k(q - q_0)^2 \tag{2.70}$$

with k being the force constant, defined as the second order derivative of the potential with respect to the spatial coordinates, at the equilibrium position:

$$k = \left(\frac{d^2V}{dq^2}\right)_{q-q_0} \tag{2.71}$$

Considering the simple spring model, it is possible to relate the force acting along the coordinate q with the force constant and the displacement, i.e. Hooke's law:

$$f(r) = -\frac{dV}{dq} = -k(q - q_0) = -k\Delta q \tag{2.72}$$

The force here expressed is the restoring force, and the minus sign stands to indicate the opposite directions of force and displacement.
It is interesting to apply this model to a system consisting of a single diatomic isolated molecule. The masses and positions of the two bonded atoms are represented by $m_1,\ r_1$ and $m_2,\ r_2$ respectively. Considering the generic displacements of these atoms, i.e. x_1 and x_2 it must be satisfied that:

$$m_1 r_1 = m_2 r_2 \tag{2.73}$$

$$m_1\left(r_1 + x_1\right) = m_2\left(r_2 + x_2\right) \tag{2.74}$$

Using these two equations the expression for the single displacement as function of the other parameters is obtained:

$$x_1 = \left(\frac{m_2}{m_1}\right) x_2 \tag{2.75}$$

and vice versa for x_2. Substituting in the equation for the force and applying Newton's equation:

$$m_1 \frac{d^2 x_1}{dt^2} = -k \left(\frac{m_1 + m_2}{m_2} \right) x_1 \tag{2.76}$$

$$m_2 \frac{d^2 x_2}{dt^2} = -k \left(\frac{m_1 + m_2}{m_1} \right) x_2 \tag{2.77}$$

Rearrangement of the equations and introduction of the *reduced mass*, i.e. $\mu = \frac{m_1 m_2}{m_1 + m_2}$ and displacement $q = x_1 + x_2$ it is possible to obtain the differential equation representing the vibrational problem:

$$\mu \frac{d^2 q}{dt^2} = -kq \tag{2.78}$$

A solution for such equation describes the variation in time of the bond length of the examined diatomic molecule:

$$q(t) = q_0 + A \sin \omega t + \phi \tag{2.79}$$

where ω is the *angular frequency* and it can be calculated as:

$$\omega = \sqrt{\frac{k}{\mu}} \tag{2.80}$$

This quantity can also be expressed in a different unit of measure, i.e. cm^{-1}. Indeed, using the linear dispersion relation of light:

$$\bar{\nu} = \frac{\nu}{c} = \frac{\omega}{2\pi} = \frac{1}{2\pi c} \sqrt{\frac{k}{\mu}} \tag{2.81}$$

Finally, the solution for the diatomic molecule vibrational problem lies around the equilibrium bond length value q_0, and the amplitude of the oscillation of such bond is given by the constant A. The situation is by far more complex in the case of a system with many atoms, i.e. polyatomic molecules. The problem can be tackled by considering many degrees of freedom for the system, within the harmonic approximation. The goal is to reduce the many body problems into a set of independent one dimensional quantum oscillators. The classical Hamiltonian for this kind of system is:

$$H = T + V = \frac{1}{2} \sum_i m_i \dot{u}_i^2 + \frac{1}{2} \sum_{ij} u_i k_{ij} u_j \tag{2.82}$$

where the kinetic energy has a diagonal quadratic form and is expressed as sum of independent terms. The potential energy instead couples all pairs of displacement through the k_{ij} coefficients. The aim is to diagonalize the Hamiltonian, which can be written in the following way:

$$\boldsymbol{H} = \frac{1}{2} \dot{\xi}^t \dot{\xi} + \frac{1}{2} \dot{\xi}^t \boldsymbol{W} \dot{\xi} \tag{2.83}$$

The matrix $\boldsymbol{W}$ can be expressed as:

$$\boldsymbol{W} = \boldsymbol{M}^{-1/2} \boldsymbol{K} \boldsymbol{M}^{-\mathbf{1/2}} \tag{2.84}$$

and it represents the potential as a quadratic form with respect to the set of mass-weighted coordinates ξ. Exploiting the diagonal representation of $\boldsymbol{WL} = \boldsymbol{L\Lambda}$ it's possible to rewrite the Hamiltonian as:

$$\boldsymbol{H} = \frac{1}{2} \dot{\xi}^t \boldsymbol{L} \boldsymbol{L}^t \dot{\xi} + \frac{1}{2} \dot{\xi}^t \boldsymbol{L\Lambda L} \dot{\xi} \tag{2.85}$$

Introducing normal coordinates is possible to rewrite the Hamiltonian featuring a diagonal representation for both kinetic and potential energy:

$$\boldsymbol{H} = \frac{1}{2}\dot{\bar{q}}^t\dot{\bar{q}} + \frac{1}{2}\dot{\bar{q}}^t\boldsymbol{\Lambda}\dot{\bar{q}} \tag{2.86}$$

in which eigenvalues Λ represent angular frequencies squared. The displacements can also be written in term of normal coordinates, starting from the equation of motion:

$$q_i(t) = q_i^0 \sin\omega_i t + \phi_i \tag{2.87}$$

$$\bar{u} = \bar{q}(\boldsymbol{M}^{-1/2}\boldsymbol{L}) \tag{2.88}$$

The reason why normal coordinates are important is the highlighting of the relation between chemical structure and vibration transition. The visualization of a specific normal modes, i.e. i^{th} mode, is possible by observation of an animation of atoms' motion.

2.4.2 Quantum theory of vibration

In this section the correlation between normal modes and vibrational wavefunction will be exposed. The Hamiltonian of a polyatomic molecular system can be written using quantum theory principles:

$$\hat{H} = \hat{T} + \hat{V} = \sum_i \left[-\frac{\hbar^2}{2}\frac{\partial^2}{\partial q_i^2} + \frac{\omega_i^2 q_i^2}{2} \right] \tag{2.89}$$

In a more convenient way it is possible to express the Hamiltonian in a dimensionless representation, exploiting the dimensionless position operator $s_i = q_i\sqrt{\omega_i\hbar}$:

$$\hat{H} = \sum_i \frac{\hbar\omega}{3}\left[\frac{\partial^2}{\partial s_i^2} + s_i^2\right] = \sum_i \hbar\omega_i \hat{h}(s_i) \tag{2.90}$$

The eigenvalues and eigenvectors associated to the one dimensional quantum oscillator are:

$$\hat{H}_{vib}(s_i)\,|n_i\rangle = \hbar\omega_i\left(n_i + \frac{1}{2}\right)|n_i\rangle \tag{2.91}$$

The eigenvectors for the vibrational problem related to normal coordinates, i.e. displacement, are n_i. Under the hypothesis of a many-body Hamiltonian obtained as the sum of multiple single Hamiltonians, it is possible to express the many-body energy eigenvalue as the sum of the single energies:

$$\hat{H}\phi(s_1,\ s_2,\ \ldots,\ s_M) = E\phi(s_1,\ s_2,\ \ldots,\ s_M) \tag{2.92}$$

$$\phi(s_1,\ s_2,\ \ldots,\ s_M) = \prod_{i=1}^{M}\phi_{n_i}(s_i) \tag{2.93}$$

$$E = \sum_{i=1}^{M}\hbar\omega\left(n_i + \frac{1}{2}\right) \tag{2.94}$$

In this situation M is the number of vibrational normal modes that can be obtained solving the equation (2.94). Usually Cartesian coordinates are used to describe the different molecular motions, and three rotational and three translational ones are identified. Thus the total number of *true* vibrations is $M = 3N - 6$, where N is the number of atoms of the system.

2.4.3 Raman scattering

Raman scattering is the inelastic scattering of photons by matter. Such interaction is possible since the electromagnetic field of the incident photons induces in the system a time-dependent dipole moment. Let E be the electric field of the incident radiation. Then:

$$E = E_0 \cos \omega_L t \tag{2.95}$$

Such electric field interacts with the electronic charge of the system, expressed in term of a dipole moment μ:

$$\mu(t) = \sum_i e_i r_i(t) \tag{2.96}$$

where e is the charge of the electron and r is the position vector.
The dipole moment variation due to the interaction of these quantities can be expressed as:

$$\Delta\mu = \alpha E + \frac{1}{2}\beta E^2 + \ \ldots \tag{2.97}$$

in which α is the polarizability of the system, while β is the hyperpolarizability, a third-rank tensor, not considered in this treatment. The polarizability can be written as:

$$\alpha = \left(\frac{\partial \mu}{\partial E}\right)_0 \tag{2.98}$$

Evidently, α is a second-rank tensor, but it will be assumed that the considered system is isotropic, i.e. μ is parallel to E. The polarizability depends on the charge distribution of the system, i.e. $\alpha = \alpha(\rho)$, so that a change in the atomic configuration is reflected in ρ and therefore α.
In the hypothesis of small displacements of nuclei around their equilibrium position, the polarizability will linearly change with the normal coordinate Q associated to the vibration:

$$Q = \sqrt{\bar{m}}\,(u_2 - u_1) \tag{2.99}$$

$$\alpha = \alpha_0 + \left(\frac{\partial \alpha}{\partial Q}\right)_0 Q + \frac{1}{2}\left(\frac{\partial^2 \alpha}{\partial Q^2}_0\right) Q^2 \tag{2.100}$$

where $\bar{m}$ is the reduced mass and u_i indicates the displacement of the atom i. The expression for the polarizability is a Taylor expansion, reported for completeness to the second order. The linear dependence is referred to the first term. Under the assumption of modeling the molecular vibrations with the harmonic oscillator it is found that the normal coordinate is:

$$Q = Q_0 \cos \omega_s t \tag{2.101}$$

and therefore the expression for the polarizability is:

$$\alpha(t) = \alpha_0 + \left(\frac{\partial \alpha}{\partial Q}_0\right) Q_0 \cos \omega_s t \tag{2.102}$$

This formulation can be used in (2.97) to obtain:

$$\Delta\mu(t) = \alpha_0 E_0 \cos \omega_L t + \frac{1}{2}\left(\frac{\partial \alpha}{\partial Q}\right)_0 Q_0 E_0 \left[\cos(\omega_L - \omega_s)t + \cos(\omega_L + \omega_s)t\right] \tag{2.103}$$

This equation shows that the dipole moment oscillates with the incident light frequency ω_L, but also with frequencies $\omega_L \pm \omega_s$, an effect of the modulation of the polarizability by the vibration of the atoms.

The classical description of an oscillating dipole is based on the electromagnetic field produced by an accelerated charge. Exploiting Maxwell's equation it is possible to express intensity of the radiation emitted by the dipole moment $\Delta\mu$ in the solid angle $d\Omega = \sin\theta d\theta d\phi$:

$$dI(t) = \frac{d\Omega}{4\pi c^3} \sin^2\theta |\ddot{\mu(t)}|^2 \tag{2.104}$$

Integrating over θ and ϕ and neglecting the cross terms it is possible to write the following expression for the intensity:

$$I(t) = AE_0^2 \left[k_0^2 \cos^2\omega_L t + k_1^2 \cos^2(\omega_L - \omega_s)t + k_2^2 \cos^2(\omega_L + \omega_s)t\right] \tag{2.105}$$

Coefficients k_i^2 have the following form:

$$k_0^2 = \alpha_0^2\ \omega_L^4 \tag{2.106}$$

$$k_1^0 = \frac{1}{4}\left(\frac{\partial\alpha}{\partial Q}\right)_0^2 Q_0^2\,(\omega_L - \omega_s)^4 \tag{2.107}$$

$$k_2^2 = \frac{1}{4}\left(\frac{\partial\alpha}{\partial Q}\right)_0^2 Q_0^2\,(\omega_L + \omega_s)^4 \tag{2.108}$$

The scattered light is expected to have peaks at frequencies ω_L and $\omega_L \pm \omega_s$. This can be demonstrated considering the Fourier's transform of the dipole moment, i.e. the power spectrum:

$$P(\omega) = \pi AE_0^2 \left\{k_0^2\delta\,(\omega - \omega_L) + k_1^2\delta\,[\omega - (\omega_L - \omega_s)] + k_2^2\delta\,[\omega - (\omega_L + \omega_s)]\right\} \tag{2.109}$$

The three terms in this equation are associated with specific features. The first one is the power scattered per unit solid angle at frequency ω_L of the incident radiation, i.e. elastic scattering (or *Rayleigh* scattering). The second and third terms are instead related to inelastic scattering (or *Raman* scattering), which is the scattering event at $\omega_L - \omega_s$, i.e. *Stokes* frequency, or $\omega_L + \omega_s$, i.e. *anti-Stokes* frequency. Since each term is proportional to k_i^2, in turn proportional to the square of the derivative of polarizability, if such derivative is zero Stokes and anti-Stokes peaks disappear for the specific normal mode. This particular feature is referred to as *Raman selection rules*.

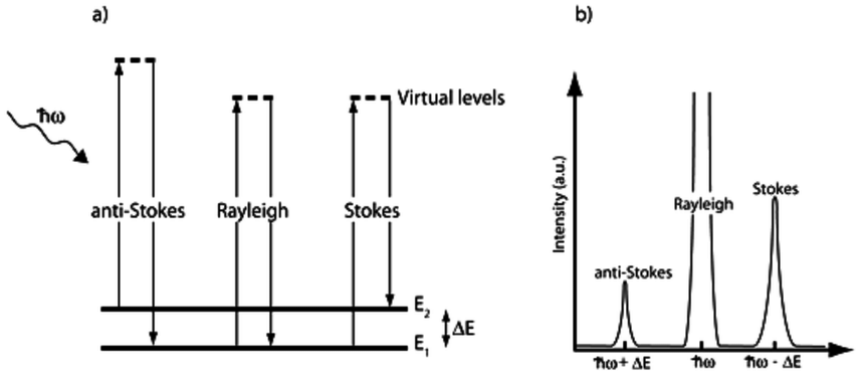

Figure 2.1. Schematic representation of the Raman process. On the left, virtual energy levels occupied by excited molecules of the sample upon interaction with incoming photon of energy $E = \hbar\omega$, where ω is the frequency of the laser; on the right, resulting Raman spectrum, with Stokes, anti-Stokes and Rayleigh lines [70].

Stokes and anti-Stokes lines are correctly predicted by the classical theory of radiation, but their

intensity ratio represents a problem. Indeed, using the equations above, it is possible to obtain:

$$\frac{I_S}{I_{aS}} = \frac{(\omega_L - \omega_s)^4}{(\omega_L + \omega_s)^4} \leq 1 \tag{2.110}$$

which is in contrast with experimental results that highlight much more intense Stokes peaks. The correction is provided exploiting a quantum theory approach in the analysis of Raman effect.
Since in general the direction of the induced dipole moment is not coincident with the electric field of the radiation, it should be used a vectorial relation, being the polarizability a second-rank tensor. For a given normal coordinate of vibration Q_s the related change in the polarizability component can be expressed as:

$$\Delta\alpha_{\rho\sigma,s} = \alpha_{\rho\sigma,s} Q_s = \left(\frac{\partial \alpha_{\rho\sigma}}{\partial Q_s}\right)_0 Q_s \tag{2.111}$$

Therefore, the normal mode associated to Q_s will appear in the obtained Raman spectrum if and only if at least one of the six components $\alpha_{\rho\sigma,s}$ is not zero. If this condition is satisfied, then the normal mode is said to be Raman *active*. In general, a normal mode may be detected depending on the configuration at equilibrium of the analyzed structure and on the symmetry of its normal modes Q_s. When the structure is known a-priori it is possible to predict the number of Raman active modes for each symmetry configuration.

Quantum theory of Raman scattering

The scattering process of the incident light involves the interaction of photons and matter (i.e. phonons). When the collision is elastic, no energy is lost in the process, while inelastic scattering makes the photon lose or gain one or more quanta of vibrational energy, producing Stokes or anti-Stokes lines respectively. Different orders of scattering are possible, and thus in first-order scattering only one phonon is involved, two in second-order scattering and so on. Let (ω_L, k_L) be the frequency and wavevector of the incident photon, (ω_{sc}, k_{sc}) the scattered photon and (w_j, q) the optical phonon participating in the scattering process indicated with $s = (q, j)$. If the collision is elastic the relation between these quantities are:

$$\omega_L = \omega_{sc} \tag{2.112}$$

$$k_L = k_{sc} \tag{2.113}$$

On the other hand, for inelastic collision:

$$\omega_L = \omega_{sc} \pm \omega_j(q) \tag{2.114}$$

$$k_l = k_{sc} \pm q \tag{2.115}$$

These equations explain that in the case of Stokes process a phonon is created, conversely in the anti-Stokes process a phonon is annihilated. Moreover, $\omega_L \gg \omega_s = \omega_j$, and thus $\omega_L \cong \omega_{sc}$ and $k_l \cong k_{sc}$. As a consequence it can be demonstrated that in the case of first-order Raman scattering only the optical modes having wavenumber $q \cong 0$ can be excited. The interaction of the incoming radiation, i.e. a photon with energy $E_L = \hbar\omega_L$ with the crystalline structure of the analyzed sample produces a perturbation of the electronic wavefunctions, since the electrons are light enough to be able to follow the variating electric field of the photon. Therefore, it is possible to model this

behavior by a non stationary state with higher energy in which the system is excited. This high energy level is called *virtual*, as it has nothing in common with the standard energy level of a crystal, it solely provides a useful way to describe the perturbation process. Only in the case of *resonant* Raman scattering the virtual state is a real state of the system, and for that the signal produced in the spectrum will be much more intense. The non-stationary nature of the virtual level forces the photon to leave it, and after that the system returns to a lower energy state. If the energy of this final level is equal to the energy of the level assumed before the perturbation, then an elastic scattering has occurred. On the other hand inelastic scattering causes the system to return in a lower or higher energy state. This event is much less probable with respect to elastic scattering. In the first case, i.e. $E_f > E_i$, the photon loses part of its energy to the system. Following energy conservation principle, the excess energy has to be conserved, and thus a phonon of energy $\hbar\omega_L - \hbar\omega_{sc} = \hbar\omega_j$ is created. If instead $E_f < E_i$, the photon gains some energy from the system. This is possible only if the system is in an excited vibrational state before the interaction with the photon, and a phonon is annihilated in the process. The correct assessment of the ratio between Stokes and anti-Stokes lines is therefore possible: the probability for the system to be in an excited vibrational state is very low. Thus, interaction with a photon is much more likely to produce Rayleigh or Stokes lines. Indeed, according to Bose-Einstein statistics, the population of the ground vibrational level is higher than that of the excited ones, and thus the ratio of the intensities is much different from (2.110):

$$\frac{I_S}{I_{aS}} \propto \left(\frac{\omega_L - \omega_s}{\omega_L + \omega_s}\right)^4 \exp\left(\frac{\hbar\omega_s}{k_B T}\right) \tag{2.116}$$

that is in fact much larger than one.

2.5 Surface Enhanced Raman Spectroscopy (SERS)

Surface Enhanced Raman Scattering (SERS) is a peculiar phenomenon consisting in an intensification of the Raman signal, observed for molecules interacting with metallic substrates, e.g. Ag and Au. It is possible to relate the SERS signal with the Raman one. Let P_{Raman} be the Raman signal generated by a sample:

$$P_{Raman} = KN\sigma_k I \tag{2.117}$$

measured in [photons/s]. The K parameter accounts for the fraction of photons collected correctly by the measurement apparatus, N is the number of illuminated molecules, σ_k is the Raman cross-section of the k-th mode integrated over the bandwidth and over all emission directions, and I is the laser intensity impinging on the sample. The relation existing between Raman and SERS scattered powers is the following:

$$P_{SERS} = G_{SERS} \cdot P_{Raman} = G_{SERS}^{Em} \cdot G_{SERS}^{Chem} \cdot P_{Raman} \tag{2.118}$$

here the contribution to the SERS effect of two particular interactions, the electromagnetic and the chemical one, is highlighted. The generic term G_{SERS} represents the global effect that the metallic surface gives to the system. The increase in the sensitivity of the measurement can be explained by considering two contributions: electromagnetic and chemical. In the first case there is

an intensification of the electromagnetic field experienced by the sample, while in the second case we have a contribution arising from the chemical interaction, i.e. formation of a bond or Van der Waals interaction, between the substrate and the sample.

2.5.1 Electromagnetic enhancement

The electromagnetic enhancement is due to mainly two contributions. The first one, is the local field enhancement. It involves the excitation of surface plasmons, that causes a strong localization and thus amplification of the incoming electromagnetic radiation in small spatial regions on the substrate. The electromagnetic field experienced in such *hot spots* is much stronger with respect to the same field experienced in the isolated case. The second contribution is instead caused by a re-radiation effect, that increases the efficiency with which the molecule radiates Raman power, since the oscillating dipole is influenced by the environment surrounding the sample.
A simplified approach can be used to describe the overall effect caused by a nanoparticle of diameter d at a distance r from an hypothetical molecule. An induced dipole can be produced in the substrate when the frequency of the oscillation of the electronic density of the surface matches the frequency of the electric field of the incident radiation. The resonance frequency depends, under the hypothesis of Rayleigh limit, i.e. $r/\lambda \leq 0.05$, on the shape, size and nature of the substrate and on the dielectric constant of the surrounding medium. The experienced electric field in a generic point in space at a distance d from the surface is given by:

$$E' = E_0 + E_{SP} \tag{2.119}$$

where E_0 is the incident electric field and E_{SP} is the field generated by the oscillating dipole. Considering the complex dielectric constant of the substrate, ε and ε_0 the dielectric constant of the surrounding medium, it is possible to write an expression for E_{SP}:

$$E_{SP} = \frac{\varepsilon - \varepsilon_0}{\varepsilon + 2\varepsilon_0} \left(\frac{r}{r+d}\right)^3 E_0 \tag{2.120}$$

and tends towards infinity as $Re(\varepsilon) \to -2\varepsilon_0$ and $Im(\varepsilon \to 0)$. The enhancement factor can be estimated assuming $E_{SP} \gg E_0$:

$$A(\omega) = \frac{E_P}{E_0} \approx \frac{E_{SP}}{E_0} = \frac{\varepsilon - \varepsilon_0}{\varepsilon + 2\varepsilon_0} \left(\frac{r}{r+d}\right)^3 \tag{2.121}$$

while the enhancement factor for the incident radiation is calculated taking into account the fact that the intensity is proportional to the square modulus of the electric field:

$$G(\omega) = |A(\omega)|^2 \tag{2.122}$$

In the same way, also the Raman electromagnetic fields (Stokes, anti-Stokes) are intensified if in resonance with the substrate surface plasmons. The global enhancement becomes:

$$G^{em}_{SERS}(\omega sc) = |A(\omega_L)|^2 \cdot |A(\omega_{sc})|^2 \tag{2.123}$$

$$G^{em}_{SERS}(\omega sc) \approx \left|\frac{\varepsilon(\omega_L) - \varepsilon_0}{\varepsilon(\omega_L) + 2\varepsilon_0}\right|^2 \left|\frac{\varepsilon(\omega_{sc}) - \varepsilon_0}{\varepsilon(\omega_{sc}) + 2\varepsilon_0}\right|^2 \left(\frac{r}{r+d}\right)^{12} \tag{2.124}$$

where the two contributions are the intensification factors considered at the frequencies of the radiation and at the scattering event, respectively. Evidently, the SERS effect depend mostly on the radii of curvature of the nanoparticle, as small radii interest the surface, while larger radii cause a long-range effect. Moreover, in the case of resonance of surface plasmons with the radiation there is a strong intensification of signals of low frequency modes, since they lay closer to the resonance condition. For the same reason, high frequency modes can fall out of resonance, hence a precise control over the several parameters in the experimental setup should be performed.

2.5.2 Chemical enhancement

Chemical enhancement has a much lower impact with respect to electromagnetic one. Nonetheless, it has important effects on the final pattern of the spectrum, since it influences Raman shifts and intensities ratios. In a first approximation, chemical enhancement depends on the type of chemical interaction that is formed between the substrate and the sample. Two main modes are highlighted: physical interaction, involving Van der Waals forces, and chemical interaction, involving the formation of a bond between the substrate and the molecule. In both these situations the electronic and geometrical structure of the molecule is altered, and thus in general the Raman cross-section will be different with respect to the isolated molecule case. It is possible to define the chemical enhancement as:

$$G_{SERS}^{chem} = \frac{\sigma_k^{ads}}{\sigma_k^{free}} \tag{2.125}$$

where σ_k^{ads} and σ_k^{free} represent the different cross sections of the k-th vibrational mode for chemical and physical interaction respectively. Also in this case there are two main contributions for the overall enhancement: non-resonant chemical effects and resonant charge transfer chemical effect. In the former, the interaction between the substrate and the molecule is non-resonant, i.e. there isn't a formation of a new electronic state, since the molecular orbitals are not close enough to the Fermi level of the metal substrate. However, such interaction may cause significant modifications in the geometry and in the electronic structure of the sample, leading to a modification in the spectra. The resonant charge transfer effect is involved whence the substrate-molecule interaction causes the formation of a *charge-transfer* state. If the electromagnetic radiation is in resonance with this state, some of the Raman modes can experience a strong enhancement, particularly those coupled with the allowed electronic transitions (i.e. resonant Raman scattering). A further cause for the chemical enhancement may be a *transient* charge-transfer effect, due to a temporary transfer of an electron between substrate and sample.
The theoretical description of the chemical enhancement is based on two different approaches. The first is a computational approach, and it is based on DFT calculations. The second one is instead a modeling approach, that proved to be successful in the description of the resonant enhancement, and will be briefly discussed.
Considering a molecule attached to a metallic substrate, if the frontier orbitals of such molecule lay close to the Fermi level of the metal, then a new electronic state may be formed, with a charge transfer. The transfer may be directed both ways, and for simplicity the metal to molecule case

will be considered. The SERS signal of the k-th vibrational mode, i.e. Q_k, can be written as:

$$P_{SERS}\left(Q_k\right) \propto \left| \frac{\mu_{KI}\mu_{FK}h_{IF}\left\langle i\right| Q_k \left|f\right\rangle}{\left[\left(\varepsilon'(\omega)+2\varepsilon_d\right)^2+\varepsilon''(\omega)^2\right]\left(\omega_{IK}^2-\omega^2+\gamma_{IK}^2\right)\left(\omega_{FK}^2-\omega^2+\gamma_{FK}^2\right)} \right|^2 \tag{2.126}$$

where the numerator is responsible for the *surface selection rules*, i.e. those vibrational modes that are to be enhanced. The subscripts $I,\ K,\ F$ indicate the ground and excited states of the molecule and the Fermi level of the substrate, respectively. The transition dipole moments are represented by μ_i. On the other hand the denominator describes the relative contribution of the plasmonic, intramolecular and charge transfer resonances to the intensity of the considered normal mode Q_k. It is composed by three factors: the first one represent the plasmonic resonance, in which ε' and ε'' are the real and imaginary part of the dielectric constant of the metal, and ε_d, real for hypothesis, is the dielectric constant of the medium. The second factor is the intramolecular resonance, featuring the transition frequency between ground state and one of the excited states localized on the molecule. The third factor is the contribution of the charge transfer state, with ω_{FK} being the transition frequency between the Fermi state and one of the excited states.
Finally, a specification regarding the aim of this work: the investigated enhancement effect is the chemical one. The electromagnetic enhancement effect will not be taken into consideration.

Chapter 3

Optimization of computational setup and analysis of Hydrogen-polyynes

3.1 Introduction

The main focus of this thesis is the simulation of the interaction between different types of CAWs, such as hydrogen-polyynes, cyano-polyynes and methyl-polyynes, with a silver nanoparticle of different dimension. The aim is to model the SERS effect, focusing on the chemical enhancement of the Raman signal. The choice of hydrogen-polyynes as benchmark for the optimization setup is mainly due to the fact that these carbon atom wires are the most studied from both the computational and experimental point of view. Furthermore, they are the polyynes having the simplest and minimal chemical structure.

The optimization of the computational setup, as well as the analysis of the results obtained from the investigation of hydrogen-terminated polyynes interacting with silver nanoparticles will be presented in this chapter. The geometry used for the metallic clusters is the result of an optimization performed in vacuum.

Such optimization is needed since different parameters may influence the results. Indeed, due to the diverse variables governing the calculations (basis-sets, functionals, and others) the results may vary one from another. As explained in the previous chapter (see section 2.3.3, section 2.3.4, and section 2.2) these parameters may be more or less suitable in the description of a generic system, and the results may be more or less precise and consistent accordingly, in particular when subtle physicochemical effects are present. Moreover, the time to perform such computations can also become an important factor to consider, as different combinations of basis-sets and functionals can greatly speed up or slow down the process.

Basis-sets featuring different characteristics have been tested, as well as different functionals. Fur-

thermore, also dispersion corrections (discussed in 2.3.5) have been considered. The benchmarking of the performances of either one or the other parameter has been done on the basis of analyses and comparisons of the various predicted spectra and interaction energies, for different systems.
Once the optimal setup has been chosen, the analysis of hydrogen-polyynes has been carried out, with the aim of investigating the features appearing in the spectra. In particular, a low frequency mode appears in the spectra of systems featuring the interaction of the polyynes with a metallic cluster. Therefore, a deepen analysis on the nature of the interaction between the cluster and the chain has to be performed, to try to assess a cause for the peculiar features measured in the spectra. Thus, the role of the size of the nanoparticles and length of the polyyne has been investigated. Also, the presence and direction of a possible charge transfer (see 2.5.2) has been addressed.

3.2 Optimization of computational setup

3.2.1 Choice of basis-set

The basis-sets that have been analyzed are the well known *cc-pVTZ*, the *AUG-cc-pVTZ* and the *6-311++G(d,p)*. The first one proved to be a very good compromise between accuracy and computational time for the simulation of Raman spectra of polyynes. The second basis-set is instead an augmented version of the first one, meaning it incorporates diffuse functions, useful when describing larger and more complex systems due to their ability in the evaluation of inter-molecular and intra-molecular long-range interactions. The choice of 6-311++G(d,p) is based on the fact that is a smaller basis-set with respect to the cc-pVTZ, but on the opposite side, it features diffuse functions.
The investigated systems are, as said, hydrogen-polyynes, of different lengths, i.e. $4, 8$ atoms (denoted as HC_4H and HC_8H), interacting with Silver nanoparticles of different size, i.e. $4, 8$ atoms (denoted as Ag_4 and Ag_8). The test batches were formed by same-length polyynes interacting with different sized clusters, and different length polyynes interacting with cluster of the same size. To be able to differentiate the influence of this parameter, the same functional, PBE0, has been used. In Figs. 3.1, 3.2 the spectra obtained for the first batch are shown. It can be observed that the peaks of the different spectra have the same shape, and also are positioned at almost the same frequency.
In the same way, the second batch highlights the same behavior: the shape and position is the same for all the basis-sets. In Fig 3.3 the AUG-cc-pVTZ spectra is not present, due to problems in computations: the energy calculated for the system failed to reach a convergent value, thus no stable configuration was found for the specific system. The problem was probably related to known SCF difficulties to reach convergence when using diffuse functions in the analysis of conjugated systems. A further analysis was performed on the interaction energies, defined with the following relationship:

$$E_{INT} = E_{dimer} - (E_{chain} + E_{cluster}) \tag{3.1}$$

where E_{dimer} is the energy of the complex formed by the Silver cluster and the CAW, while E_{chain} and $E_{cluster}$ are the energies of the hydrogen-polyyne and cluster respectively.

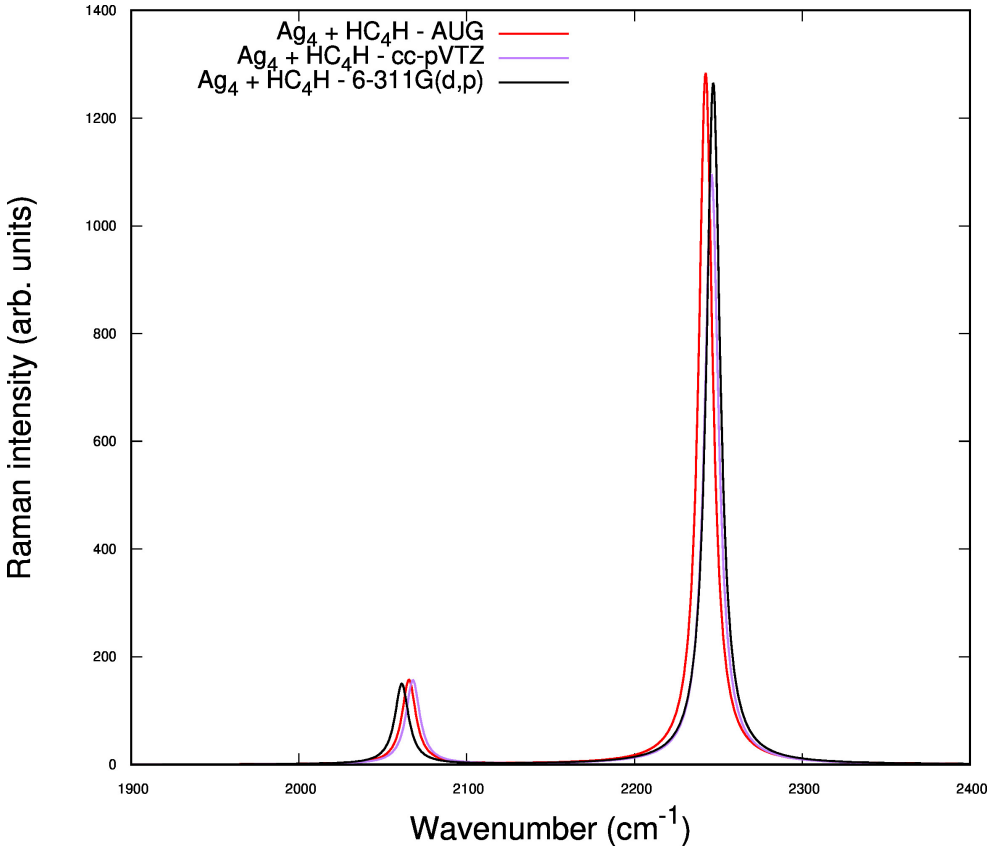

Figure 3.1. Effect of the basis-set on the spectra of system $Ag_4 + HC_4H$

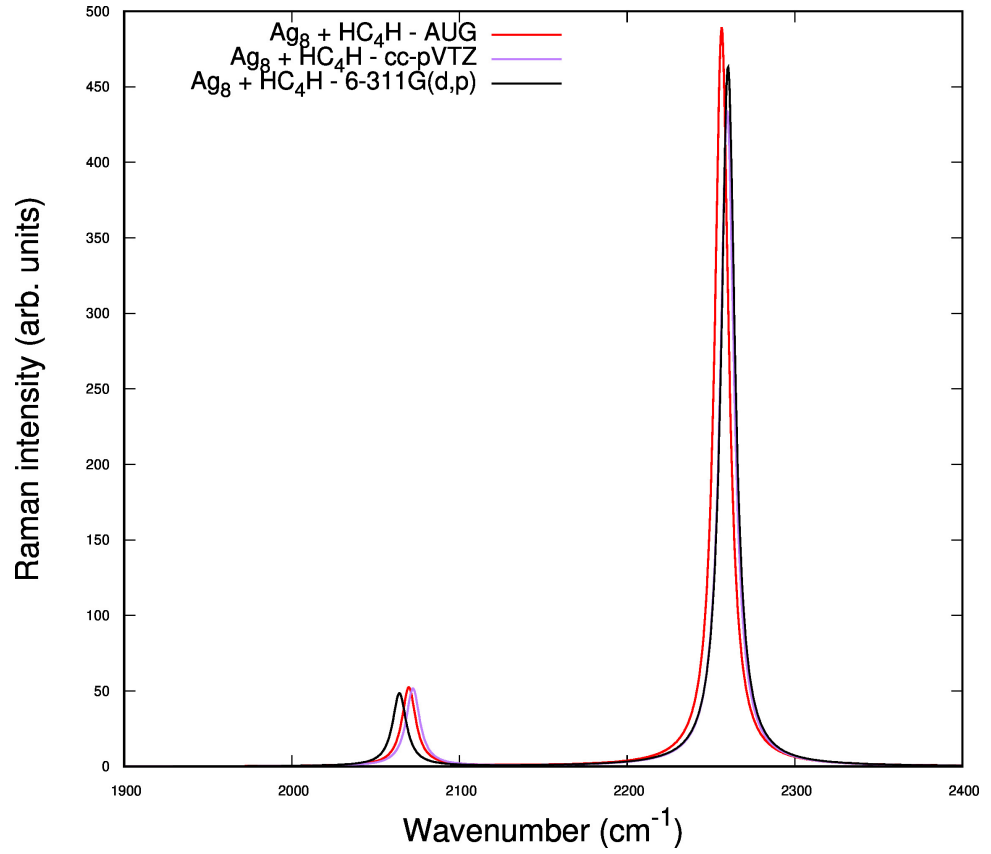

Figure 3.2. Effect of the basis-set on the spectra of system $Ag_8 + HC_4H$

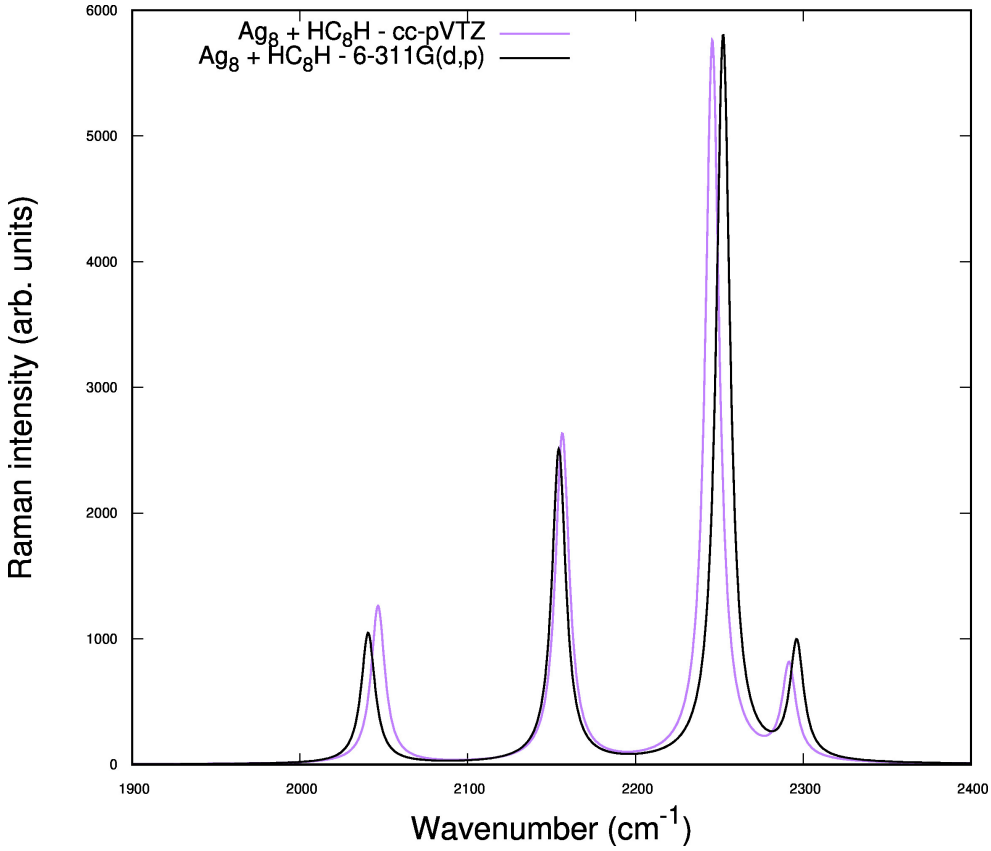

Figure 3.3. Effect of the basis-set on the spectra of system $Ag_8 + HC_8H$

The obtained values, reported in table 3.1 are consistent with the use of different basis-sets; indeed, a trend was individuated and coherent for all the systems.

Systems	**AUG-cc-pVTZ**	**cc-pVTZ**	**6-311++G(d,p)**
$\mathbf{Ag_4 + HC_4H}$	-3.12	-2.85	-4.23
$\mathbf{Ag_4 + HC_8H}$	-5.34	-5.20	-6.13
$\mathbf{Ag_8 + HC_4H}$	-4.90	-4.64	-5.21
$\mathbf{Ag_8 + HC_8H}$	/	-6.03	-6.24

Table 3.1. Interaction energies, in $kcal/mol$ for different basis-sets.

Therefore, considering the spectra and interaction energies, the choice of one of the three proposed basis-sets does not seem to be crucial. Therefore, 6-311++G(d,p) has been selected. In this way, it is possible to have diffuse functions in the description of the different systems, i.e. hydrogen-polyynes, methyl-polyynes and cyano-polyynes, without having to sustain the burden of the higher complexity and computational cost of the AUG-cc-pVTZ.

3.2.2 Choice of exchange-correlation functional

In order to investigate the effect of the functional choice on the modeling of the CAW-silver nanoparticle system, the same analysis, reported in the previous section, was performed using B3LYP hybrid functional and comparing the results obtained with the PBE0 one, both briefly introduced in the previous chapter, in section 2.3.4. PBE0 has been used in previous studies (for example, see references [71–73]) giving good results in the evaluation of Raman spectra of *sp* systems featuring π conjugation. On the other hand B3LYP is widely used in DFT studies, and has given good results for a variety of systems.
In order to study the effect of the exchange-correlation functional employed, metallic clusters of $8, 16$ atoms interacting with polyynes of $4, 8$ atoms long were investigated. To have comparable results cc-pVTZ was used for both cases. The spectra obtained are summarized in Figures. 3.4, 3.5, 3.6:

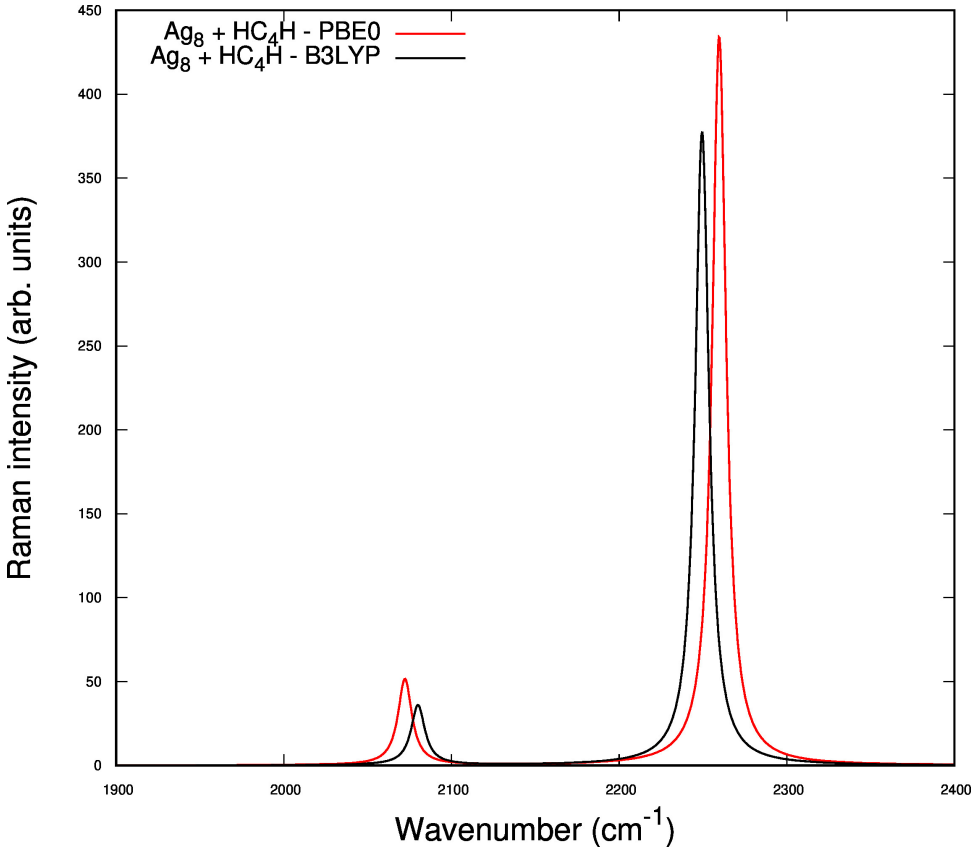

Figure 3.4. Effect of the two different functionals (PBE0 and B3LYP) for $Ag_8 + HC_4H$

From the analysis of the different spectra we can see that a general difference in the frequencies of the peaks of the two functionals. The maximum shift measured for the case of the 4 atom long polyyne is 10 cm^{-1} for the peaks with the highest intensities located at 2250 (B3LYP) and 2260 cm^{-1} (PBE0) (see Fig. 3.4). In the case of the 8 atom long polyyne the highest difference is of 23 cm^{-1} and is measured for the peaks at 2223 (B3LYP) and 2246 cm^{-1} (PBE0), those with the highest intensities, as in the previous case. For the final sample, the 4 long polyyne interacting with the cluster of 16 atoms, the maximum shift is of 20 cm^{-1} and still measured for the peaks with the highest intensity (at 2249 and 2269 cm^{-1}). It is noticeable that the differences are more evident in the case of $Ag_8 + HC_8H$, which is not a case, since probably PBE0 overestimates π conjugation

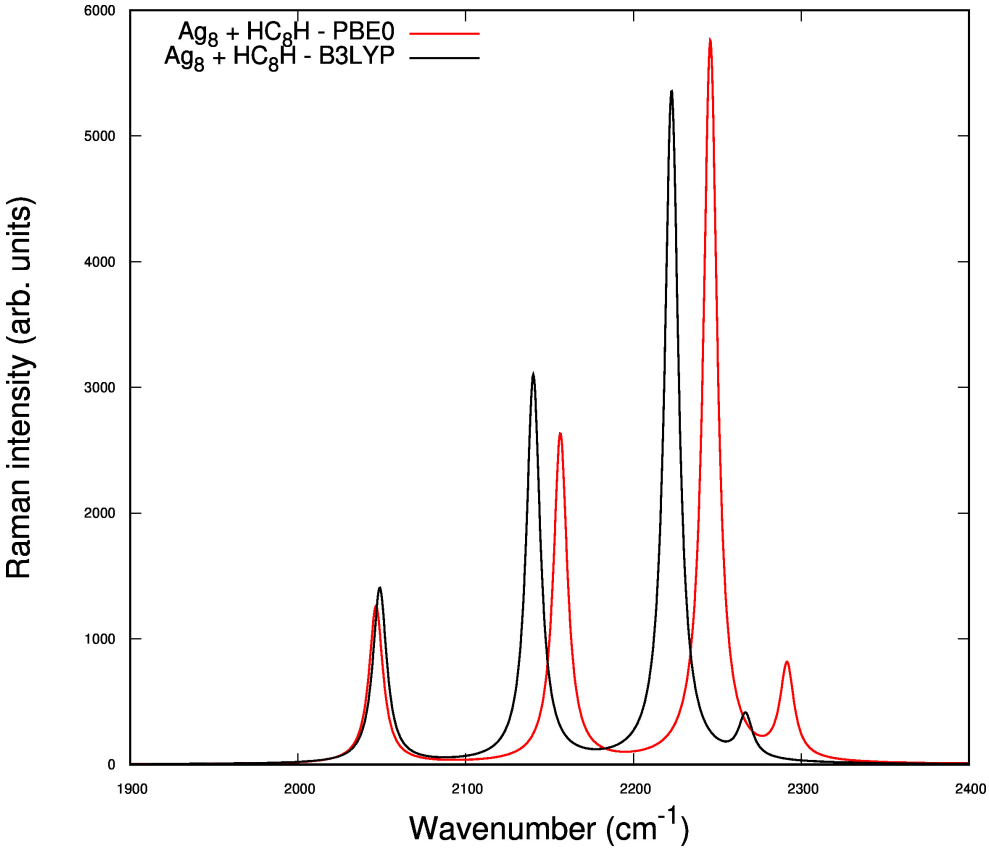

Figure 3.5. Effect of the two different functionals (PBE0 and B3LYP) for $Ag_8 + HC_8H$

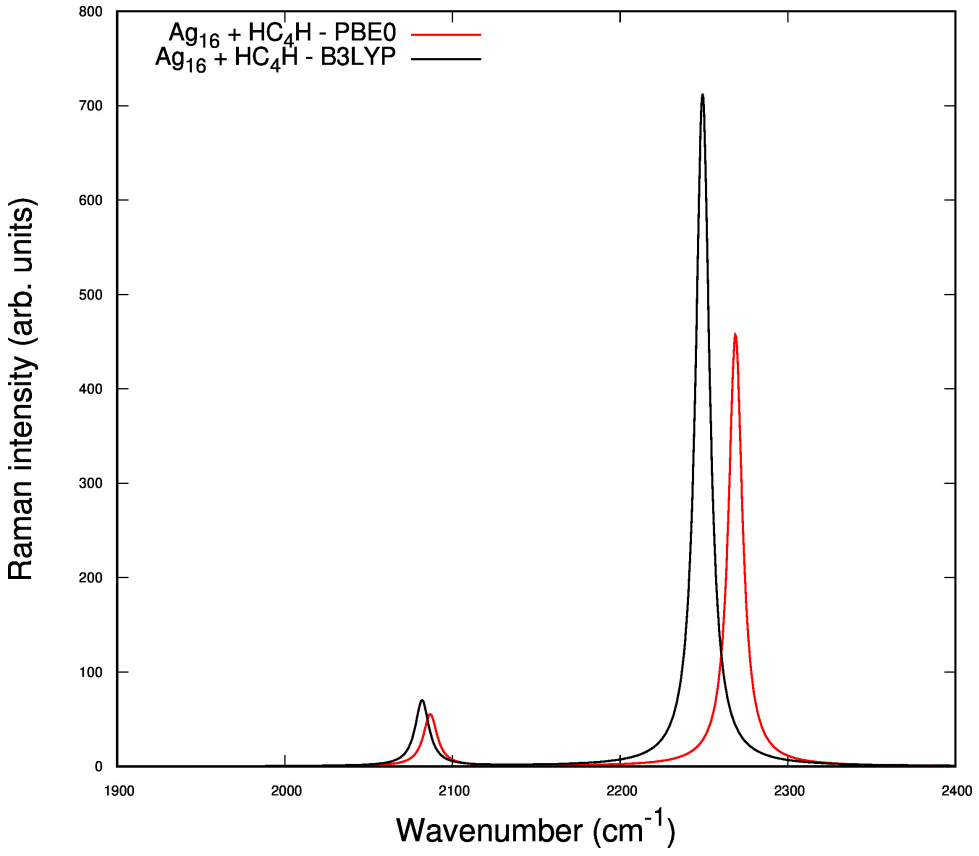

Figure 3.6. Effect of the two different functionals (PBE0 and B3LYP) for $Ag_{16} + HC_4H$

with respect to B3LYP (which in turns underestimates it). In the case of $Ag_{16} + HC_4H$ (Fig. 3.6) the shift of the peaks at 2249 and 2269 cm^{-1} is smaller with respect to the $Ag_8 + HC_8H$ system and similar to $Ag_8 + HC_4H$, plus the relative distance of the two peaks is lower for the B3LYP functional (167 cm^{-1} versus 187 cm^{-1} for PBE0), thus confirming the fact that the conjugation of the chain causes discrepancies in the results yielded by the two functionals. Similarly to the case of the basis-sets, also for functionals interaction energies were considered in the comparisons. In table 3.2 the different energies are reported:

Systems	**PBE0**	**B3LYP**
$\mathbf{Ag_8 + HC_4H}$	-5.20	-2.05
$\mathbf{Ag_8 + HC_8H}$	-6.03	-2.54
$\mathbf{Ag_{16} + HC_4H}$	-4.51	-2.06

Table 3.2. Interaction energies, in $kcal/mol$ for different functionals.

There is a significant discrepancy between the predicted values, but this is expected, due to the differences of the two functionals in the estimation of the exchange-correlation energy. Specifically, the B3LYP functional predicts a much more waker interaction with respect to PBE0. However it is possible to see that a trend develops and is similar for each column: the energy of the shorter polyyne is lower with respect to the longer one. The physical meaning and a more in depth analysis will be discussed later on. The differences observed in the spectra and in the interaction energies may originate from the characteristics of the functionals, especially considering their different mathematical definition. Considering that the overall shape of the spectra and the trend identified in the interaction energies, the choice of the functional seems to not alter significantly the results. Therefore PBE0 was selected, also considering the satisfying results obtained in the previously mentioned studies, where this functional was used to investigate *sp* hybridized systems (and in particular their Raman spectra).

3.2.3 Long range interactions and dispersion corrections

The effect of intermolecular Van der Waals interactions (see section 2.3.5) has been considered. As discussed in the previous chapter, one of the problems that affects DFT based calculations is the poor evaluation of interactions of weak magnitude, such as Van der Waals interactions, even if wide basis-sets featuring diffuse functions are used. The assessment of the effect of dispersion corrections (GD3 corrections) has been done on a single dimer, formed by the 8 atoms-long polyyne and the silver nanoparticle with 8 atoms. Again, the analysis of the spectra and interaction energies was considered to check whether the corrections introduced any notable differences. The test were carried out using the same basis-set, i.e. cc-pVTZ, with PBE0 and B3LYP functionals, to check whether long range interactions are modeled differently using one or the other. As seen in

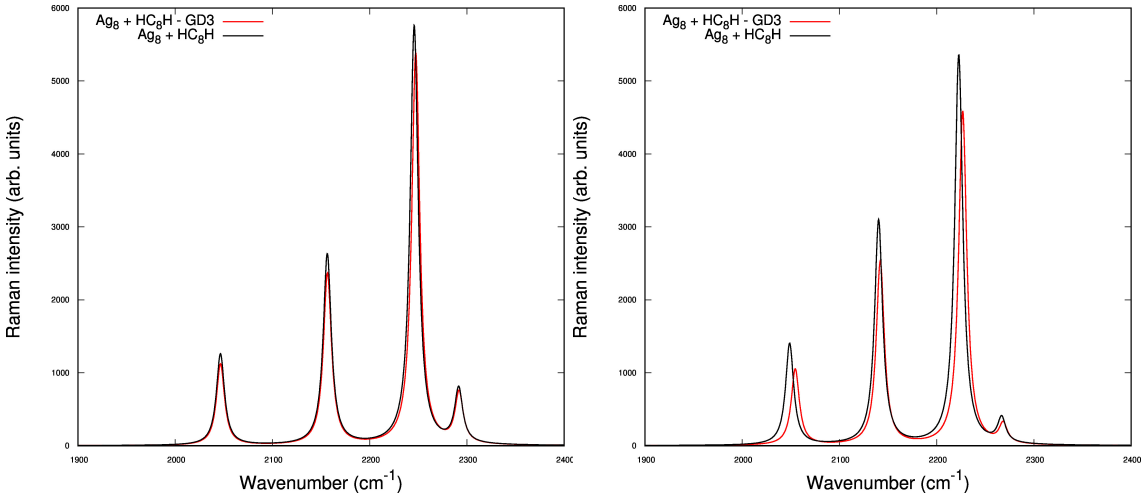

(a) (b)

Figure 3.7. Comparison between the spectra obtained with and without Grimme's GD3 correction for the case of: a) PBE0 - cc-pVTZ; b) B3LYP - cc-pVTZ. In red, the spectra obtained *with* the corrections, in black the one *without* them.

Fig. 3.7 the spectra obtained are very similar, with minor shifts of the peaks, in the order of few cm^{-1}, and the intensity ratios are consistent in both setups, for every normal mode with relevant intensities detected. A second test based on the interaction energies of the observed systems was also performed, since GD3 corrections add an additional energy term related to long range interaction both for the monomer and the dimer equilibrium energies, which may have some considerable impact on the interaction energy calculated for the system. The results reported in Table 3.3 show that a consistent difference arises in the evaluation of the interaction energies:

Systems	**GD3**	**No GD3**
PBE0	-8.25	-6.03
B3LYP	-5.05	-2.54

Table 3.3. Effect on the interaction energies of Grimme's corrections. The values are in $kcal/mol$.

Nonetheless, the magnitude of such difference is consistent, and, between 1.5 and 2.2 $kcal/mol$. Considering this result, the shape of the spectra, and the additional computational resources needed for the evaluation of the dispersion interaction GD3 corrections have not been added to the final computational setup.

3.3 Analysis of Hydrogen polyynes

In the previous section the process that led to the choice of parameters for the computational setup has been described. The selected basis-set was 6-311++G(d,p), and PBE0 the exchange-correlation functional. With such setup the analysis of different samples has been performed, and in this section the results obtained for hydrogen-polyynes interacting with different silver clusters will be discussed. The systems investigated are the same used in the optimization setup, i.e. a silver nanoparticle of different size, $4, 8$ atoms, and hydrogen-polyynes of different length, $4, 8$ atoms long. The interaction energies and spectra have been analyzed to assess the role of the size of the cluster and the length of the chain on the results. Finally, an analysis of the charge transfer effect and its dependence on the length of chain will be presented.

3.3.1 Interaction energies and SERS spectra

The influence of chain length and size of the cluster has been investigated upon comparisons between the spectra and interaction energies obtained for the different systems. Firstly, the spectra of the hydrogen-polyynes have been analyzed, to check whether the distinctive peaks referred to *sp* carbon hybridization were correctly predicted. In Fig. 3.8 it is indeed possible to observe in both cases the ECC mode, assigned to the most intense peak, and, in the spectrum of HC_8H, it is well visible also the β mode peak, at a lower frequency. Their eigenvectors are reported in Fig. 3.9.

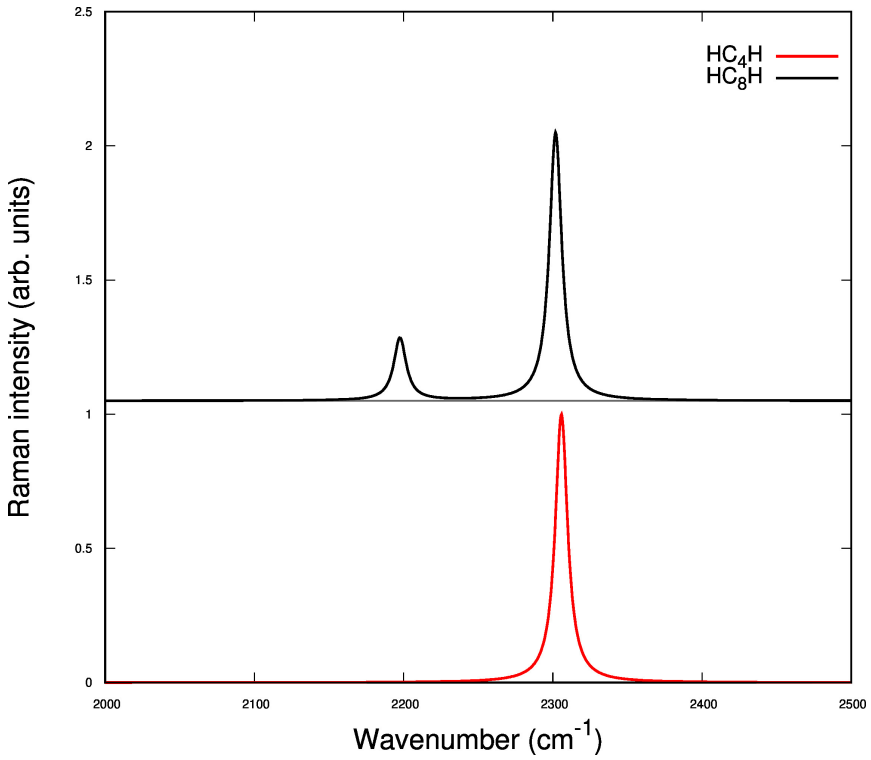

Figure 3.8. Normalized spectra for isolated hydrogn-polyynes.

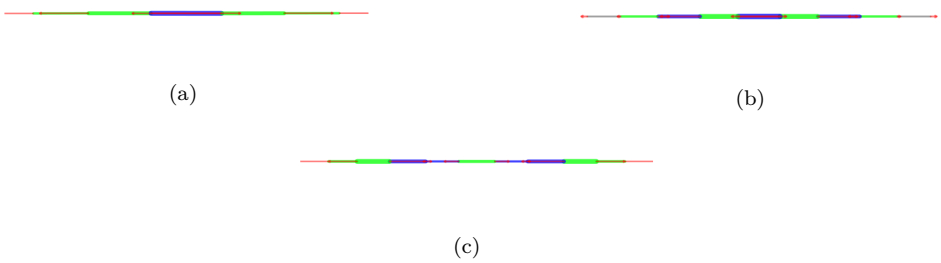

(a) (b)

(c)

Figure 3.9. Eigenvector of the two hydrogen-polyynes: a) ECC mode of HC_4H, at 2306 cm^{-1}; b) ECC mode of HC_8H, at 2302 cm^{-1}; β mode of HC_8H, at 2198 cm^{-1}.

The analysis of the interaction energies (see table 3.4) suggest that the interaction is stronger with increasing size of the cluster and increasing length of the linear carbon chain. If the size of the cluster is fixed, i.e. considering the effect of the length of the chain, a difference of 1.8 $kcal/mol$ between $Ag_4 + HC_4H$ and $Ag_4 + HC_8H$ is measured. For the other two systems, i.e. $Ag_8 + HC_4H$ and $Ag_8 + HC_8H$ the gap reduces to 1.23 $kcal/mol$. On the other hand, if the length of the chain is fixed, it is possible to highlight the effect of the size of the cluster: for the systems $Ag_4 + HC_4H$ and $Ag_8 + HC_4H$ the difference in the interaction energies is of $2.2 kcal/mol$; for $Ag_4 + HC_8H$ and $Ag_8 + HC_8H$ systems such difference decreases to 1.43 $kcal/mol$. In both cases, i.e. for fixed size of the cluster and then for fixed length of the chain, the difference between the interaction energies of the considered systems is reducing ($1.8 \rightarrow 1.23$ $kcal/mol$ and $2.2 \rightarrow 1.43$ $kcal/mol$). It is therefore possible to hypothesize that such difference will reach a plateau, meaning that, at some point, the increase in the size of the cluster at fixed chain length or the increase of the chain length at fixed cluster dimensions, will not produce an appreciable increase in the interaction energies.

Cluster / **Polyyne**	**Ag_4**	**Ag_8**
HC_4H	-3.01	-5.21
HC_8H	-4.81	-6.24

Table 3.4. Predicted interaction energies, in $kcal/mol$ for hydrogen-polyynes interacting with silver nanoparticles.

Another result obtained form this evaluation is that the system with the longest chain and biggest cluster is the most stable. This can be explained by the presence of a higher number of molecular orbitals available for the interaction between the cluster and the chain. The optimized geometry, corresponding to the more stable configuration, for every system predicts the interaction of the silver cluster with the first carbon atom of the chain (as visible in Fig. 3.10).
An interesting insight is provided by the analysis of the spectra, which confirm the interaction of the chain and the cluster. In fact, a general enhancement of the signal is measured, and in addition new peaks arise due to the activation of new normal modes. To better compare the effect of the interaction between the two monomers, the spectra have been discussed separately for each length

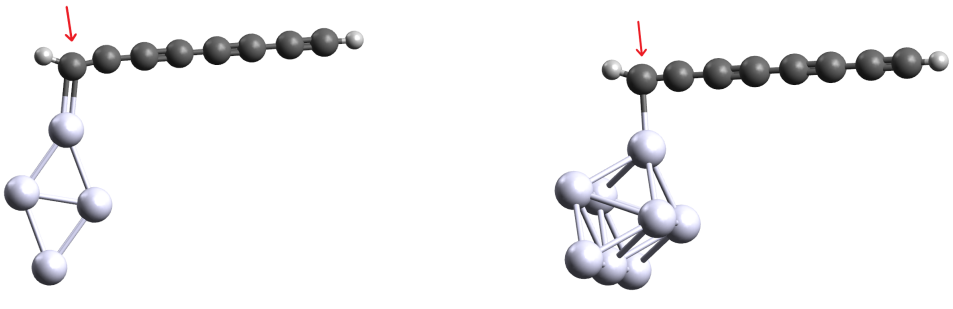

(a) (b)

Figure 3.10. Structure of the optimized systems: a) $Ag_4 + HC_8H$; b) $Ag_8 + HC_8H$. The red arrow indicates the first carbon atom of the chain. A clarification: the bonds reported in the picture may not be correct: the visualization software may render some details about the system in an approximated way, based only on the atoms' distances.

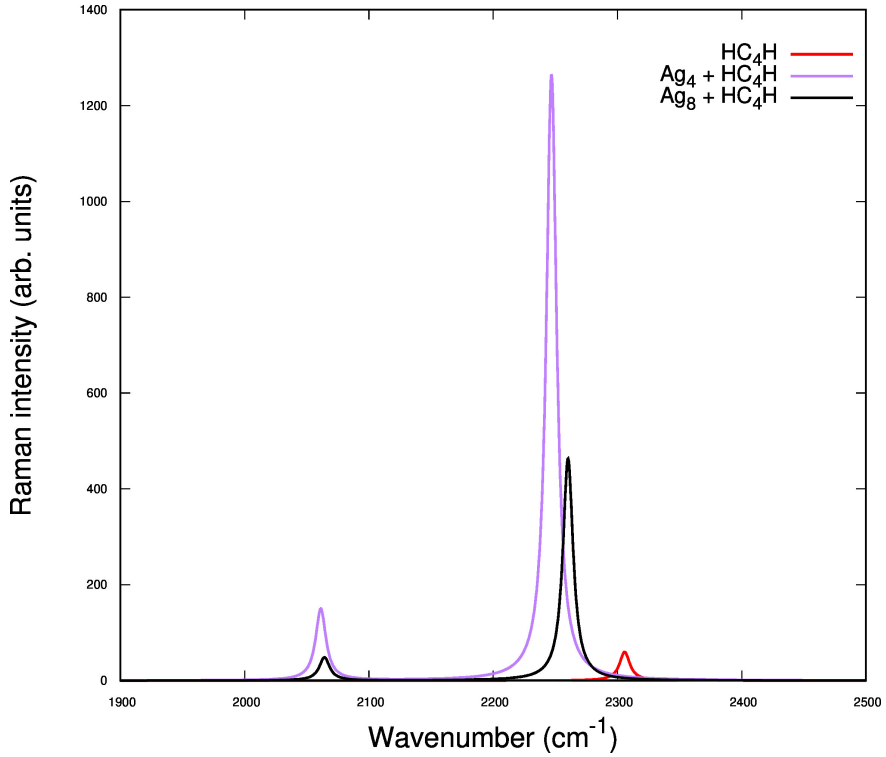

Figure 3.11. Predicted SERS spectra of systems composed by polyyne of 4 atoms long, and different sized clusters

of the linear chain (C_4 and C_8). As a starting case, Raman spectra related to the polyyne C_4 interacting with Ag_4 and Ag_8 clusters are discussed and reported in Fig 3.11. It is possible to observe a downshift of the most intense peak and the appearance of a peak at lower frequencies (at 2068 cm^{-1} for Ag_4 and 2072 cm^{-1} for Ag_8), which is not predicted for the isolated polyyne. The relative intensities of the normal modes suggest a different behavior from the one described on the basis of the interaction energies, i.e. the smaller cluster could have a more intense interaction with the polyyne. Moreover, the shift confirms the values of the intensities, as indeed the peaks of the $Ag_4 + HC_4H$ are at lower frequencies with respect to $Ag_8 + HC_4H$ (specifically, at 2246 versus 2260 cm^{-1}). The shape of the spectra suggests that the cause behind the increase in the

intensities of the signals and the redshift of the peaks is not related to the interaction energy, since the latter is higher for the system with the bigger cluster (see table 3.4). Instead, by comparing the different optimized geometries, reported in Fig. 3.12, it is possible to associate the redshift and the enhancement of the peaks to the degree of distortion of the chain caused by the interaction with the cluster. The higher distortion seems indeed caused by the smaller cluster, as visible in Figs. 3.12a and 3.12b. The newly activated normal modes, not predicted for the isolated chain, is caused in principle by the peculiar interaction with the cluster, which has also the effect of distorting the chain, which in turns loses its symmetry. A possible interpretation for the smaller distortion

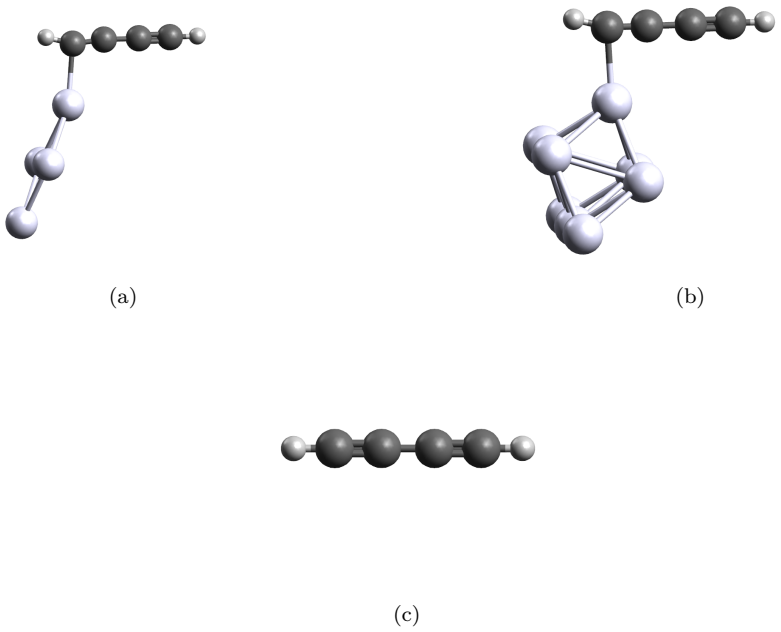

(a) (b)

(c)

Figure 3.12. Optimized geometries of: a) $Ag_4 + HC_4H$; b) $Ag_8 + HC_4H$; c) HC_4H.

induced by the bigger cluster is that the relative difference between the size of the cluster and the polyyne is too big. In this case, it has to be expected that for longer chains the deformation produced by the bigger cluster is noticeable and more evident when compared to this situation. As for the peculiar behavior of the spectra, i.e. the downshift of the peaks, a possible explanation may be the effect of the cluster on the electronic structure of the polyyne: the interaction of both nanoparticles with the chain results in a redshift of the spectra which has its main cause in the modification of the nature of the normal mode. The appearance and nature of the low frequency peak in both dimers has been investigated with the inspection of the related eigenvectors. Taking as example the case of $Ag_4 + HC_4H$, since similar considerations are possible also for $Ag_8 + HC_4H$, it is possible to observe, in Fig 3.13, a strong contribution due to the stretching of the triple bond of the two carbon atoms in the immediate vicinity of the silver cluster, with the other bonds having an opposite behavior. This suggest a strong interaction taking place between the such atoms and the cluster, causing the appearance of the associated peak at low frequencies. As for the other active mode, it resembles a modified ECC mode, further suggesting a rupture of the collective oscillation of the bonds in the isolated hydrogen-polyyne, due to its interaction with the nanoparticle. The same general considerations apply also for the case of polyyne HC_8H, even if the predicted spectra are much different. Indeed, as in the case of the shorter polyyne, new peaks appear, related to new active modes, which are produced, in same fashion of the $Ag_i + HC_4H$ systems, by the effect of the

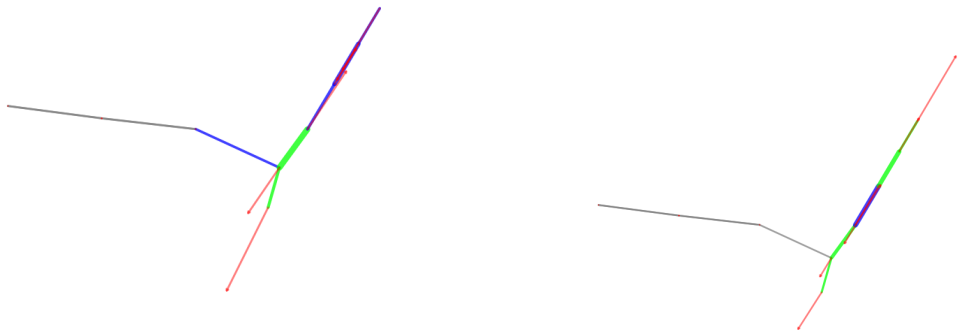

(a) 2068 cm^{-1} (b) 2246 cm^{-1}

Figure 3.13. Schematic view of the eigenvectors of $Ag_4 + HC_4H$. The cluster is positioned parallel to the view, and thus is seen as a line on the left of the chain. The frequency of the modes is indicated. The colored segments indicate a stretching (green) or compression (purple) of the specific bond while red arrows indicate the direction of the motion of the associated atom.

peculiar interaction with the cluster. Previously, the spectrum of the isolated HC_4H was showing a lone peak while now, due to the interaction with the nanoparticle, two distinct and redshifted modes are observable; a same situation is verified for the 8 atom long polyyne: the spectra of HC_8H featured two active normal modes, while the interaction with the cluster produces the activation of a total of four new modes, which are still redshifted with respect to those belonging to the isolated polyyne. The frequencies at which the peaks related to such active modes are located are: 2020, 2142, 2223, 2282 cm^{-1} for $Ag_4 + HC_8H$, and 2041, 2154, 2252, 2296 cm^{-1} for $Ag_8 + HC_8H$. The spectra for the systems $Ag_i + HC_8H$ are reported in Fig. 3.14. For these systems, the intensities of the peaks associated to the different clusters are much more similar in opposition with the HC_4H chain, indicating a similar deformation of the chain for each interacting cluster, as visible in Fig. 3.15. Similarly to the case of the shorter polyyne, also in this systems the shift of the peaks can be related to the peculiar effect of the cluster that increases the conjugation of the chain. In this regard, the values of the BLA and energy gap between the HOMO and LUMO of the molecule have been calculated for HC_8H and $Ag_8 + HC_8H$. Specifically, the BLA is calculated as the difference between the average length of the triple bonds and the average of the single bonds of the chain; the energy gap is instead calculated during the optimization process. The values reported in table 3.5 highlight the effect of the cluster in increasing the conjugation of the chain, as indeed both parameters decrease when the polyyne is interacting with the cluster. The increased conjugation can also be observed in cases (i.e. $Ag_4 + HC_8H$ and $Ag_8 + HC_8H$): the overall behavior of the spectra is similar, and a downshift is predicted. Moreover, by comparing the two plots, i.e. Fig. 3.11 and Fig. 3.14, it would seem that the shift is independent on the size of the polyyne or of the cluster, and it is then a phenomenon that is manifesting upon the interaction of the isolated polyyne with the nanoparticle. Indeed, taking into account the eigenvectors related to the peaks located at 2247 cm^{-1} for the $Ag_4 + HC_4H$ and the one located at 2228 cm^{-1} for the $Ag_4 + HC_8H$ system, it is possible to observe a similarity in the oscillation of the bonds (see Fig. 3.16). The behavior can be associated to a modification and localization of the ECC mode and it is caused again by the interaction with the cluster. Thus, the downshift of the considered normal mode is consistent for both systems. A more in depth investigation on the magnitude of this relation has

been performed, by inspecting the bond length between the first atom of the chain and the closest atom of the silver nanoparticle (see Fig. 3.10), and reported later in the discussion. The analysis of the eigenvectors confirms the nature of the low frequency band at 2020 cm^{-1} for $Ag_4 + HC_8H$ and 2042 cm^{-1} for $Ag_8 + HC_8H$: it is still related to the stretching of the triple bond of the carbon atoms in the vicinity of the cluster, as shown in Fig 3.17. The other eigenvectors (see Fig. 3.18) represent different combinations of stretching and compression of the single and triple bonds in the chain.

System	**BLA**	**Energy Gap**
$\mathbf{HC_8H}$	0.135	4.735
$\mathbf{Ag_8 + HC_8H}$	0.122	2.041

Table 3.5. Bond length alternation, in Angstroms, and energy gap, in eV for HC_8H and $Ag_8 + HC_8H$. Both parameters show decreasing values upon the interaction with the cluster.

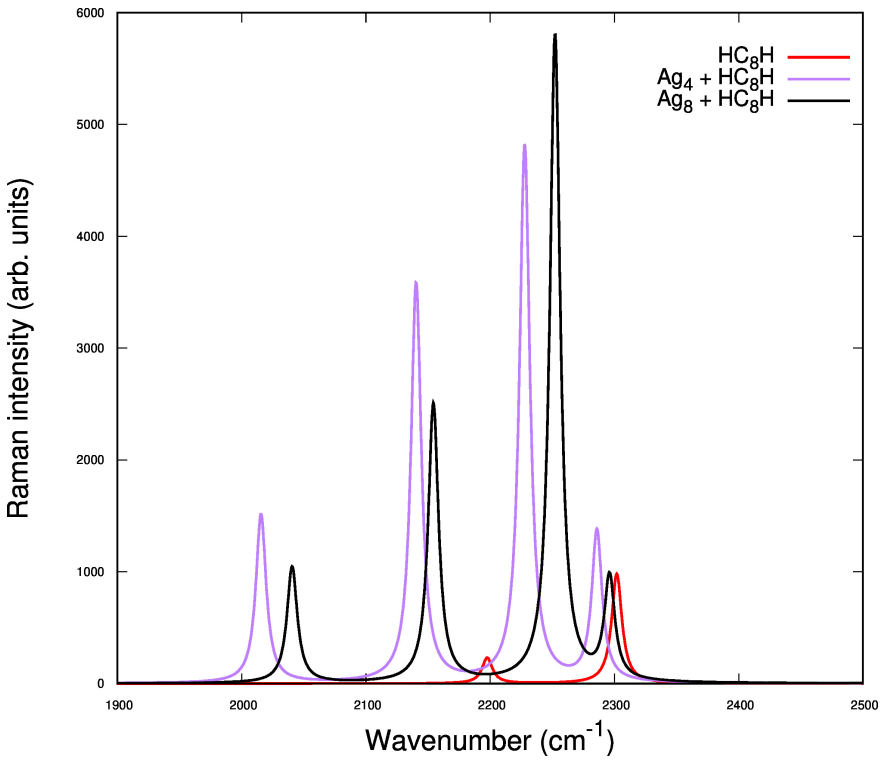

Figure 3.14. Predicted SERS spectra of systems composed by polyyne of 4 atoms long, and different sized clusters

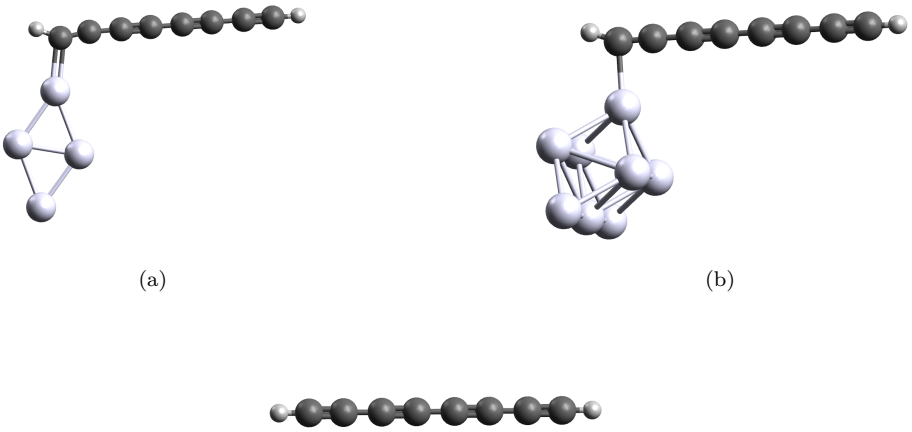

(a) (b)

(c)

Figure 3.15. Optimized geometries of: a) $Ag_4 + HC_8H$; b) $Ag_8 + HC_8H$; c) HC_8H.

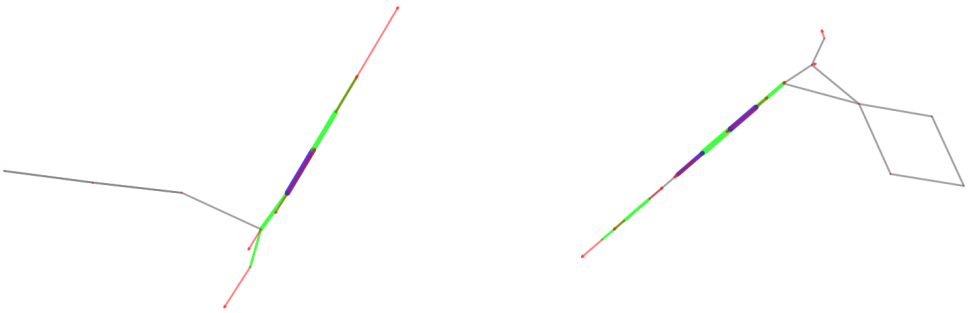

(a) (b)

Figure 3.16. Eigenvectors related to the ECC mode for: a) $Ag_4 + HC_4H$; b) $Ag_4 + HC_8H$.

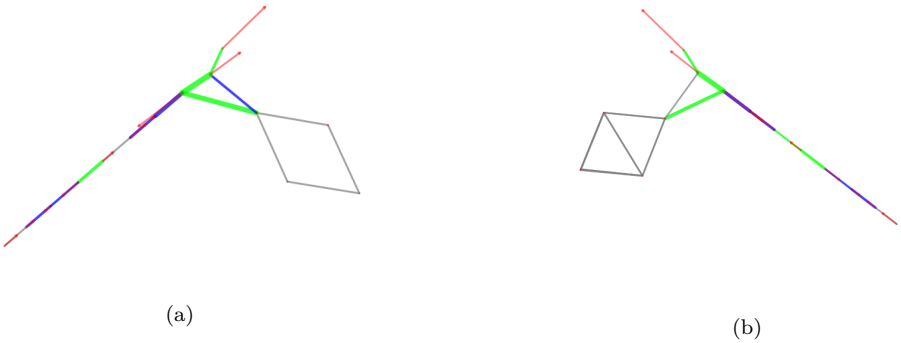

(a) (b)

Figure 3.17. Eigenvectors related to the low frequency mode for the case of: a) $Ag_4 + HC_8H$ at 2020 cm^{-1}; b) $Ag_8 + HC_8H$ at 2042 cm^{-1}.

This fact could be related to the modification of the ECC mode of the isolated chain, with a visible localization of such mode. This is more evident in the case of the longer polyyne, that has more

active normal modes, but the same also happens for the two measured for HC_4H. A possible explanation for this peculiar behavior of the ECC mode resides in the nature of the interaction of the chain with the cluster: a modification in the bonds of the various atoms, and specifically in their length and related force constant, may be the cause for the activation of different carbon-carbon stretching modes similar to ECC in different portion of the chain. In this context, it has been performed an analysis on the force constants in internal coordinates of the carbon-carbon bonds, reported later.

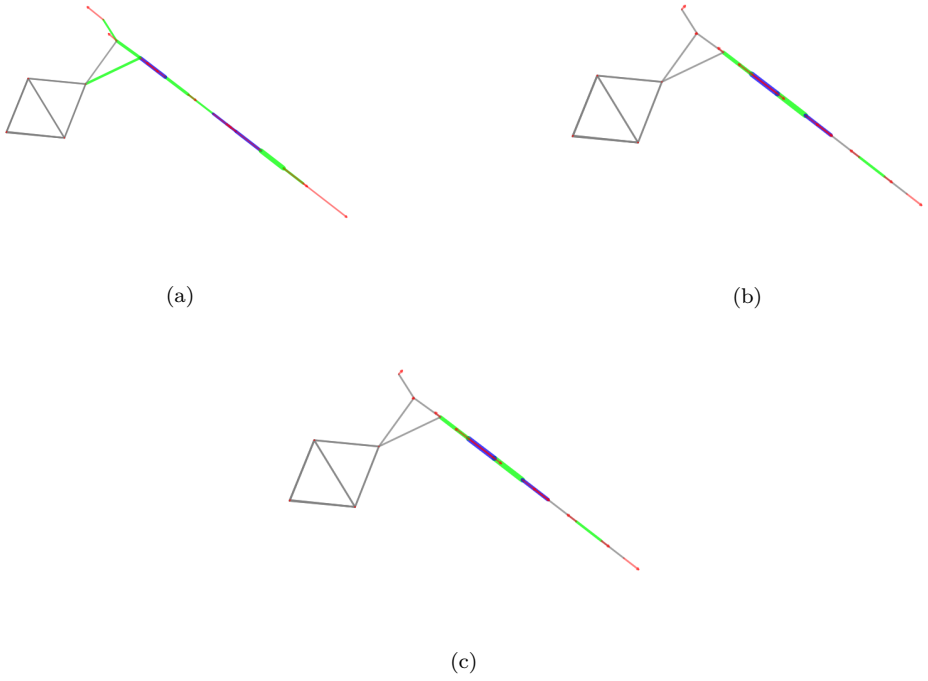

(a) (b)

(c)

Figure 3.18. Eigenvectors related to the normal modes of $Ag_8 + HC_8H$ systems, at frequencies: a) 2154 , b) 2252 , c) 2296 cm^{-1}. The same behavior is observed also for $Ag_4 + HC_8H$

As anticipated earlier, a parameter that may be of help in the interpretation of the behavior of the system is the set of the bond lengths and their associated force constants. Specifically, the force constants of the bonds of the polyyne interacting with the cluster are compared with those of the isolated polyyne. The case of $Ag_8 + HC_8H$ is taken as example, and the values are reported in table 3.6. It is possible to notice a decrease of more than a half in the bond force constant of the triple bond of the two carbon atoms in the vicinity of the cluster (and similar values are measured for all the other systems): from 16.371 to 6.3576. Such predicted values are a proof of the relevant interaction with the cluster, which is indeed the reason of the low frequencies predicted for the normal modes associated to the vibrations of the bonds involved in the interaction itself. Furthermore, a corresponding variation in the bond length of those two carbon atoms is also measured: from 1.210 Å of the isolated polyyne to 1.234 Å of the cluster and polyyne system. The calculated values of force constant and bond length are very different with respect to the same parameters of the other carbon-carbon bonds along the chain. For this reason the considered triple bond behaves as if it was an isolated bond, not participating in the collective vibration, instead oscillating on its own. Indeed, by looking at the related eigenvector reported in Fig. 3.17b it is possible to see how the vibration is highly localized on the bond between the first two atom of the chain. A general decrease in the values of the other force constants is predicted, with a related

variation of the bond lengths, which could explain the downshift of the other normal modes. This fact is mainly caused by the peculiar interaction between the chain and the cluster, which is also responsible for an increased conjugation on the chain, which is also, as explained before, influenced by the length of the polyyne. Such interplay is indeed the cause of a modification of the electronic structure of the chain, and as discussed in section 1.2.3, the mutual influence of electronic and vibrational properties is a typical phenomenon of these systems. Moreover, the conjugation may be also affected by a charge transfer between the chain and the nanoparticle.

Bond	**Bond length, with cluster**	**Bond length, isolated**	**Force constant, with cluster**	**Force constant, isolated**
$\mathbf{H-C_1}$	1.069	1.065	6.2640	6.4699
$\mathbf{C_1 \equiv C_2}$	1.234	1.210	6.3576	16.3710
$\mathbf{C_2-C_3}$	1.344	1.353	8.2858	8.0663
$\mathbf{C_3 \equiv C_4}$	1.225	1.220	14.952	15.4700
$\mathbf{C_4-C_5}$	1.340	1.345	8.4019	8.2723
$\mathbf{C_5 \equiv C_6}$	1.222	1.220	15.229	15.470
$\mathbf{C_6-C_7}$	1.351	1.353	8.1094	8.0663
$\mathbf{C_7 \equiv C_8}$	1.211	1.210	16.281	16.371
$\mathbf{C_8-H}$	1.065	1.065	6.4692	6.4699

Table 3.6. Analysis of the bond lengths and force constants for the case of the cluster and polyyne system vs isolated polyyne. The first and second atom of the chain, directly interacting with the cluster are C_1 and C_2. The values of the bond lengths are in Angstroms, while the unit of measure for the force constant are $mdyne/\text{Å}$.

In order to further quantify the interaction between carbon atoms near the cluster and the cluster itself, we decided to analyze the distance between the first two carbon atoms of the chain and the nearest silver atom. Indeed it is possible to predict an ideal Van der Waals type of interaction whence the bond length of two atoms is equal to the sum of the their Van der Waals radii:

$$L_{bond} \approx R_1^{VdW} + R_2^{VdW} \tag{3.2}$$

The Van der Waals radii of carbon and silver are 1.70 Å and 1.72 Å respectively, while the bond length we are considering are 2.262 Å for the first atom, and 2.578 Å for the second one, and thus both are much shorter that the sum of the Van der Waals radii, 3.42 Å. This could justify an interaction between the carbon atoms and the silver one that is stronger than a simple Van der Waals interaction, adding another interesting result in the investigation of the interaction occurring between the chain and the nanoparticle. For comparison, the values of such bond length obtained for all of the systems are reported in 3.7. It is possible to observe that the lowest value for the first carbon are obtained for $Ag_4 + HC_8H$ and $Ag_8 + HC_8H$, suggesting that the higher the conjugation

on the chain, the stronger the interaction with the cluster. On the other hand, the length of the bond of the second carbon atom and the cluster is lower when the cluster itself is bigger. Thus the effects that mostly influence this parameter, and therefore the interaction between the chain and the nanoparticle are the conjugation on the chain and the size of the cluster.

System	**Bond length (C_1-Ag)**	**Bond length (C_2-Ag)**
$\mathbf{Ag_4 + HC_4H}$	2.370	2.874
$\mathbf{Ag_4 + HC_8H}$	2.241	2.865
$\mathbf{Ag_8 + HC_4H}$	2.339	2.596
$\mathbf{Ag_8 + HC_8H}$	2.262	2.578

Table 3.7. Analysis of the bond lengths between the first and second carbon atom of the chain (see Fig. 3.10) and the closest silver atom belonging to the cluster. The reported values are measured in Angstroms.

It is possible to observe that the lowest value for the first carbon are obtained for $Ag_4 + HC_8H$ and $Ag_8 + HC_8H$, suggesting that the higher the conjugation on the chain, the stronger the interaction with the cluster. On the other hand, the length of the bond of the second carbon atom and the cluster is lower when the cluster itself is bigger. Thus the effects that mostly influence this parameter, and therefore the interaction between the chain and the nanoparticle are the conjugation on the chain and the size of the cluster.

3.3.2 Analysis of the charges

In order to understand if a possible charge transfer effect takes place in the interaction of the two monomer, and contributes to the effect described above, the charges associated to the polyyne and cluster were also investigated for all the studied systems. The goal is to prove whether a charge transfer exists and if so, to investigate its direction, i.e. from the cluster to the chain or the opposite. The methods used in this analysis are the well known "CHarges from ELectrostatic Potentials using a Grid-based method" (CHELPG, [74]) and "CHarges from IR Intensity parameters" (CHIRI, developed by Milani et al. [75]). The former is based on a fitting of charges based on the electrostatic potential predicted for the optimized geometry of the considered systems. The latter is based on atomic charges (IR charges) that are extracted from the computed atomic polar tensors (APT) by means of DFT ab-initio calculations. These charges can be gathered also by the polar tensors, i.e. the derivatives of the dipole with respect to the Cartesian coordinates of the atoms. Therefore, one of the advantages of this method is the correlation of charges with an experimentally measurable property. If a planar molecule is analyzed, the relationship between charge and APT components is described by the following expression:

$$q_\beta = \boldsymbol{P}_\beta^{yy} \tag{3.3}$$

Where β indicates the considered atom of the molecule, yy indicates the out-of-plane diagonal element of the APT $\boldsymbol{P_\beta}$. The definition of IR charges is unfortunately exact only for planar molecules. With a suitable set of corrective parameters, which involved the identification of a "reference" atom (which is the silver atom of the cluster closest to the chain), the calculations could be performed and approximated also for the systems investigated in this work, which are non planar (with the exception of the isolated polyynes). In table 3.8 the total charge of the silver cluster is reported using both computational methods. Due to the overall charge neutrality of the dimer, the total charge on the polyyne has the same value reported, but with opposite sign.

System	CHELPG	CHIRI
$\mathbf{Ag_4 + HC_4H}$	-0.06013	-0.08098
$\mathbf{Ag_8 + HC_4H}$	0.01979	0.02456
$\mathbf{Ag_4 + HC_8H}$	-0.04732	-0.13946
$\mathbf{Ag_8 + HC_8H}$	0.01342	-0.05568

Table 3.8. Calculated values of the charge of the silver cluster. The charge of the polyyne is the same, but with opposite sign. The reported values are in units of the electron charge, e.

The values obtained from the calculations are too small to be an actual proof of a possible charge transfer, but peculiar behaviors could be identified. The first one is a trend that highlights how the chain tends to accommodate more negative charge as the length increases for fixed dimensions of the cluster. This may be caused to the fact that there is a higher conjugation on the chain itself, and thus more orbitals available to accommodate such charge. The other interesting datum we can extract from these values is that the direction of an eventual negative charge transfer effect looks to be directed towards the cluster. There are three exceptions: CHELPG measures a positive charge for the system $Ag_8 + HC_8H$, while both methods do so for the $Ag_8 + HC_4H$ system. The charge on the cluster reported in the other cases is negative, suggesting that the polyyne is positively charged, for both lengths of the chain. Nonetheless the values obtained are still very small in modulus, ad as such a more in depth analysis of this behavior should be performed.
In order to further investigate these trends obtained from the analysis of the charge distributions for the dimers, the ionization energy of such systems has been considered, to check the energetically favored direction of the charge transfer. It is possible to calculate such quantity with the following expression:

$$E_{ION} = IP - EA \tag{3.4}$$

where IP is the ionization potential of the species acting as an electron donor and EA is the electron affinity of the electron acceptor. It is possible to define E_{ION} as the work required for the formation of charged species in the case of the charge transfer of one electron from the polyyne to the cluster (Ag^-; CAW^+) or vice versa (Ag^+; CAW^-). Whence the equilibrium energies of the charged polyynes is obtained, the value of the ionization energy can be defined. The values of $IP = 4.6\ eV$ and $EA = -1.3\ eV$ are taken for ${Ag_i}^+$ and ${Ag_i}^-$ respectively, as indicated in [31].

The results of the calculations are reported in table 3.9.

System	$\mathbf{E}_{ION}$ $[eV]$
$\mathbf{Ag^- + HC_4H^+}$	8.56
$\mathbf{Ag^- + HC_8H^+}$	7.35
$\mathbf{Ag^+ + HC_4H^-}$	3.97
$\mathbf{Ag^+ + HC_8H^-}$	3.59

Table 3.9. Calculated values of E_{ION} for different chain length.

The energies obtained indicate that the configuration in which the polyyne is negatively charged is energetically favored, in opposition with the result obtained by the analysis of the charges. This behavior underlines the necessity of more detailed and in depth studies about the charge transfer effect, especially when taking into account the questionable reliability of the calculated charges. The values calculated for the analysis of the ionization energies highlight a trend (see Fig.3.19), which suggests that the more stable system is the one with the longer chain, as confirmed also in the initial investigation of the interaction energies (see section 3.3.1). A final consideration on the results obtained until now regarding the analysis of the charges: this investigation did not successfully justified the shape of the spectra generated by the interaction of the cluster with the polyynes. In previous studies it was hypothesized that the downshift of the peaks was caused by a charge transfer between the two monomers. The results obtained suggest instead that the primary cause for the modification of the spectra is the strong interaction between the cluster and the chain, which, as said, is stronger than a classic Van der Waals-like interaction. A more detailed study should be carried out to shine light on the effect of the eventual charge transfer taking place in these systems.

A further investigation was tried in order to verify which of the methods employed above could better describe the charge transfer effect. For this reason, the comparison of the spectra of the artificially charged polyynes with the spectra of the interacting system has been performed. Indeed, similarities in such spectra could confirm a preferential direction for the charge transfer. As we can see in the plots, the spectra for the negatively charged isolated polyynes correctly predict a downshift of the peaks, but fail to model the low frequency peak that we see in the spectra of the interacting systems. This confirms the hypothesis advanced above, i.e., rather than being the charge transfer the cause for the modification of the shape of the spectra, it is the interaction between the cluster and the chain to induce a chemical SERS effect. Therefore, a more detailed study is needed in order to model the charge transfer phenomenon, to check whether it is significant for the modification of the spectra.

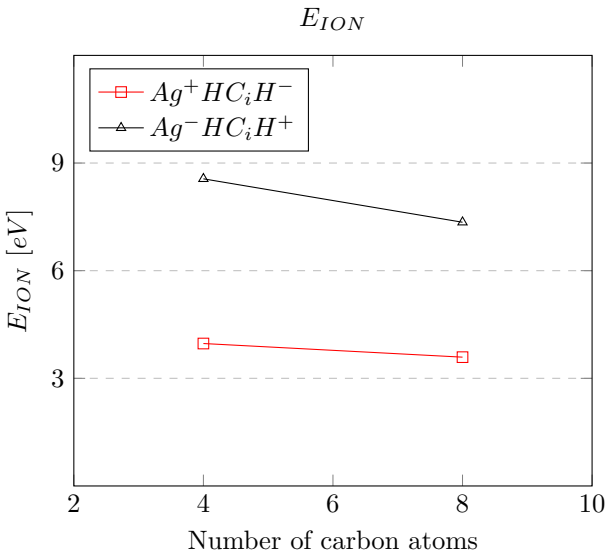

Figure 3.19. Plot of the ionization energies, E_{ion} for the different systems analyzed. Lower energies indicate a more stable configuration.

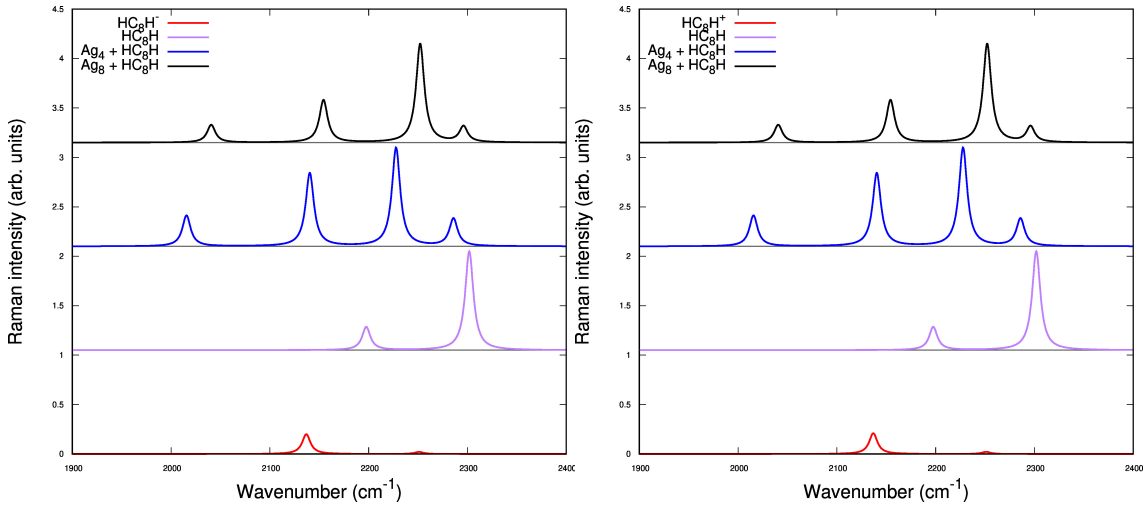

(a) (b)

Figure 3.20. Comparison of the spectra of the charged hydrogen-polyyne with the spectra of isolated neutral polyyne, $Ag_4 + HC_iH$ and $Ag_8 + HC_8H$.

3.3.3 Comparison with experimental data

The comparison with experimental data is necessary to check whether there exists an agreement between the computation and the experiments. The spectra reported in Fig. 3.21 represent the experimental SERS spectra of a sample containing silver nanoparticles interacting with HC_8H polyyne. The spectra obtained from the computations have to be scaled down to account for the used functional (i.e. PBE0) overestimation of the π conjugation (see section 3.2.2). The scale factor for the specific functional and basis-set used (i.e. PBE0 and 6-311++G(d,p)) is 0.9594, taken from the Computational Chemistry Comparison and Benchmark DataBase (CCCBDB, [76]). The red line represents the spectrum obtained experimentally, and features five peaks, which are located at about 1890, 1930, 2070, 2250, 2290 cm^{-1}. The right most peaks, i.e. at 2250 and 2290 cm^{-1},

indicated in Fig. 3.21 by the red arrows, are related to the acetonitrile solution.

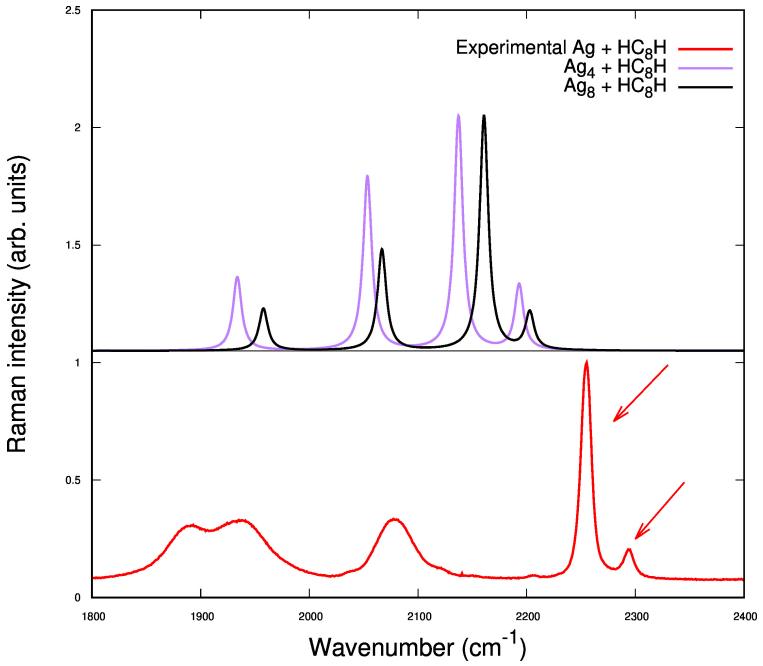

Figure 3.21. Experimental SERS spectrum of liquid solutions of size-selected polyynes with four triple bonds [43]. The calculated spectra, in purple and black, have been scaled down. The arrows indicate the peaks related to the acetonitrile.

The peaks which represent the polyynes interacting with silver nanoparticles are those at 1890, 1930, 2070 cm^{-1}. It can be observed that there exists a non-negligible shift between the experimental measures and the predicted ones even after the scaling of the values. This may be caused by the different size of the silver nanoparticles in solution, that are bigger than the model ones used in the computations. As evident, the peaks measured in the experiment are broad and cover a wide range of frequencies. This behavior is caused by the effect of the dimensional distribution of the nanoparticles in the solution, which is in agreement with the results of the computations, as indeed discussed in section 3.3.1: the calculated spectra are in fact influenced by the dimension of the cluster. The solution experimentally prepared features silver nanoparticles of non-zero dimensional distribution and, moreover, a convolution of the measured signals, for the whole set of of different systems (i.e. silver nanoparticle interacting with the polyynes) had to be performed, thus resulting in the broadening of the mentioned peaks. In this regard, a correspondence with the calculated spectra can be individuated: broad bands arise in the experimental spectra in the range of 1850 and 1950 cm^{-1} and between 2050 and 2110 cm^{-1}. These features may be related to the different peaks predicted for hydrogen-polyynes interacting with the silver clusters.
A more in depth understanding on the discrepancies highlighted for the two cases, i.e. the experimental measures versus the calculated ones, may be obtained by a study focused on the effect of the size of the particles. In this regard, a more precise model of the clusters should be introduced in the computations, to better reflect the experimental environment. Moreover, convolution of the predicted spectra of different systems could be calculated, to check its influence on the broadening of the peaks.

Chapter 4

Analysis of methyl- and cyano-polyynes

4.1 Introduction

In order to further investigate the nature of the interaction between the cluster and the carbon chain, the study has been extended towards methyl- and cyano-terminated polyynes. The computations have been performed using the same optimized setup discussed in the previous chapter, i.e. PBE0 as exchange-correlation functional and 6-311++G(d,p) as basis-set. The predicted results have then been compared with experimental SERS data obtained in [43]. These are linear chains having as terminal groups a hydrogen atom on one side, and on the other a CH_3 or CN group respectively, as shown in Fig. 4.1

(a) (b)

Figure 4.1. Optimized configurations for a)methyl-polyyne, and b) cyano-polyyne. In blue the nitrogen atom.

The properties of such systems may be different with respect to hydrogen-polyynes, due to the presence of the end group, as discussed in chapter 1.
The main goal was the study of the interaction between the polyyne and the metal cluster, and in this context this analysis was focused on the effect of the terminal group, and therefore we considered a unique chain length (i.e. 8 atoms) and cluster size (i.e. Ag_8). Due to the asymmetry

introduced in the chain by the presence of the end group, two different configurations were assumed and then optimized. In the first one, the cyano and methyl end groups were placed on the same side of the silver cluster (identified as $Ag_8 + CH_3C_8H$ and $Ag_8 + CNC_8H$), while in the second case on the opposite side (i.e. $Ag_8 + HC_8CH_3$ and $Ag_8 + HC_8CN$). Similarly to the hydrogen-polyynes, an investigation of the interaction energies and on the Raman spectra was performed. Moreover, the same analysis of the bond lengths and their force constants was carried out, in order to confirm the nature and magnitude of the peculiar interaction between the chain and the cluster. As for the case of hydrogen-polyynes, the charges of the dimer and the spectra of charged monomers were analyzed to assess the presence and direction of a possible charge transfer between the cluster and the chain.

4.2 Methyl-polyynes

4.2.1 Interaction energies and SERS spectra

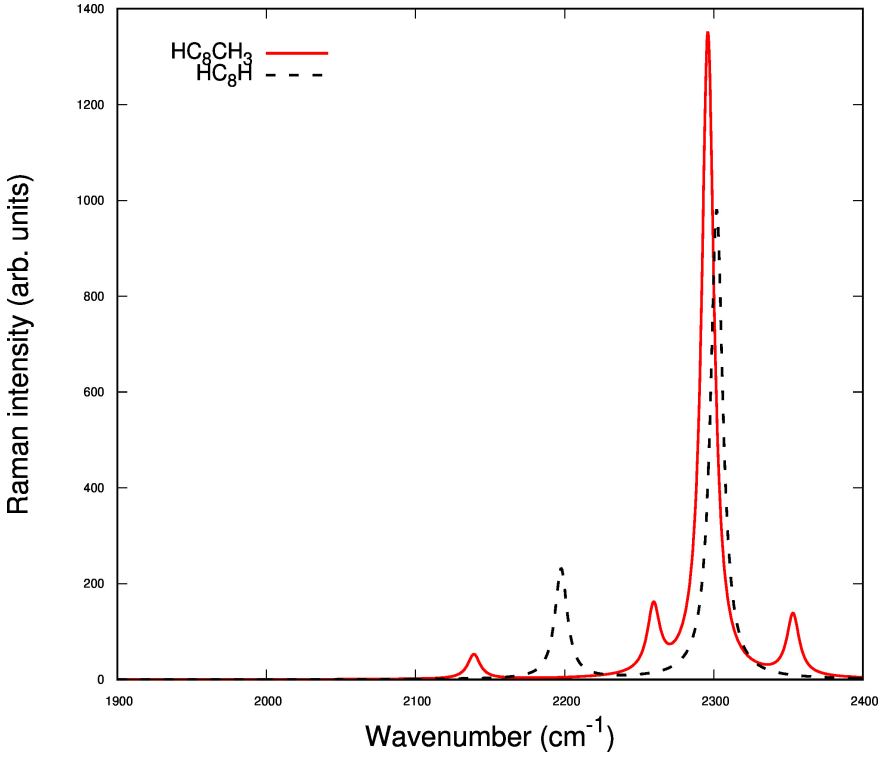

Figure 4.2. Predicted Raman spectrum of HC_8CH_3, in red. The spectrum of HC_8H is reported for comparison with the dotted black line.

Due to the presence of the end group the vibrational properties of the methyl-polyyne are different with respect to the isolated one, thus the Raman spectrum of the former is different from the latter. In Fig 4.2, both the spectra are reported; the appearance of new peaks can be noticed in the methyl-polyyne's Raman spectrum when compared to the hydrogen-polyyne's one. The frequencies associated to Raman active normal modes of the methyl-terminated species can be found at 2139, 2260, 2296, 2353 cm^{-1}. The new peaks visible in the spectrum of HC_8CH_3 are

probably caused by the end groups, which are in this case different (H and CH_3), whereas in the hydrogen-polyynes they were the same (both H). The only exception is for the peak with the highest intensity: it can still be related to the ECC mode, as visible in Fig. 4.3. Its minor shift can be correlated to an increase in the conjugation of the chain, due to the hyperconjugation affecting the C−H bonds in the methyl end group, as predicted by the analysis of the BLA and energy gap for the isolated methyl-polyyne. Specifically, the calculated values report a BLA of 0.133 Å and an energy gap of 4.680 eV, which are lower with respect to those of the HC_8H hydrogen-polyyne, thus indicating a slightly higher conjugation of the chain.

(a) 2302 cm^{-1} (b) 2296 cm^{-1}

Figure 4.3. Eigenvectors associated to the ECC mode of a) HC_8H, b) HC_8CH_3. The frequencies of the normal modes are also reported.

As a first investigation of the polyyne-cluster interaction in the case of methyl-terminated chain, the interaction energies of the two configurations discussed above were calculated: the first one featuring the methyl group on the same side of the chain as the cluster, the other one with the CH_3 group and the nanoparticle at opposite sides of the polyyne. The calculated values are reported in table 4.1, where it is possible to see that one of the two configurations is more stable and energetically favoured, i.e. the one in which the cluster interacts with the chain in the vicinity of the CH group.

System	$\mathbf{E}_{INT}$ $[kcal/mol]$
$\mathbf{Ag_8 + HC_8H}$	-6.24
$\mathbf{Ag_8 + HC_8CH_3}$	-6.40
$\mathbf{Ag_8 + CH_3C_8H}$	-4.88

Table 4.1. Calculated values of the interaction energies for the two different stable configurations of methyl-polyyne. The value of $Ag_8 + HC_8H$ is reported for comparison.

The interaction energy increases of about 0.16 $kcal/mol$ from $Ag_8 + HC_8H$ to $Ag_8 + HC_8CH_3$, and since the values obtained differ by less then a single $kcal/mol$, the obtained results are comparable with the numerical error related to the basis-sets (e.g. basis-set superposition error), or in the inaccurate description of the dispersion interactions. As for the less stable configuration, it could be suggested that the presence of the methyl group in the vicinity of the cluster has some effects on the interaction between the silver atom and the first carbon of the chain (highlighted in Fig. 4.4a): the steric hindrance is the cause for the lower interaction energy.
Additional insights can be obtained by the analysis of the BLA and energy gap between the HOMO and LUMO, as done for the system $Ag_8 + HC_8H$ in the previous chapter. The trend of such parameters is reported in table 4.2. A comparison between The two parameters decrease when the

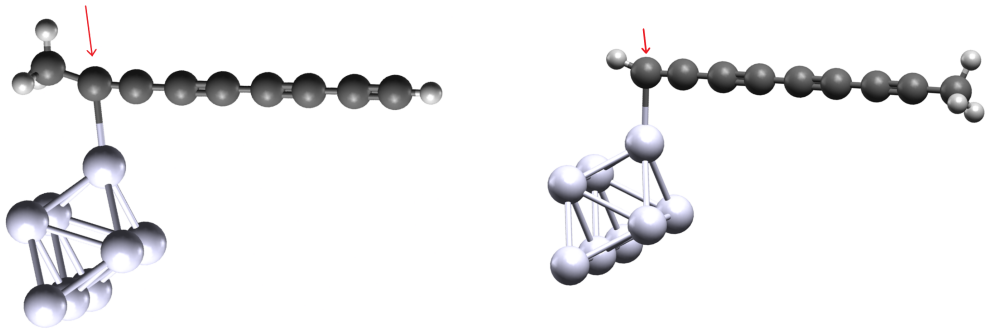

(a) (b)

Figure 4.4. Structure of the optimized systems: a) $Ag_8 + CH_3C_8H$; b) $Ag_8 + HC_8CH_3$. The red arrow indicates the first carbon atom of the chain.

methyl-polyyne is interacting with the cluster, and thus it is possible to affirm that an increased conjugation on the chain is due to the interaction between the polyyne and the cluster itself. The values reported for the two configurations, i.e. $Ag_8 + HC_8CH_3$ and $Ag_8 + CH_3C_8H$ indicate that the position of the methyl terminal group is slightly influencing the conjugation on the chain, but the small discrepancies of the values indicate that its effect on the interaction with the cluster has to be further analyzed.

System	**BLA**	**Energy Gap**
$\mathbf{Ag_8 + HC_8H}$	0.122	2.041
$\mathbf{Ag_8 + HC_8CH_3}$	0.121	2.095
$\mathbf{Ag_8 + CH_3C_8H}$	0.127	2.204

Table 4.2. Calculated values of the BLA, in Angstroms, and energy gap, in eV for the two different stable configurations of methyl-polyyne. The value of $Ag_8 + HC_8H$ is reported for comparison.

The implications related to the two different configurations have been also investigated by the analysis of the spectra. The spectra for both the configurations are compared to the spectrum of the isolated methyl-polyyne in Fig. 4.5.
Some differences are visible: for the case of $Ag_8 + HC_8CH_3$ there is a modification in the overall shape of the Raman spectrum, possibly caused by the way the chain interacts with the cluster and the magnitude of such interaction. On the other hand the spectrum of the system with the cluster and the methyl end group on the same side resembles the one of the isolated chain, but is redshifted. The same effect shown for the case of hydrogen-polyynes can be observed for the system $Ag_8 + HC_8CH_3$: the interaction of the cluster with the carbon atoms in its vicinity influences the activation of the normal mode, which localizes in the portion of the chain closest to the nanoparticle, at about 2050 cm^{-1}. Also in this case we can hypothesize that a decrease in the force constant of the triple bond of the two carbon atoms interacting with the cluster is taking place, and this is caused by the interaction itself. This results in the activation of that low frequency normal mode.

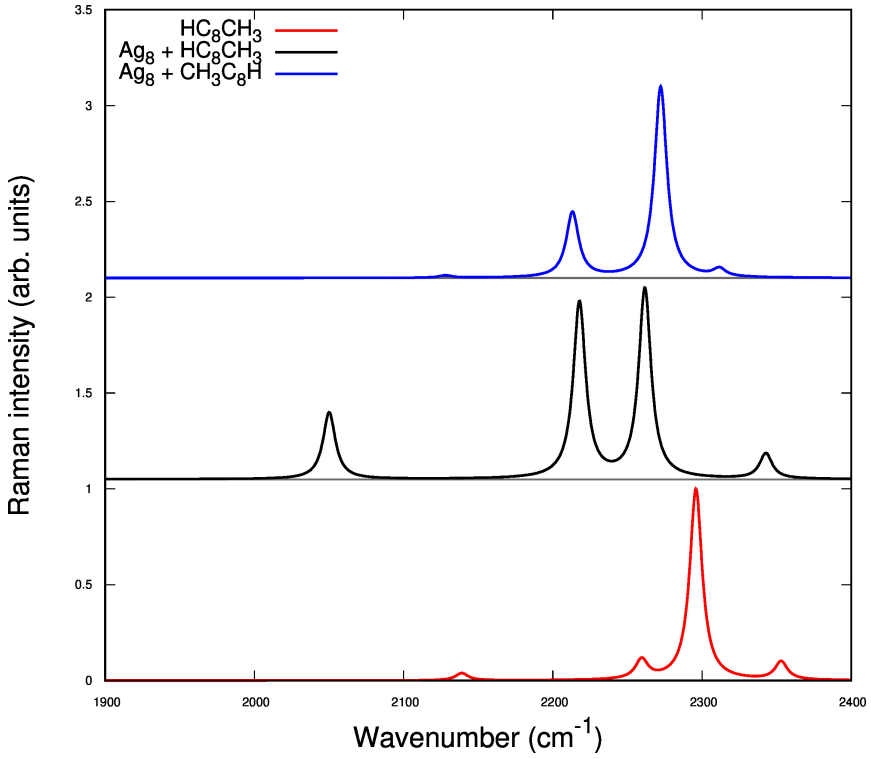

Figure 4.5. Comparison of the predicted normalized spectra for methyl-polyynes interacting with the cluster in different configurations: in blue, the configuration featuring the methyl group on the same side of the cluster, in black the one with cluster and end group on opposite sides. In red, the spectrum of the isolated methyl-polyyne.

Furthermore, the enhancement of the peak at 2218 cm^{-1} is due to a modification of the ECC mode, that is now focused on the specific part of the chain where the nanoparticle interacts with the polyyne; such peculiar interaction is also the cause for the modification to the ECC mode. The same consideration applies for the peak at 2343 cm^{-1}. Instead, for the $Ag_8 + CH_3C_8H$ system, the presence of the methyl group on the same side of the cluster weakens the interaction of the cluster itself with the carbon atoms, resulting only in a shift of the signals, as indeed the overall shape of the spectrum is similar to the isolated polyyne case: there is an enhancement in the intensity of each mode, and the low frequency peak does not appear. To better assess such enhancement of the signals due to the interaction with the cluster, the non-normalized spectra are reported in Fig. 4.6, for both configurations.

The analysis of the eigenvectors associated to the normal modes could provide some interesting insights: a similar shape between the eigenvectors of the normal modes of the system $Ag_8 + CH_3C_8H$ and the isolated methyl-polyyne can be expected, while a modification in the nature of the oscillation of the bonds should be expected in the case of $Ag_8 + HC_8CH_3$, especially for the low frequency normal mode, similarly to the case of the hydrogen-polyynes.

In this regard, the eigenvectors related to the low frequency normal mode of $Ag_8 + HC_8CH_3$, $Ag_8 + CH_3C_8H$ and HC_8CH_3 are reported. In Fig. 4.7 it is possible to see a comparison of the low frequency mode for both the configurations and the isolated polyyne.

The different behavior of the $Ag_8 + HC_8CH_3$, highlighted in Fig. 4.7a, is caused by the interaction with the cluster, that is inducing a modification in the triple bond of the first two carbon atoms of the chain (highlighted in Fig. 4.4). By looking at the eigenvectors related to $Ag_8 + CH_3C_8H$

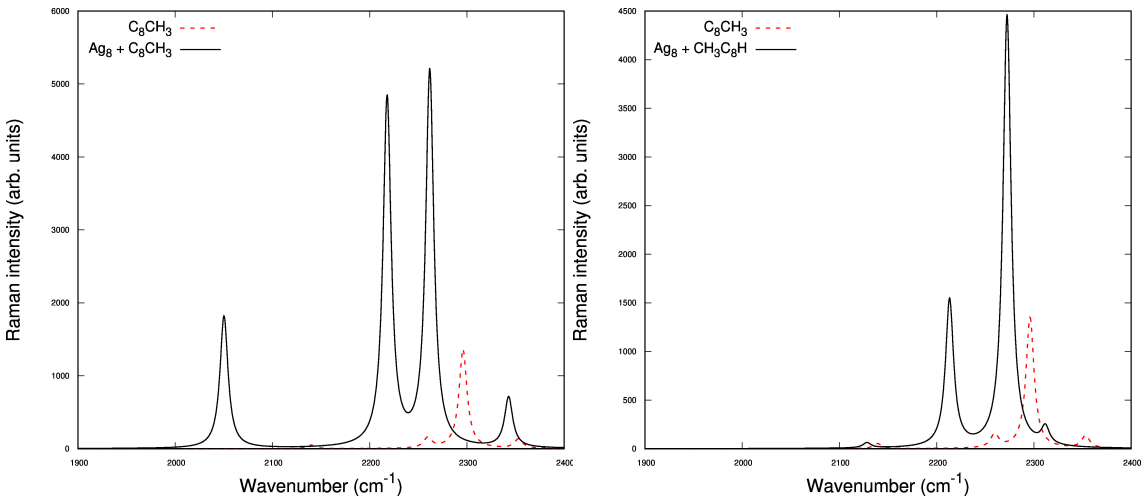

(a) (b)

Figure 4.6. Non-normalized spectra of: a) HC_8CH_3 and $Ag_8 + HC_8CH_3$; b) HC_8CH_3 and $Ag_8 + CH_3C_8H$

.

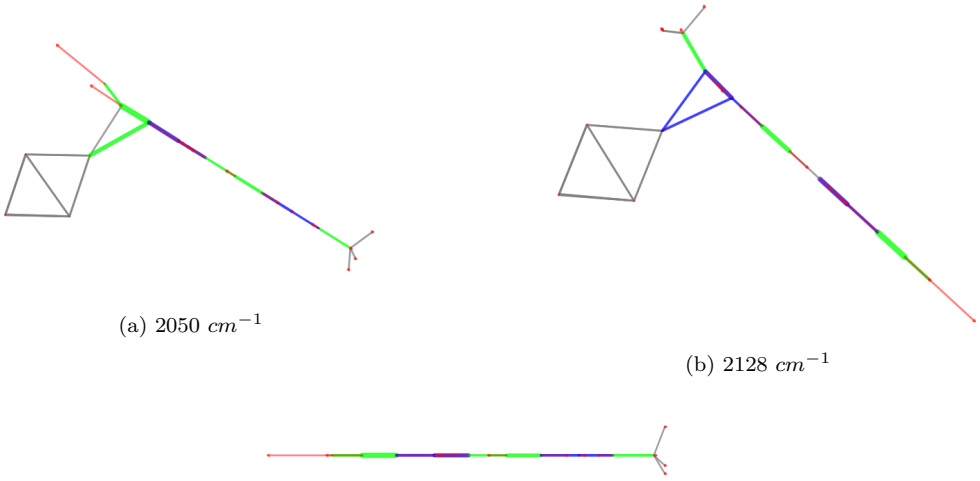

(a) 2050 cm^{-1}

(b) 2128 cm^{-1}

(c) 2139 cm^{-1}

Figure 4.7. Eigenvectors associated to the low frequency normal mode for a) $Ag_8 + HC_8CH_3$, b) $Ag_8 + CH_3C_8H$, c) HC_8CH_3. The difference in the oscillation between a) and b), c) is visible. The frequencies of the normal modes are also reported.

and HC_8CH_3, it is possible to observe similarities with the one of $Ag_8 + HC_8CH_3$, but the analysis of the spectra underlines huge differences: an higher relative intensity and especially a noticeable shift (of about 100 cm^{-1}) are predicted for the peak of $Ag_8 + HC_8CH_3$ with respect to the isolated polyyne. The behavior of $Ag_8 + CH_3C_8H$ is instead different with respect to $Ag_8 + HC_8CH_3$: the low frequency peak is absent, and the reason is the position of the methyl group on the same side of the cluster, that weakens the interaction of the silver cluster with the first two atoms of the chain. The observation of the eigenvectors associated to the most intense peak, located between 2260 and 2300 cm^{-1}, reported in Fig. 4.8 further confirms the different behavior induced by the position of the end group. In fact, the oscillations of the bonds in the case of the $Ag_8 + CH_3C_8H$ are associated to the ECC mode, visible also in the isolated polyyne; on the other hand, the same normal mode

for the system $Ag_8 + HC_8CH_3$ highlights a localization of the oscillations on a specific part of the chain, and this is mainly caused by the peculiar interaction with the cluster.

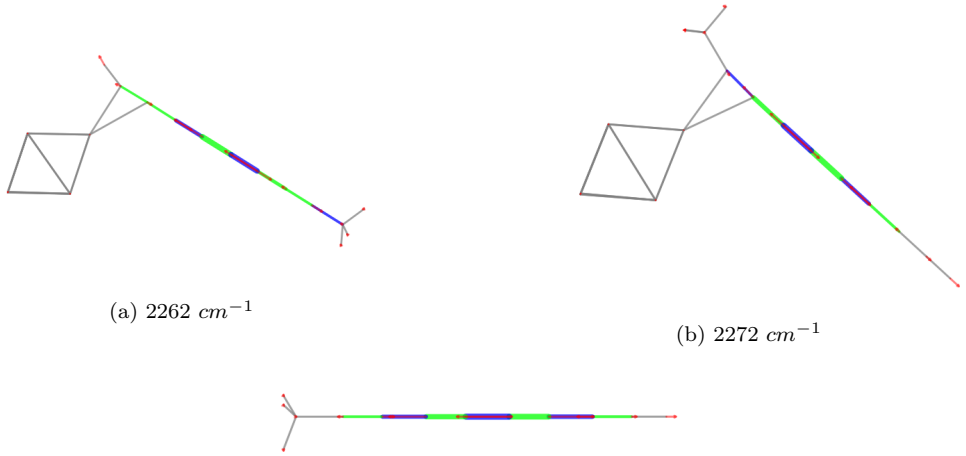

(a) 2262 cm^{-1}

(b) 2272 cm^{-1}

(c) 2296 cm^{-1}

Figure 4.8. Eigenvectors associated to the highest intensity normal mode for a) $Ag_8 + HC_8CH_3$, b) $Ag_8 + CH_3C_8H$, c) HC_8CH_3. The frequencies of the normal modes are also reported.

Moreover, the oscillations of the bonds of $Ag_8 + HC_8CH_3$ (Fig. 4.8a) can be related to a modified ECC mode, focused only on a specific part of the chain; on the other hand, a collective ECC oscillation is visible in the case of both the isolated methyl-polyyne (Fig. 4.8c) and the $Ag_8 + CH_3C_8H$ system. The nature of the interaction with the cluster is again the probable cause for the differences in the eigenvectors: for the $Ag_8 + HC_8CH_3$ system, the interaction with the cluster is stronger, and causes the activation of localized normal modes. On the other hand, the methyl group on the same side of the cluster has a shielding effect, which results in a weakened interaction between the nanoparticle and the polyyne, preventing the strong localization of the ECC mode, and thus causing the similarities in the eigenvectors of $Ag_8 + CH_3C_8H$ and HC_8CH_3.
The situation changes again for the other two peaks, located at about 2200 cm^{-1} and at about 2350 cm^{-1}, whose eigenvectors are reported in Fig. 4.9 and 4.10 respectively. For each system, the peak at ≈ 2200 cm^{-1} can be associated to a different collective oscillation of the carbon-carbon bonds. Moreover, the strong interaction with the cluster is underlined by the high intensity of the peak of $Ag_8 + HC_8CH_3$ with respect to the other two systems. As for the $Ag_8 + CH_3C_8H$ system, we can see that the overall behavior is basically the same showed in the isolated polyyne (see Figures. 4.9b and 4.9c), but the oscillation is more localized on the triple bond of the two initial carbon atoms of the chain.
The right-most peak, at ≈ 2350 cm^{-1}, is instead related to a localized oscillation on the side of the methyl group in the case of the HC_8CH_3 and $Ag_8 + HC_8CH_3$ systems, as showed in Fig. 4.10. As it is possible to see in the spectra, these peaks are predicted in both those systems, and have a similar frequency and intensity, with a downshift in the case of the interaction with the silver cluster, due to the already discussed effect of the interaction of the cluster itself with the chain, causing an increased conjugation on the chain. On the other hand it is evident a difference in the spectrum of the other system, i.e. $Ag_8 + CH_3C_8H$. In this case, the position of the methyl group on the same side of the cluster results in a lower frequency and intensity; the cause of this behavior is the presence of the cluster itself, which screens the effect of the methyl group on the chain.

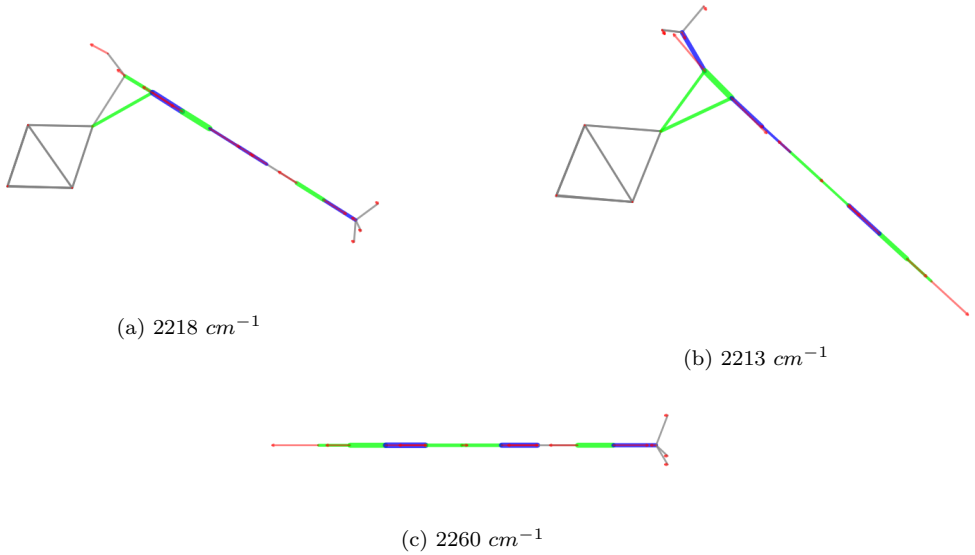

(a) 2218 cm^{-1}

(b) 2213 cm^{-1}

(c) 2260 cm^{-1}

Figure 4.9. Eigenvectors associated to the normal mode at around 2200 cm^{-1} for a) $Ag_8 + HC_8CH_3$, b) $Ag_8 + CH_3C_8H$, c) HC_8CH_3. The frequencies of the normal modes are also reported.

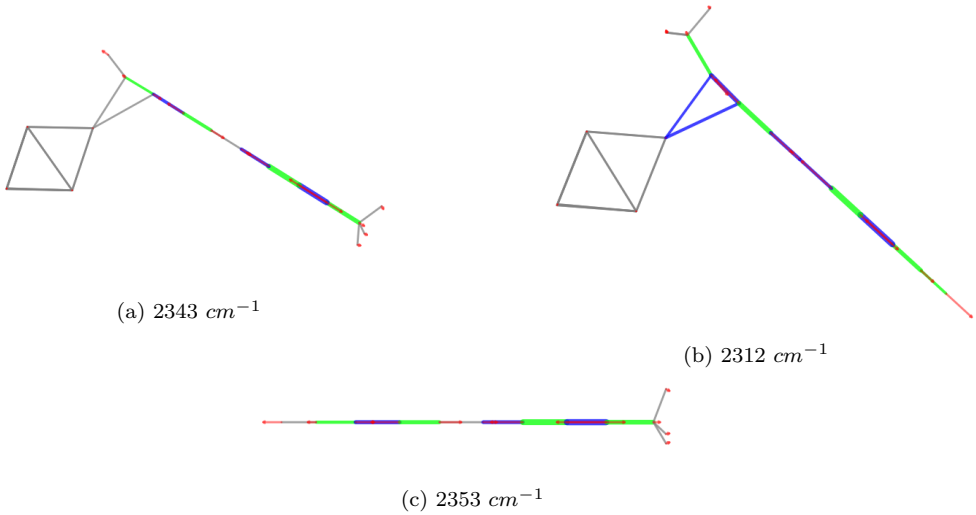

(a) 2343 cm^{-1}

(b) 2312 cm^{-1}

(c) 2353 cm^{-1}

Figure 4.10. Eigenvectors associated to the right-most normal mode, i.e. $\approx 2350\ cm^{-1}$ for a) $Ag_8 + HC_8CH_3$, b) $Ag_8 + CH_3C_8H$, c) HC_8CH_3. The frequencies of the normal modes are also reported.

Summarizing, the analysis of the spectra and the eigenvectors highlights a very different behavior caused by the relative positions of the end group and the silver cluster. In one case, with the cluster opposite to the methyl group, the behavior observed is similar to the case of hydrogen-polyynes, suggesting a strong interaction between the molecular orbitals of the nanoparticle and those of the first carbon atoms of the polyyne, causing the appearance of the low frequency mode. The geometry of the chain is also influenced, and this is visible by the enhancement of the signals and by the localization of the collective oscillations on the side of the cluster. On the other hand, when the cluster is on the same side of the methyl group, the interaction effect is weakened, and in fact the low frequency mode is not detected, since the interaction is different with respect to the $Ag_8 + HC_8CH_3$ system. Furthermore, the shape of the spectra is similar to that of the isolated polyyne, with the difference in the enhancement of the intensity of the peaks, as visible in Fig. 4.6. The

cause could be the hindering effect of the methyl group, which weakens the interaction between the chain and the cluster, thus preventing the modification of the ECC mode. The interaction with the nanoparticle also causes differences in the behavior of the other peaks as well: the one close to 2200 cm^{-1} is a result of the modification of the ECC mode, and its intensity is grater for $Ag_8 + HC_8CH_3$, while mildly increased in the case of $Ag_8 + CH_3C_8H$. The last peak, located at about 2300 cm^{-1}, moves closer to the high intensity peak in the case of $Ag_8 + CH_3C_8H$ due to the fact that the methyl group is on the same side of the cluster, and thus the bonds influenced by such end group are involved also in the interaction with the cluster, while in the other two cases are free to vibrate, and indeed the peaks for HC_8CH_3 and $Ag_8 + HC_8CH_3$ are similar in frequency and intensity.
To better explain all these effects, a further analysis can be done on the bond lengths and force constants, similarly to the case of hydrogen-polyynes. The values are reported in table 4.3, along with the data of hydrogen-polyynes for comparison. In such table, the values for the bond length of the triple bond interacting with the cluster are reported for the dimers and the isolated polyyne. The bond length between the closest silver atom and the first carbon atom of the chain, involved in the considered triple bond, near to the silver atom is also reported.

System	**Bond length**, C≡C	**Bond length**, C−Ag	**Force constant**, C≡C
$\mathbf{Ag_8 + HC_8CH_3}$	1.232	2.275	6.4793
$\mathbf{Ag_8 + CH_3C_8H}$	1.229	2.410	6.7362
$\mathbf{HC_8CH_3}$	1.211	/	16.3360
$\mathbf{CH_3C_8H}$	1.213	/	16.1070
$\mathbf{Ag_8 + HC_8H}$	1.234	2.262	6.3576
$\mathbf{HC_8H}$	1.210	/	16.3710

Table 4.3. Analysis of the bond lengths and force constants for the case of the two different configuration of the methyl-polyynes. The bottom values of the hydrogen-polyynes are for comparison. The bond lengths are measured in Angstroms, while the force constants are in $mdyne/Å$.

The first observation that can be made regarding the systems $Ag_8 + HC_8CH_3$ and $Ag_8 + CH_3C_8H$, is that, even if the values of the C≡C bond length are similar, i.e. 1.232 Å versus 1.229 Å, there is a small difference in the values of the silver-carbon bond of about 0.15 Å, in agreement with the predicted values of the interaction energies. This discrepancy can be correlated with the values obtained in the calculations of the interaction energies, with that of $Ag_8 + HC_8CH_3$ grater than the one of $Ag_8 + CH_3C_8H$, and in the changes in the overall shape of the spectra of the two configurations. Indeed, a stronger interaction between the cluster and the chain is suggested in the case of $Ag_8 + HC_8CH_3$, due to the absence of the methyl group, which instead is positioned at the end of the chain. Moreover, the value is close to the case of the hydrogen-polyyne interacting with the nanoparticle, further highlighting the similarities of these two systems. As for the case of the hydrogen-polyynes, also for the methyl-polyyne the interaction with the cluster seems to be

stronger than a simple Van der Waals interaction, since the bond length is smaller than the sum of the Van der Waals radii. The bond length analysis cannot alone justify the different shape of the spectra of the two methyl-polyynes interacting with the silver cluster. Indeed, it could in principle explain the activation of the low frequency mode for the $Ag_8 + HC_8CH_3$ system, considering the reduction of the force constant, but at the same time it fails to explain the behavior of the spectrum of $Ag_8 + CH_3C_8H$, which, as discussed above, is subjected to the effect of the relative position of the cluster and the methyl group and their effect on the triple bond of the first two carbon atoms of the chain. In fact, the interaction of the carbon atoms sharing the triple bond that interacts with the cluster is slightly different in the two cases, given the presence of the methyl group. Therefore, the difference in the nature of the two terminal groups, i.e. CH_3 versus H, and their influence on the chain seem to be the main causes of the discrepancies in the predicted spectra.

4.2.2 Analysis of the charges

The analysis of the charges for these systems was performed with the same procedure followed for hydrogen-polyynes and using the same methods, i.e. CHELPG and CHIRI, already introduced in the previous chapter. The aim is again the investigation of a possible electron charge transfer as one of the reasons behind the SERS chemical enhancement effect on the spectra of the polyynes interacting with the metal cluster, and, if so, to understand the direction of such charge transfer. The values obtained from the calculations are reported in table 4.4, and are referenced to the cluster (thus the charge of the polyyne is opposite in sign).

System	CHELPG	CHIRI
$\mathbf{Ag_8 + HC_8CH_3}$	-0.003492	-0.14988
$\mathbf{Ag_8 + CH_3C_8H}$	-0.023691	-0.12624

Table 4.4. Analysis of the charges of the systems of methyl-polyynes interacting with the silver nanoparticle. The values are in electron charge units, e.

The values are still small, but bigger (in modulus) with respect to those obtained for the hydrogen-polyynes, at least by using the CHIRI method. Both methods indicate that in each configuration the electronic charge transfer is directed towards the cluster, which acts as electron acceptor, with the chain consequently behaving as an electron donor. However, concerning the amplitude of the charge transfer, the two methods are in contrast with each other, with CHELPG suggesting a greater charge transfer for the configuration featuring the methyl group on the same side of the cluster, and vice versa for CHIRI. Nonetheless, the values obtained with CHELPG are very small, almost negligible, and therefore the trends obtained are mostly affected by numerical errors. Moreover, the behavior highlighted by CHELPG seems to be in principle in contrast with the hypotheses which suggested a more pronounced effect for a longer chain due to the increased conjugation, further indicating a possible low precision for the considered method. To have a second datum supporting

the discussion on the charges, the spectra for the charged species were analyzed. Following the same procedure as the hydrogen-polyynes case, this investigation has been carried out to verify whether the spectra of the positively or negatively charged species could be associated with the spectrum of the dimer in any of its configurations. The obtained spectra are reported in Fig. 4.11.

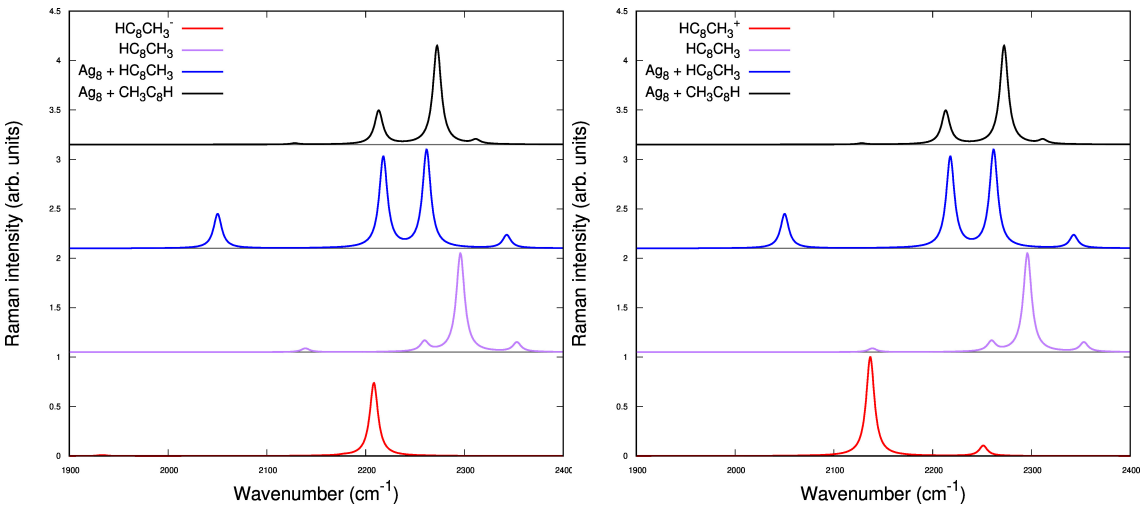

(a) (b)

Figure 4.11. Comparison of the spectra of the charged methyl-polyyne with the spectra of isolated neutral methyl-polyyne, $Ag_8 + HC_8CH_3$ and $Ag_8 + CH_3C_8H$. Specifically are reported the plot of: a) negatively charged methyl-polyyne; b) positively charged methyl-polyyne.

The reported spectra, as visible, have few differences. Firstly, only one peak is visible for the negatively charged methyl-polyyne (Fig. 4.11a) at 2208 cm^{-1}, associated to a collective oscillation of the carbon-carbon bonds, similar to the ECC mode, and localized on the part of the chain close to the methyl group. In reality, a second peak is predicted, at lower frequencies, i.e. 1933 cm^{-1}, but with a negligible intensity, as reported in Fig. 4.12. The redshift predicted for the $HC_8CH_3{}^-$ is higher with respect to the $HC_8CH_3{}^+$ polyyne. This is consistent with the results obtained for the hydrogen-polyynes, and thus it would seem that the spectrum of the negatively charged chain is more similar to the dimer one. Therefore, it seems that the problems highlighted in the previous chapter persist. Indeed, as already discussed in the previous chapter, these results are in contrast with the charges analysis performed with the CHELPG and CHIRI methods, that suggested a dimer in which the polyyne is positively charged (see table 4.4). In this comparison, we can see instead that the negatively charged polyyne is the one that better represents the redshift of the frequencies of the normal modes measured in the dimers. Both of the charged systems fail to correctly assess the presence of the low frequency normal mode (visible in the blue spectra in Fig. 4.11) already discussed in the above section. Furthermore, this confirms that the main cause for the peculiar shape of the spectra measured for the dimer is the presence of the silver cluster, which induces a strong modification on the geometry of the chain, resulting in the activation and enhancement of the already discussed normal modes, that weren't present in the isolated polyyne. Considering the obtained results it would seem that the description of the interaction between a nanoparticle and a polyyne is not well described by the model of the charged species. It follows that some more in depth analysis is needed to shine light on the phenomenon of the charge transfer.

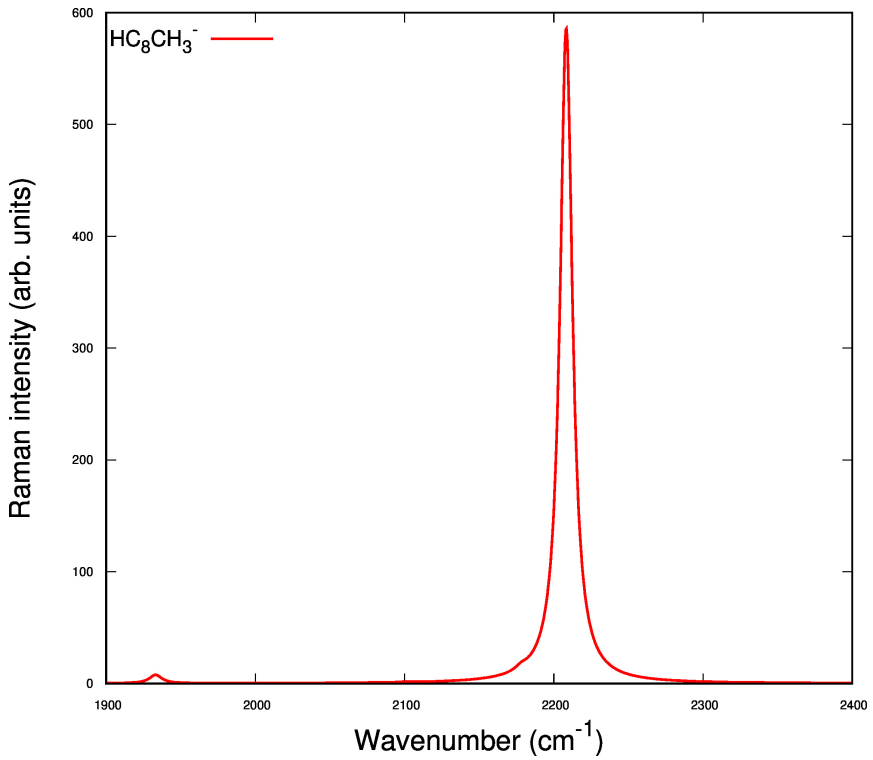

Figure 4.12. Non-normalized spectrum of $HC_8CH_3^-$. Both peaks can be observed at frequencies 2208 and 1933 cm^{-1}.

4.3 Cyano-polyynes

4.3.1 Interaction energies and SERS spectra

The analysis of cyano-polyynes follows the same steps of the previous two cases. The nature of the C≡N group is very different with respect to the methyl group, therefore, it is to be expected a difference in the behavior of the spectrum of the isolated polyyne. The Raman spectrum is reported in Fig. 4.13. The first observation is the rigid redshift of the overall spectrum. This is similar to the case of the methyl-polyynes, because the addition of another carbon atom, moreover sharing a triple bond with a nitrogen atom, increases the conjugation of the chain. This is confirmed by the analysis of the BLA and energy gap, already discussed for the cases of hydrogen-polyynes and methyl-polyynes. The calculated values are reported in table 4.5. As shown, there is a decrease of the values of the two parameters, and it indicates an increased conjugation of the chain, due to the presence of the CN terminal group. Regarding the appearance of the right-most peak, at a frequency of 2375 cm^{-1}, it is possible to observe that it is generated by a normal mode composed mainly by the stretching of the C−C single bond near the CN group, and the C≡N triple bond itself, as visible in the eigenvector related to that normal mode (Fig. 4.14e). The normal mode showing the highest intensity, located at 2271 cm^{-1} can be assigned to the ECC mode (Fig. 4.14c). The other signals are related to oscillations which have some reminiscence of the ECC mode (synchronous stretching and compression of the single/triple bonds), but localized on different bonds along the chain, and arise due to the asymmetry of the molecule.

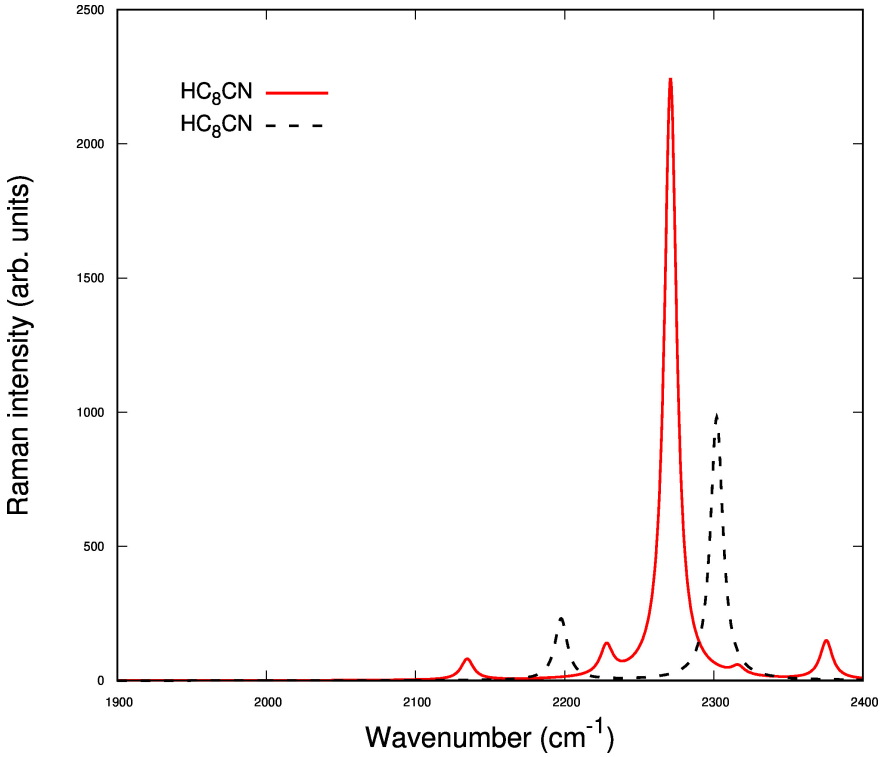

Figure 4.13. Predicted Raman spectrum of HC_8CN

System	BLA	Energy Gap
$\mathbf{HC_8H}$	0.135	4.735
$\mathbf{HC_8CH_3}$	0.133	4.680
$\mathbf{HC_8CN}$	0.127	4.299

Table 4.5. Bond length alternation, in Angstroms, and energy gap, in eV for isolated hydrogen-, methyl-, and cyano-polyynes of the same length.

The next step is the analysis of the interaction between the chain and the silver nanoparticle. As for the case of methyl-polyynes, the relative position of the cyano group with respect to the one of the cluster has to be investigated. For this reason, two possible initial configurations were prepared and optimized, i.e. one featuring the cyano group and the silver cluster on the same side, the other on opposite sides, as shown in Fig. 4.15a and 4.15b. Interestingly, both the optimization processes converged to very similar geometries, each of them featuring the silver cluster on the opposite side of the cyano group; this suggests only one energetically possible configuration for these interacting monomers, as the CN group does not represent a preferential site for the interaction with the cluster.

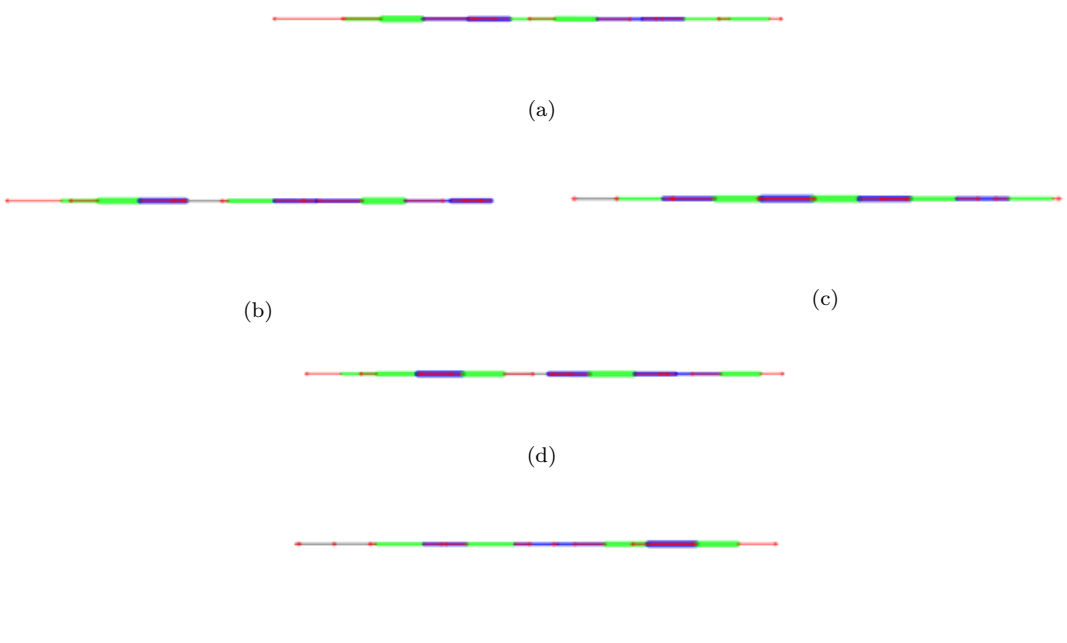

Figure 4.14. Eigenvectors of the system HC_8CN related to: a) the ECC mode; e) CN bond. Eigenvectors a), b), d) are related to different modes of carbon-carbon bond stretching.

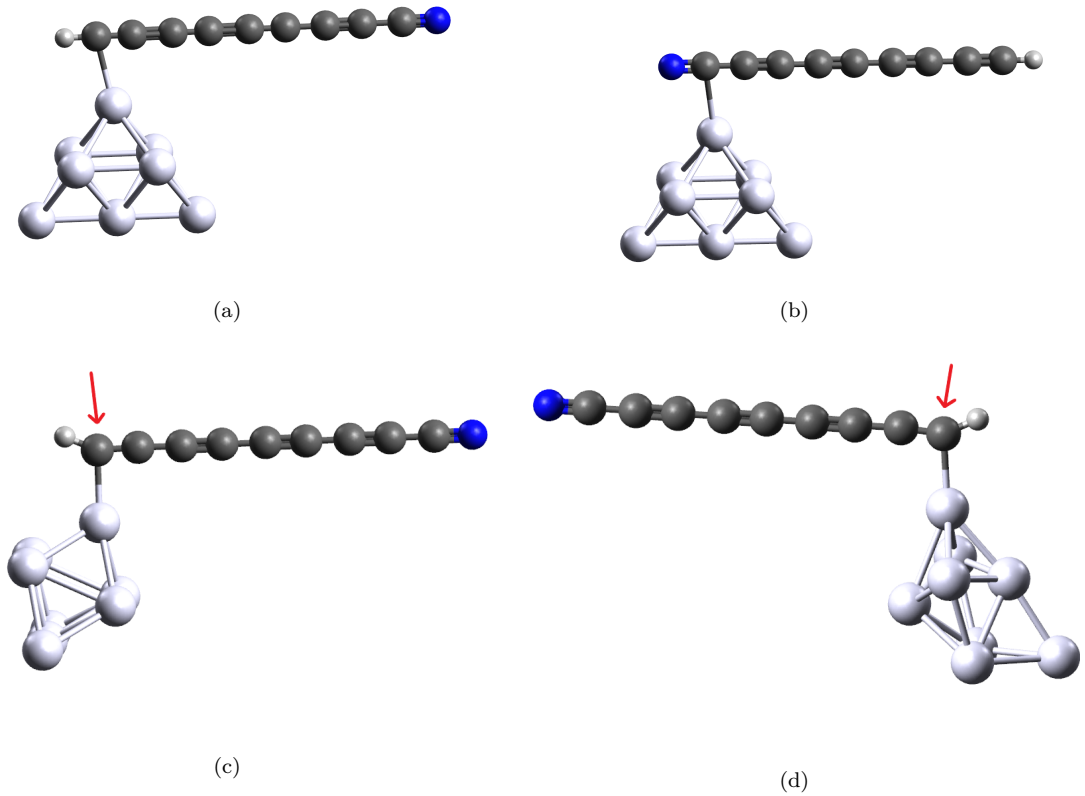

Figure 4.15. Initial and optimized geometries of the systems. Panels a) and c) refer to the case of Ag_8 + HC_8CN; b) and d) to $Ag_8 + CNC_8H$ configuration instead. The red arrows indicate the first atom of the chain.

An interesting behavior can be observed for the system in Fig. 4.15d: the initial configuration (Fig. 4.15b), featuring the cluster in the vicinity of the CN end group, resulted in a predicted optimized geometry in which the cluster itself moved to the opposite side to find the interaction site granting the minimum energy configuration; in the process, also the cluster's geometry was modified, since another minimum energy configuration was found. Apparently, the presence of the strong triple bond shared by the atoms of the C≡N group represents an obstacle for the cluster to interact with the carbon atoms of the chain. For this reason, it is forced to move along the chain, until the last carbon atom is reached, when the minimum of the potential surface of the geometry is assumed. This behavior confirms what already discussed for the methyl-polyynes, i.e. the nature of the end group is fundamental, as it greatly influences the interaction between the cluster and the chain.
Due to the fact that the two configuration are similar, the optimized systems will be indicated with their initial geometry configuration. To be more clear, the system of Fig. 4.15d will be described as $Ag_8 + CNC_8H$, while the system of Fig. 4.15c will be described as $Ag_8 + HC_8CN$.
The analysis of the interaction energies provided some other interesting insights. The values are reported in table 4.6.

System	$\mathbf{E}_{INT}$
$\mathbf{Ag_8 + HC_8H}$	-6,24
$\mathbf{Ag_8 + HC_8CN}$	-6.91
$\mathbf{Ag_8 + CNC_8H}$	-7.95

Table 4.6. Calculated values of the interaction energies for the two different stable configurations of cyano-polyynes. The value of $Ag_8 + HC_8H$ is reported for comparison. The values are in $kcal/mol$.

The first thing to notice is the fact that even if having a similar final configuration, the two systems have a difference of 1.04 $kcal/mol$. This value cannot be completely associated to an error in the calculations, and thus it would indicate that the difference is induced by the different shape of the two silver clusters interacting with the CH side of the polyynes (see Fig. 4.15d and 4.15c). Indeed, in the journey from one side of the polyyne to the other, a different minimum in energy related to a specific geometry has been found for the cluster. This configuration is probably one of many, and thus the result reported is important in highlighting the influence of the nanoparticle's shape on the interaction it could have with the polyynes. As for the comparison with the values obtained in the hydrogen-polyynes, the differences are 0.67 $kcal/mol$ and 1.71 $kcal/mol$. This increase can be associated to the already discussed higher electronic conjugation of the chain.
In order to verify the effect of the shape of the cluster and to analyze the interaction with the cluster, the predicted spectra were investigated, and are reported, for both optimized configurations, in Fig. 4.16. The observation that can be done are in general those already reported for the other studied systems, i.e. hydrogen-polyynes and methyl-polyynes. A redshift of the peaks is predicted for both configurations, and probably due to the specific interaction of the cluster with the chain, which also induces a stronger conjugation on the chain, as shown in table 4.7. The values reported for the dimers $Ag_8 + HC_8CN$ and $Ag_8 + CNC_8H$ indicate a strong decrease in both BLA and energy

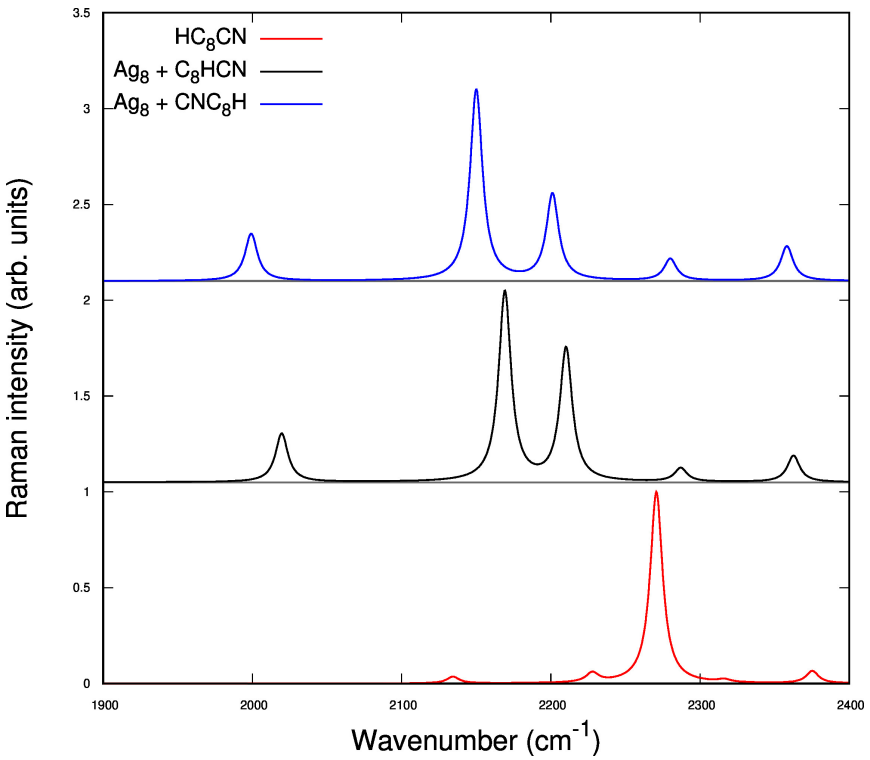

Figure 4.16. Comparison of the predicted normalized spectra for cyano-polyynes interacting with the cluster. In blue, the configuration initially featuring the cyano group on the same side of the cluster, in black the one with cluster and end group initially on opposite sides. In red, the spectrum of the isolated cyano-polyyne.

gap, as already seen in the case of both the hydrogen-polyynes and methyl-polyynes. The shift in the spectra is higher for the $Ag_8 + CNC_8H$ system, an this can be induced by the different shape assumed by the silver cluster at the end of the optimization processes, which then is responsible for a modification in the interaction with the chain, that results stronger with respect to the $Ag_8 + HC_8CN$ system.

System	BLA	Energy Gap
$\mathbf{Ag_8 + HC_8H}$	0.135	4.735
$\mathbf{Ag_8 + HC_8CH_3}$	0.121	2.095
$\mathbf{Ag_8 + CH_3C_8H}$	0.127	2.204
$\mathbf{Ag_8 + HC_8CN}$	0.108	1.660
$\mathbf{Ag_8 + CNC_8H}$	0.103	1.361

Table 4.7. Bond length alternation, in Angstroms, and energy gap, in eV for different dimers. The values indicate an higher conjugation for the cyano-polyynes dimers.

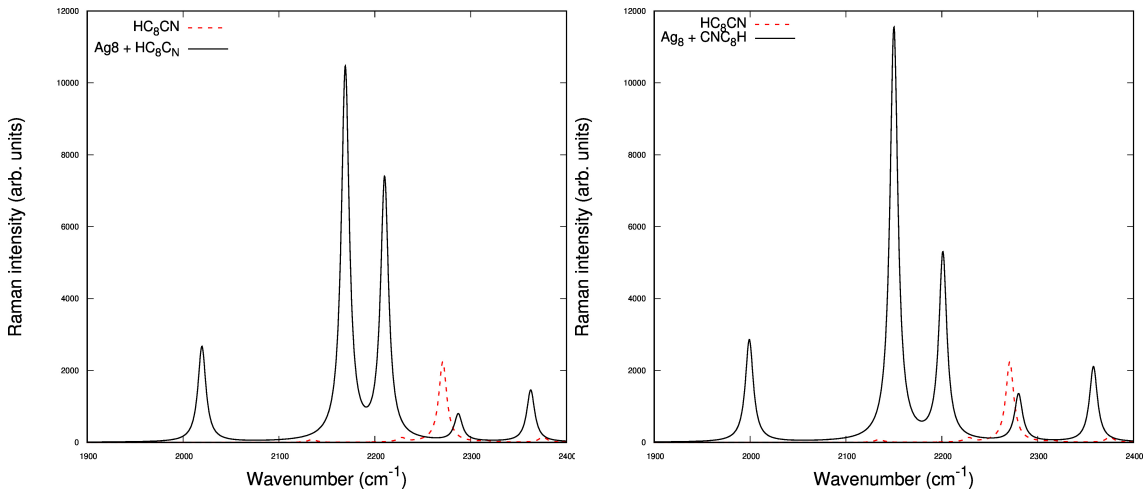

(a) (b)

Figure 4.17. Non-normalized spectra of: a) HC_8CN and $Ag_8 + HC_8CN$; b) HC_8CN and $Ag_8 + CNC_8H$

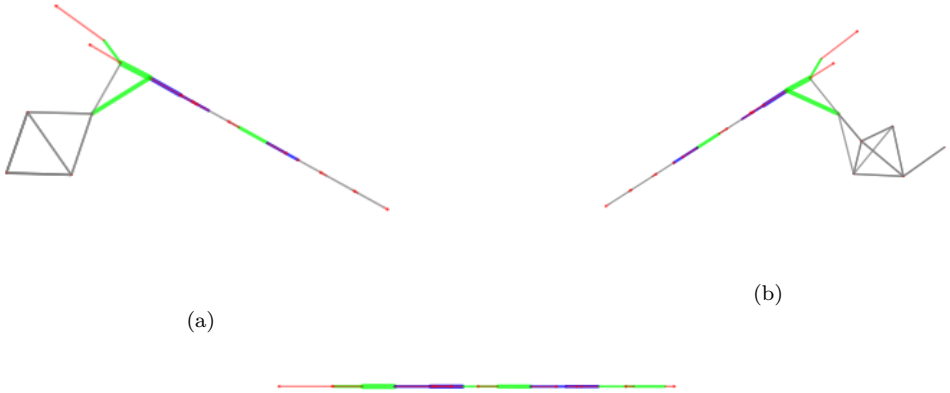

(a) (b)

(c)

Figure 4.18. Eigenvectors related to the low frequency mode for the case: a) $Ag_8 + CNC_8H$ at 1999 cm^{-1} ; b) $Ag_8 + HC_8CN$ at 2020 cm^{-1}; c) HC_8CN at 2134 cm^{-1}.

An enhancement of the peaks is observed in the non-normalized spectra (see Fig. 4.17), with the already mentioned low frequency mode arising in the left side of the spectra, at 2020 cm^{-1} and 1999 cm^{-1} for the $Ag_8 + HC_8CN$ and $Ag_8 + CNC_8H$ respectively. The nature of this peak can be assessed by the inspection of the eigenvectors, reported in Fig. 4.18. The same behavior showed in the case of hydrogen-polyynes and methyl-polyynes, is observed. The peak located at about 2010 cm^{-1} is associated to the oscillation of the triple bond interacting with the cluster (see Fig. 4.15d and 4.15c). The eigenvectors of the systems $Ag_8 + CNC_8H$ and $Ag_8 + HC_8CN$ are very similar, as expected by their similar optimized geometry, while it is very different from the one of the isolated cyano-polyyne. The nature of the low frequency peak is then determined by the peculiar interaction between the polyyne and the nanoparticle. Similarly to the other investigated systems, a modification in the internal force constants is expected, as well as a modification of the bond lengths. Due to the increase interaction energy calculated for cyano-polyynes with respect to methyl- and hydrogen-polyynes, a shorter silver-carbon bond (i.e. between the closest silver atom and the closest two atoms of the chain) should also be predicted. As for the peaks located at

2169 cm^{-1} and 2150 cm^{-1} for systems $Ag_8 + HC_8CN$ and $Ag_8 + CNC_8H$ respectively, the analysis of the eigenvectors, reported in Fig. 4.19 suggests a behavior seen in the other cases: the modes resemble the ECC one, but localized only on the extreme of the chain. Also in this case the eigenvectors are similar for both dimers, while are very different from those of the isolated polyyne. The effect of the cluster is then again underlined: it modifies the nature of the normal modes of the chain.

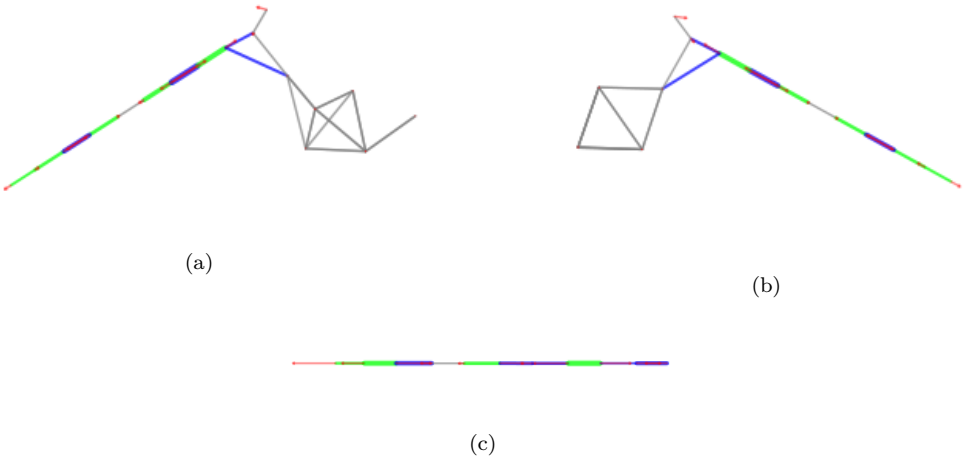

(a) (b)

(c)

Figure 4.19. Eigenvectors related to the normal modes of: a) $Ag_8 + CNC_8H$ at 2150 cm^{-1} ; b) $Ag_8 + HC_8CN$ at 2169 cm^{-1}; c) HC_8CN at 2228 cm^{-1}.

The same happens also for the peaks at 2210 cm^{-1} and 2201 cm^{-1} for $Ag_8 + HC_8CN$ and $Ag_8 + CNC_8H$ respectively. The ECC mode, very well visible for the isolated polyyne, is not predicted for the dimers. The normal modes have some characteristics of the ECC mode, but again the interaction with the nanoparticle influences the nature of the vibration, changing it, and localizing the oscillation on a specific bonds on the chain. The eigenvectors are reported in Fig. 4.20.

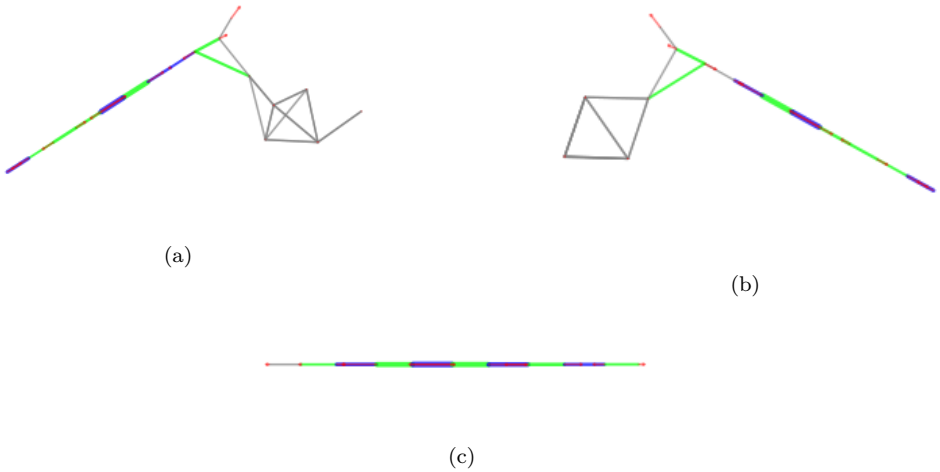

(a) (b)

(c)

Figure 4.20. Eigenvectors related to the normal modes of: a) $Ag_8 + CNC_8H$ at 2201 cm^{-1} ; b) $Ag_8 + HC_8CN$ at 2210 cm^{-1}; c) HC_8CN at 2271 cm^{-1}.

Another peak is predicted at 2287 cm^{-1} and 2280 cm^{-1}, always for $Ag_8 + HC_8CN$ and $Ag_8 + CNC_8H$ respectively, reported in Fig. 4.21, and represents again a localized mode on the central bonds of the chain. This peak is not predicted for the isolated polyyne: this may indicate that such

normal mode is enhanced by the interaction with the cluster. At last, the peak at high frequencies,

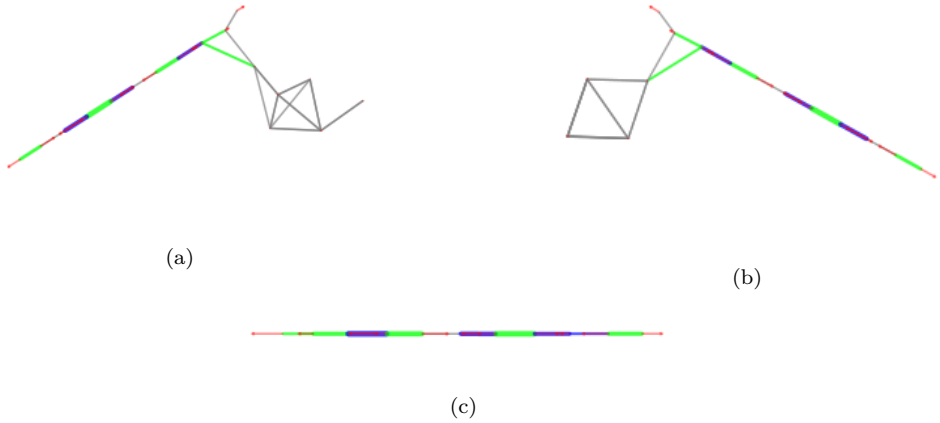

Figure 4.21. Eigenvectors related to the normal modes of: a) $Ag_8 + CNC_8H$ at 2280 cm^{-1} ; b) $Ag_8 + HC_8CN$ at 2287 cm^{-1}; c) HC_8CN at 2316 cm^{-1}.

specifically at 2363 cm^{-1} and 2358 cm^{-1} for systems $Ag_8 + HC_8CN$ and $Ag_8 + CNC_8H$ respectively, is associated to the vibration of the triple bond of the C≡N group, as shown in Fig. 4.22. This is observed also for the isolated polyyne. The fact that its characteristics are not altered by the presence of the cluster is due to the distance that these two have between them and also by the fact that the cyano triple bond is one of the strongest in nature.

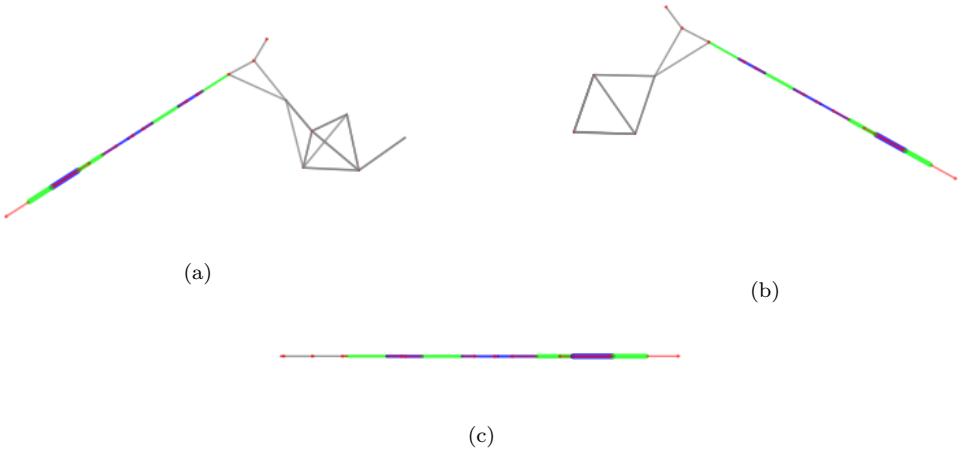

Figure 4.22. Eigenvectors related to the normal modes of: a) $Ag_8 + CNC_8H$ at 2358 cm^{-1} ; b) $Ag_8 + HC_8CN$ at 2363 cm^{-1}; c) HC_8CN at 2375 cm^{-1}.

In this regard, a possible explanation for the instability of system featuring the cluster on the same side of the CN group could be suggested on the base of the electronegativity of such terminal group: the high electronic density found on the CN group at the end of the chain, differently from the CH terminal group, may be the cause of the impossibility to instantiate a stable interaction with the cluster. However, more in detail analysis should be carried out in order to better investigate this behavior.

A further comment has to be done on the discrepancies of the spectra of the dimers: the overall trend is more or less the same and instead the shift in frequencies can be attributed to the stronger interaction caused by the different shape of the cluster. Indeed, it can be hypothesized that a

different shape modifies the internal force constants of the bonds of the chain, causing a minor shift. This would mean that for different geometries, different interaction energies are predicted, and therefore spectra with higher rigid shifts are obtained. This can also explain the particular behavior of the experimental spectra. As it will be seen in the next section, the peaks measured in experiments are usually very broad. These feature can be caused by the convolution of signals belonging to systems having a peculiar cluster configuration; the obtained bands are more or less shifted depending on the interaction of the chain with the cluster itself. Finally, the influence of the shape of the cluster on the spectra may be considered as a general effect. Therefore, also for other systems, a little change in the geometry of the nanoparticle would cause a modulation of the spectrum.
Also for cyano-terminated polyynes, an analysis of the internal force constants and on the bond lengths of the dimers has been performed. The results are reported in table 4.8

System	**Bond length**, C≡C	**Bond length**, C−Ag	**Force constant**, C≡C
$\mathbf{Ag_8 + HC_8CN}$	1.239	2.225	6.4793
$\mathbf{Ag_8 + CNC_8H}$	1.243	2.195	6.6342
$\mathbf{HC_8CN}$	1.210	/	16.385

Table 4.8. Analysis of the bond lengths, in Å and force constants for the case of the two cyano-polyynes dimers analyzed. The values for the isolated chain are also reported. The bond lengths are measured in Angstroms, while the force constants in $mdyne/$Å.

The obtained results are consistent with those predicted for the hydrogen-polyynes and methyl-polyynes. A softening in the force constant of the carbon-carbon triple bond is experienced due to the peculiar interaction with the silver cluster. The nature of such interaction seems to be again stronger than a classical Van der Waals interaction, as the carbon-silver bond is shorter than the sum of the two Van der Waals radii. Moreover we can hypothesize that the modulation of the force constants of the bonds may cause variations in the frequencies of the related normal modes. The values related to the two different configurations are similar, but a small decrease in the length of the silver carbon bond for the $Ag_8 + CNC_8H$ is predicted, indicating that the downshift of the spectra and the increased interaction energy arise from a slightly stronger interaction between the cluster and the chain. Besides, this also adds importance to the considerations done before about the shape and geometry of the cluster. A comparison with the case of the methyl-polyynes and hydrogen-polyynes shows that the system $Ag_8 + CNC_8H$ has the lower value in the silver-carbon bond, indicating furthermore that it features the strongest interaction between the cluster and the chain. The low value of the force constant is in agreement with the low frequency of the normal mode located at about 2000 cm^{-1} described and discussed above, which is again a direct consequence of the peculiar nature of the interaction taking place between the monomers. A general softening of the force constants is then to be expected also for cyano-polyynes, as seen for hydrogen-polyynes, due to the similarities in the effects of the cluster on the parameters analyzed. It is therefore confirmed once again that the effect of the cluster is that of modifying the behavior

of the chain, resulting in the activation of new normal modes, the localization of the ECC mode on specific bonds, which can be related and explained also by the the softening of the force constants.

4.3.2 Analysis of the charges

In order to check the presence and the magnitude of the electron charge transfer effect, and its direction, also for these systems the analysis of the charges has been carried out. The results reported were obtained with the CHIRI method, discussed in the previous chapter. As for the CHELPG one, no value could be obtained due to computational issues encountered in the calculations of the charges. The calculated values are reported in table 4.9. Again, these are referred to the silver cluster, i.e. the charge of the polyyne has an opposite sign.

System	**CHELPG**	**CHIRI**
$\mathbf{Ag_8 + HC_8CN}$	/	0.28113
$\mathbf{Ag_8 + CNC_8H}$	/	0.16331

Table 4.9. Analysis of the charges of the systems of cyano-polyynes interacting with the silver nanoparticle. The values are in unit of electron charge, e.

The first observation is that the values calculated with the CHIRI method yield a completely opposite result with respect to those obtained in the study of the charges of hydrogen polyynes and methyl polyynes. Indeed, it would seem that the polyynes tend to behave as electron acceptors instead of electron donors, probably because the CN group has a strong electron attractive behavior, thus forcing the polyyne to withdraw charge from the cluster; on the other hand, when the terminal groups are H and CH_3 this behavior does not take place. The values obtained are too big to justify this inversion in the trend with a simple numerical error, or a poor precision in the evaluation of the direction of the charge transfer, as instead was possible for the case of hydrogen-polyynes. Indeed, it has been suggested above that the particular configuration of the atoms of the nanoparticle could induce some modification in the spectra and in the interaction energies, therefore, it would be possible to expect also a modification of the charge. Nonetheless, this hypothesis should be further investigated by some more in depth analysis on the possible influence of the shape of the cluster on this particular parameter.
The results showed above can be compared with the information obtained by the analysis of the spectra of the charged isolated cyano-polyynes, reported in Fig. 4.23. The predicted spectra seems to be in agreement with the results of the analysis of the charges with the CHIRI method. Indeed, the negatively charged polyyne spectrum is similar to the spectra obtained for the $Ag_8 + CNC_8H$ and $Ag_8 + HC_8CN$ systems, correctly describing both the redshift of the signals and also the appearance of the low intensity peak. This was instead not accomplished by the Raman spectra computed for the charged species for hydrogen-polyynes and methyl-polyynes. However, the other peaks predicted for the dimers are not correctly modeled, especially high frequency ones. This could be a

proof that confirms the hypotheses suggested in the discussion of the results of methyl-polyynes and hydrogen-polyynes, i.e. that the model that assumes the charge transfer as the reason for the downshift of the peaks and the general modifications of the spectra is not successful in interpreting the considered interaction. It is still worth highlighting that in the case of cyano-polyynes the spectra of the charged species (specifically HC_8CN^-) and the analysis of the charges are in good agreement, differently from the case of methyl- and hydrogen-terminated polyynes, in predicting an electron acceptor behavior of the polyyne. Finally, it has to be stressed the fact that a more in depth analysis is needed to model the effect of the charge transfer, due to the inconsistent results obtained for the different systems analyzed.

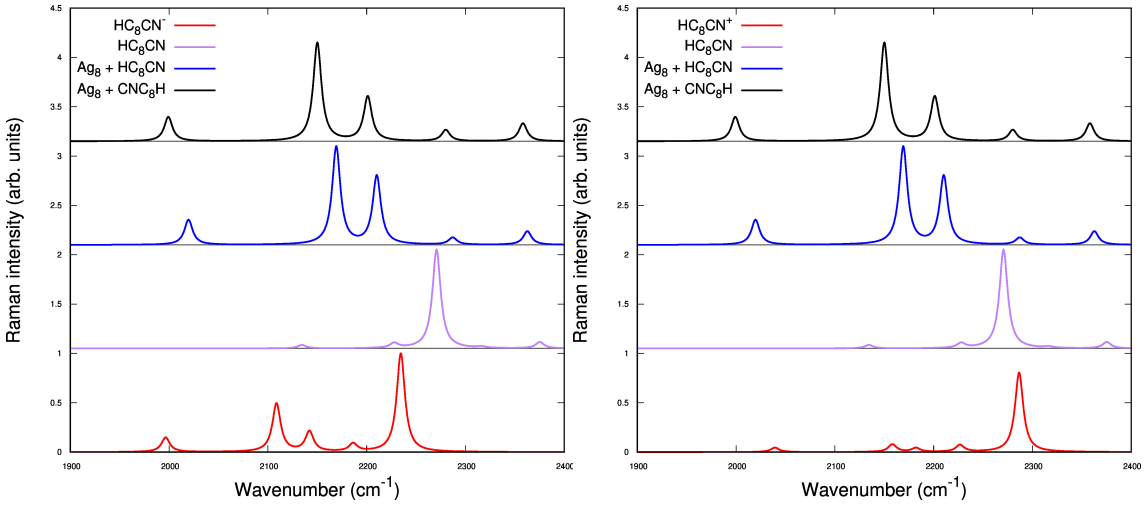

(a) (b)

Figure 4.23. Comparison of the spectra of the charged cyano-polyyne with the spectra of isolated neutral cyano-polyyne, $Ag_8 + HC_8CN$ and $Ag_8 + CNC_8H$. Specifically are reported the plot of: a) negatively charged methyl-polyyne; b) positively charged methyl-polyyne.

4.4 Comparison with the experimental data

The predicted results for methyl- and cyano-terminated polyynes have been compared with the experimental data obtained by Peggiani et al. [43], in order to verify whether the results obtained from the calculations may be in agreement with experimental measures. In Fig. 4.24 are reported the comparison between computed and experimental Raman spectra for the analyzed species.
The experimental spectra has been obtained from a solution of acetonitrile, which is causing an high intensity peak at 2350 cm^{-1}. The frequencies considered and reported in the spectra do not show the peaks related to the acetonitrile solution, which contains cyano- and methyl-polyynes of the same length of those investigated in this chapter, interacting with silver nanoparticles of various dimensions. As for the case of hydrogen polyynes, the calculated spectra have to be scaled down, with a factor of 0.9594 in order to correct the approximations assumed by using DFT methods regarding the chain's conjugation. The scale factors for the specific functional and basis-set used

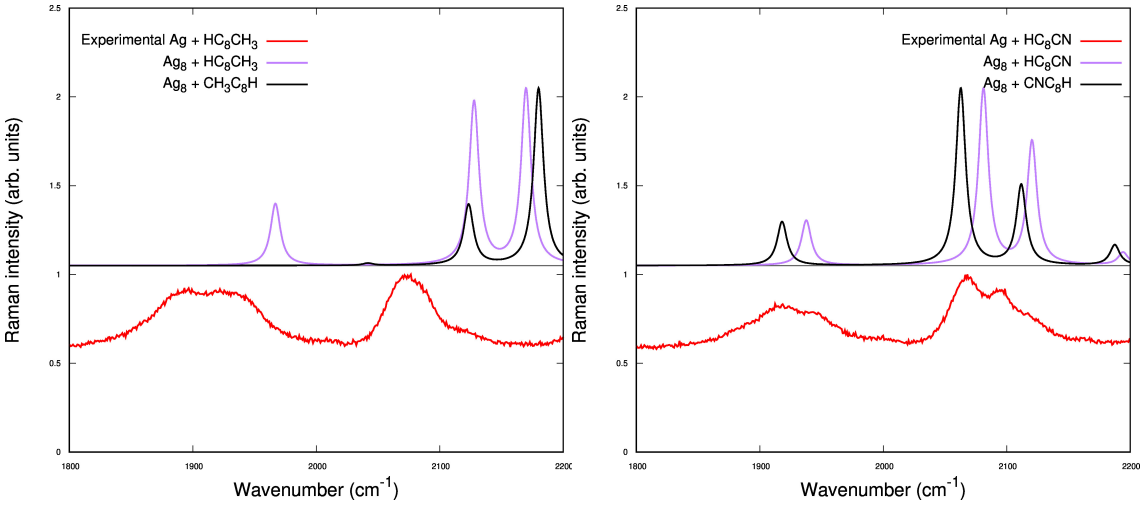

(a) (b)

Figure 4.24. Experimental SERS spectrum of liquid solution of size-selected polyynes. a) comparison of SERS experimental measure with predicted SERS signals of methyl-polyynes; b) comparison of experimental SERS and predicted SERS for cyano-polyynes [43].

(i.e. PBE0 and 6-311++G(d,p)) are again taken from the Computational Chemistry Comparison and Benchmark DataBase (CCCBDB, [76]). The peaks measured for methyl-polyynes are found at about 1910 and 2080 cm^{-1}. The calculated spectra predict peaks for the methyl-polyynes at about 1950 cm^{-1} for the low frequency peak, and between 2100 and 2200 cm^{-1} for the other high intensity normal modes. It would seem that both the low frequency signal and the other peaks are not precisely located at similar frequency, but overall the proposed model featuring a silver cluster interacting with the polyyne successfully describes the low frequency band, whereas the charged species model fails to do so. The reason behind the discrepancies between the experimental data and the calculations may be the influence of the size of the nanoparticle, which is larger in the case of the experiment, and therefore causes a downshift of the normal modes, as hypothesized when discussing the effect of the shape of the cluster in the analysis of the calculated results for cyano-polyynes. The broadening of the peaks measured in the experiment may be caused by the already discussed effect of the convolution of the various signal for the systems present in solution, i.e. polyynes interacting with nanoparticles of different sizes. It would seem that the low frequency normal mode in the experimental spectrum suffers more from this effect, even if the predicted spectra only show a high intensity low frequency peak for the $Ag_8 + HC_8CH_3$ system. However, it has to be taken into account the fact that a lower equilibrium energy was calculated for the $Ag_8 + CH_3C_8H$ system, which indicates that most of the synthesized dimers should possess the $Ag_8 + HC_8CH_3$ configuration. Furthermore, the broadening effect may also be influenced by the specific interaction with the nanoparticle: the dimensions of the cluster is much greater with respect to the size of the chain, and thus a small difference in the local interaction site may result in the broadening of the peaks. However, the effect of the local properties of the interaction sites have been correctly assessed by the studied model. As for the signal at about 2080 cm^{-1}, it may be associated to the high intensity normal modes reported in the calculated spectra. As visible, the broadening of the measured peak is not intense as for the case of the low frequency mode. Finally, the peaks predicted in the case of the calculated spectra at frequencies greater than 2200 cm^{-1} have probably a too low intensity to be detected in the experimental analysis.

As for the cyano-polyynes, the frequencies measured in the experiment are similar to those of the methyl-polyynes, i.e. the low frequency normal mode is located at about 1910 cm^{-1} and the other at about 2070 cm^{-1}. For the latter, the presence of a shoulder is to be noted, representing a similar effect highlighted also by the asymmetry of the same band measured in the methyl-polyynes: the shape of peaks underlines the presence of different systems in solution. On the other hand, the predicted spectra is in good agreement concerning the frequency related to the low frequency peak, which is located at around 1900 cm^{-1}. The other peaks appearing in the experimental spectrum are predicted to be between 2030 and 2110 cm^{-1}. The shape of the experimentally measured peaks is also in agreement with the calculations. Indeed, for the low frequency normal mode, the broadening of the signal may be due to the effect of the different possible cluster's configurations, as already discussed, and in this case particularly visible by observing the predicted spectra (in black and purple, in Fig. 4.24b). As for the measured peaks at about 2080 cm^{-1}, it may be observed a good agreement with the predicted spectra. Indeed, the convolution of the theoretical spectrum for the $Ag_8 + HC_8CN$ resembles the experimental spectrum, which is in fact a confirmation on the hypothesis proposed for the effect of the different cluster's shape. As visible, in both the calculated spectra, the peak at about 2110 cm^{-1} is less intense than the close peak at 2030 cm^{-1}, so that the former may appear as a shoulder of the latter. Finally, similarly to the case of methyl-polyynes, the peaks at frequencies above 2180 cm^{-1} are related to modes that are probably too weak to be detected in the experimental measures.

Conclusions and future perspective

In this thesis work an investigation of the peculiar interactions taking place between differently terminated polyynes and a silver cluster has been carried out, to give an interpretation on the origin of the SERS chemical effect observed in multiple studies. The model used was built on the base of experimentally investigated systems, formed by a polyyne and a metal nanoparticle.
The first task was to find the best computational setup able to describe precisely the peculiar interaction taking place between the two monomers. The analysis focused on the effect of the following computational parameters: basis-sets, exchange-correlation functionals and dispersion corrections, and was performed by analyzing the trends observed for the interactions energies, the Raman spectra and the modification of the molecular structure.
The comparison between the effect of the basis-sets was performed on systems consisting of polyynes of $4, 8$ atom long interacting with clusters formed by $4, 8$ atoms; the selected basis-sets were: cc-pVTZ (providing a good compromise between accuracy and computational time), AUG-cc-pVTZ (augmented version of the first one, incorporating diffuse functions) and 6-311++G(d,p) (smaller than cc-pVTZ, but featuring diffuse functions). In each case the same functional was used, i.e. PBE0, for consistency. The overall shape of the different spectra was similar for each basis-set and an analogous trend was highlighted in the interaction energies. Therefore, the choice of either basis-set proved to be not crucial and thus 6-311++G(d,p) was selected, in order to describe accurately the interaction, but keeping at the same time an affordable computational cost.
The same process was employed to investigate the effect of the exchange-correlation functional. The selected functionals were PBE0, suited for the description of *sp* systems featuring π conjugation, and B3LYP, that yielded good results in a variety of case studies. The samples used in this analysis were systems formed again by polyynes of different lengths ($4, 8$ atoms), interacting with clusters of different size ($4, 8, 16$ atoms). The overall shape of the spectra proved to be similar in each case, but differences in the frequencies were predicted, as expected. The inspection of the calculated interaction energies highlighted also a difference in the values: a weaker interaction between the cluster and the polyynes was predicted by B3LYP functional with respect to PBE0. However, a trend was found and resulted to be similar for both the exchange-correlation functionals adopted, in agreement with the analysis of the basis-sets. Considering the influence of the characteristics of the two functionals on both the spectra and interaction energies, the choice of either PBE0 or B3LYP did not seem to significantly alter the results. Therefore, considering the successful results in previous studies on *sp* carbon systems, PBE0 was selected.

The influence of dispersion corrections was assessed on a single test sample to verify its relevance in describing the intermolecular interaction between the polyyne and the cluster: an 8 atom long polyyne interacting with a cluster of 8 silver atoms. The basis-set used was cc-pVTZ, and both the functionals PBE0 and B3LYP were considered. The predicted spectra were very similar for every setup; on the other hand, the interaction energies featuring the corrections were quite different from those who did not, as expected. Considering the results, the decision was to avoid to use the corrections in the final setup, since they overestimate the interaction.
The first case study concerned hydrogen-polyynes. The study of the interaction energies highlighted an increase stability for systems featuring longer chains and bigger clusters. In the simulated SERS spectra, the peculiar interaction taking place between the chain and the cluster was responsible for the activation of new vibrational normal modes, and the modification of the existing ones; in particular, the appearance of a low frequency peak was observed, and could be associated to a strong vibration localized on the triple bond that mostly interact with the cluster. Such interaction caused also a strong modification and localization of the ECC mode on specific sections of the chain. The analysis of the bond length alternation and energy gap performed on the system $Ag_8 + HC_8H$ showed an increased conjugation with respect to the isolated polyyne. The bond lengths between the silver atoms of the cluster and the carbon atoms of the chain involved in the interaction were considered and proved to be smaller than the sum of the Van der Waals radii of the two considered atoms, indicating that the magnitude of the interaction of the cluster with the polyyne was stronger than a Van der Waals-like interaction. Moreover, the force constants for the bonds of the chain were analyzed: the values decreased with respect to the case of the isolated polyyne, in agreement with the downshift of the signals in the spectra. An analysis of the charges was performed, using CHELPG and CHIRI methods, to evaluate the accuracy of a model based on a charge transfer. The values obtained suggested a direction of a negative charge transfer towards the cluster. Moreover, an analysis of the spectra of charged isolated polyynes was carried out: the more accurate description of the interaction was given by the negatively charged isolated chain. However, this model failed to assess the origin of the low frequency peak, completely due to the specific local interaction which can be predicted only by explicitly considering the presence of the cluster. A final comparison between the theoretical and experimental data was carried out and a good agreement of the SERS spectra was observed.
The study has been extended towards methyl- and cyano-terminated polyynes, using the same computational setup employed in the case of hydrogen-polyynes. The presence of a different terminal group on one side of the chain introduced an asymmetry, therefore two initial configurations were prepared and subsequently optimized, i.e. $Ag_8 + HC_8CH_3$ and $Ag_8 + HC_8CN$ and $Ag_8 + CNC_8H$ and $Ag_8 + CH_3C_8H$.
For the case of methyl-polyynes, a first assessment of the BLA and energy gap of the isolated chain indicated a slightly increased conjugation of the chain with respect to hydrogen-polyynes, due to the hyperconjugation of the CH bonds of the methyl terminal group. The analysis of the interaction energies of the dimers, showed that $Ag_8 + HC_8CH_3$ is more stable with respect to $Ag_8 + CH_3C_8H$, due to the weakening effect caused by steric hindrance of the methyl group on the interaction with the cluster. This effect is also visible in the spectra of the two configurations: for $Ag_8 + HC_8CH_3$ the interaction with the cluster causes the appearance of new normal modes. In particular a low frequency active normal mode was predicted, and the eigenvector analysis demonstrated that it was related to the vibration of the triple bond that mostly interacted with the metal nanoparticle. The other normal modes were related to a strong localization of the collective oscillation of the

bonds on specific parts of the chain. The spectrum of the $Ag_8 + CH_3C_8H$ configuration showed instead a rigid shift of the signals that appeared in the spectrum of the isolated polyyne, and no new signals were predicted; moreover the nature of the vibrations of the bonds was similar to the case of the isolated molecule. The analysis of the bond lengths and force constants showed a similar behavior for both the configurations, in agreement with the interaction energies. However the investigation of such parameters, confirmed that the main reason for the modification of the spectra is the peculiar interaction between the cluster and the chain. The evaluation of the accuracy of the charge transfer model in the description of the peculiar behavior of these systems was also performed. The analysis of the charges by means of CHELPG and CHIRI methods found that the chain has a tendency to charge positively, but the results were not in agreement with each other, and a deeper investigation is therefore required. The analysis of the spectra of charged isolated chains resulted unsuccessful: a rigid red-shift of the ECC peak can be predicted better by the negatively charged polyyne spectra, but no low intensity peak is observed. The optimization of the two possible configurations highlighted that the interaction with the cluster can not take place on the side of the cyano group, as it is energetically unfavored. For this reason the cluster modified its position and shape until a minimum energy was reached in the vicinity of the hydrogen terminal group. The diverse shape of the cluster influenced the interaction energies: different values were obtained for the two configurations with very similar final geometries. This peculiarity is also causing differences in the spectra of the two configurations. As for the cases of hydrogen-polyynes and methyl-polyynes, the appearance of new peaks in the spectra, related to newly activated normal modes is observed. The low frequency peak can be still related to the strong vibration of the triple bond that mostly interact with the cluster, and the eigenvectors of the other Raman active normal modes show that the collective oscillation of the triple and single bonds localizes on a specific part of the chain. The values calculated for the bond lengths between the cluster and the carbon atoms of the polyyne are both smaller with respect to the sum of the Van der Waals radii, thus also for this system the interaction taking place seems stronger that a Van der Waals-like interaction. The model based on the charge transfer in this case predicts an opposite behavior with respect to the cases of hydrogen-polyynes and methyl-polyynes, as indeed the calculated charge on the chain has a negative value. The analysis of the spectra of the isolated charged polyynes confirms the observations of the previous cases, as the negatively charged chain correctly predicts the redshift of the spectra of the dimers. Surprisingly, the calculated spectrum is also able to predict the presence of a low frequency peak. In this regard, further analyses on the charge transfer model have to be performed to give a definitive evaluation on the accuracy of this model to describe the interaction between the cluster and the chain. Finally, a comparison between the experimental spectra obtained for cyano- and methyl-polyynes and the corresponding calculated ones was carried out. The predicted SERS spectra for methyl-polyynes is blueshifted with respect to the experimental one, but describes a very similar spectral pattern. The calculated spectra of the cyano-polyynes are instead very precise in the modeling of the experimental data. The discrepancies in the shape of the peaks can be related to the unavoidable differences between the systems produced in laboratory and those analyzed with the computations, in particular, the nanoparticles obtained in solutions during the experiments are bigger with respect to the cluster model.

The results presented in this thesis may be exploited in the future to build and study more precise models, to understand the peculiar interactions that take place between metal nanoparticles and polyynic chains. The nature of the interaction should be further investigated, by a detailed analysis on the modification of the electronic structure of both the cluster and the chain. Indeed, the

molecular orbitals engaged in the formation of the chemical bond should be studied. Moreover, the electronic density and the charge distribution on both the monomers should be better assessed, to verify the presence of a charge transfer and its direction. The influence of the geometry and shape of the metallic cluster should be better investigated, because it affects in a non negligible way the electronic and vibrational properties of the dimers. Moreover, a better model should be used for the description of the experimental situation, since the mean size of the experimentally-obtained nanoparticles is greater than the one of the clusters studied in this work. In this regard, it would be interesting to understand how the local geometry of the surface of the nanoparticle influences the properties of the polyynes and the interaction between the two.

Ringraziamenti

Sicuramente il primo e più grande ringraziamento va ai miei genitori, che mi hanno sostenuto e incoraggiato in ogni momento di questa esperienza al PoliMi, sin dal primo giorno di università. Senza di loro questo percorso non sarebbe stato possibile, e per questo avranno sempre la mia infinita gratitudine.
Un ringraziamento speciale va anche a tutti gli altri membri della mia famiglia, specialmente a quelli che non sono più qui.
Ci tengo inoltre a ringraziare Elena, per tutto l'amore ed il sostegno ricevuti, e per rendere la vita una esperienza meravigliosa. Grazie anche a tutti i miei amici e compagni di corso, che con la loro simpatia e bontà di spirito hanno saputo alleggerire i momenti più difficili e rendere memorabili quelli più simpatici e divertenti.
Un sentito ringraziamento va anche, e soprattutto, al prof. Carlo Casari, per l'opportunità di svolgere questo lavoro di tesi presso il dipartimento e per la sua generosissima disponibilità. Molti, moltissimi ringraziamenti, che non saranno mai abbastanza, al Dr. Alberto Milani, che mi ha proposto di scrivere questa tesi, ed al Dr. Patrick Serafini. Entrambi sono stati fondamentali nella elaborazione di questo lavoro, dal primo all'ultimo giorno, con la loro sapienza, pazienza, simpatia, e disponibilità. La mia stima nei loro confronti sarà sempre illimitata.

List of Figures

List of Tables

Acronyms

SWCNT	Single Wall Carbon NanoTube
MWCNT	Multi-Wall Carbon NanoTube
CAW	carbon atom wire
CAWs	carbon atom wires
BLA	Bond Length Alternation
SERS	Surface Enhanced Raman Spectroscopy
DFT	Density Functional Theory
SCF	Self-Consistent-Field
RHF	restricted Hartree-Fock
MO	molecular orbital
STO	Slater-type orbitals
GTO	Gaussian-type orbitals
LDA	Local Density Approximation
LSDA	Local Spin Density Approximation
GEA	Gradient Expansion Approximation
GGA	Generalized Gradient Approximation

Bibliography

[1] A. Hirsch, "The era of carbon allotropes," *Nature materials*, vol. 9, no. 11, pp. 868–871, 2010.

[2] K. S. Novoselov, A. K. Geim, S. V. Morozov, D. Jiang, Y. Zhang, S. V. Dubonos, I. V. Grigorieva, and A. A. Firsov, "Electric field effect in atomically thin carbon films," *science*, vol. 306, no. 5696, pp. 666–669, 2004.

[3] A. H. Castro Neto, F. Guinea, N. M. R. Peres, K. S. Novoselov, and A. K. Geim, "The electronic properties of graphene," *RvMP*, vol. 81, no. 1, pp. 109–162, 2009.

[4] A. Armano and S. Agnello, "Two-dimensional carbon: a review of synthesis methods, and electronic, optical, and vibrational properties of single-layer graphene," *CJournal of Carbon Research*, vol. 5, no. 4, p. 67, 2019.

[5] S. Iijima and T. Ichihashi, "Single-shell carbon nanotubes of 1-nm diameter," *nature*, vol. 363, no. 6430, pp. 603–605, 1993.

[6] S. Sheshmani, A. Ashori, and M. A. Fashapoyeh, "Wood plastic composite using graphene nanoplatelets," *International Journal of Biological Macromolecules*, vol. 58, pp. 1–6, 2013.

[7] X. Zhao, Y. Liu, S. Inoue, T. Suzuki, R. Jones, and Y. Ando, "Smallest carbon nanotube is 3 å in diameter," *Physical review letters*, vol. 92, no. 12, p. 125502, 2004.

[8] R. Zhang, Y. Zhang, Q. Zhang, H. Xie, W. Qian, and F. Wei, "Growth of half-meter long carbon nanotubes based on schulz–flory distribution," *Acs Nano*, vol. 7, no. 7, pp. 6156–6161, 2013.

[9] M.-F. Yu, O. Lourie, M. J. Dyer, K. Moloni, T. F. Kelly, and R. S. Ruoff, "Strength and breaking mechanism of multiwalled carbon nanotubes under tensile load," *Science*, vol. 287, no. 5453, pp. 637–640, 2000.

[10] S. J. Tans, M. H. Devoret, H. Dai, A. Thess, R. E. Smalley, L. Geerligs, and C. Dekker, "Individual single-wall carbon nanotubes as quantum wires," *Nature*, vol. 386, no. 6624, pp. 474–477, 1997.

[11] A. Tikhomirov, V. Nedzvetskii, M. Lipka, G. Andrievskii, and V. Klochkov, "Chronic alcoholization-induced damage to astroglia and intensification of lipid peroxidation in the rat brain: Protector effect of hydrated form of fullerene c 60," *Neurophysiology*, vol. 39, no. 2, pp. 105–111, 2007.

[12] M. Wang and S. Lin, "Ballistic thermal transport in carbyne and cumulene with micron-scale spectral acoustic phonon mean free path," *Scientific reports*, vol. 5, p. 18122, 2015.

[13] M. Liu, V. I. Artyukhov, H. Lee, F. Xu, and B. I. Yakobson, "Correction to carbyne from first-principles: Chain of c atoms, a nanorod or a nanorope," *ACS nano*, vol. 11, no. 5, pp. 5186–5186, 2017.

[14] C. S. Casari, M. Tommasini, R. R. Tykwinski, and A. Milani, "Carbon-atom wires: 1-d systems with tunable properties," *Nanoscale*, vol. 8, no. 8, pp. 4414–4435, 2016.

[15] C. S. Casari and A. Milani, "Carbyne: from the elusive allotrope to stable carbon atom wires," *MRS Communications*, vol. 8, no. 2, pp. 207–219, 2018.

[16] S. Yang and M. Kertesz, "Linear c n clusters: Are they acetylenic or cumulenic?" *The Journal of Physical Chemistry A*, vol. 112, no. 1, pp. 146–151, 2008.

[17] A. Milani, M. Tommasini, M. Del Zoppo, C. Castiglioni, and G. Zerbi, "Carbon nanowires: Phonon and π-electron confinement," *Physical Review B*, vol. 74, no. 15, p. 153418, 2006.

[18] A. Milani, M. Tommasini, and G. Zerbi, "Carbynes phonons: A tight binding force field," *The Journal of chemical physics*, vol. 128, no. 6, p. 064501, 2008.

[19] M. Tommasini, A. Milani, D. Fazzi, M. Del Zoppo, C. Castiglioni, and G. Zerbi, "Modeling phonons of carbon nanowires," *Physica E: Low-dimensional Systems and Nanostructures*, vol. 40, no. 7, pp. 2570–2576, 2008.

[20] M. Tommasini, D. Fazzi, A. Milani, M. Del Zoppo, C. Castiglioni, and G. Zerbi, "Intramolecular vibrational force fields for linear carbon chains through an adaptative linear scaling scheme," *The Journal of Physical Chemistry A*, vol. 111, no. 45, pp. 11 645–11 651, 2007.

[21] F. Innocenti, A. Milani, and C. Castiglioni, "Can raman spectroscopy detect cumulenic structures of linear carbon chains?" *Journal of Raman Spectroscopy: An International Journal for Original Work in all Aspects of Raman Spectroscopy, Including Higher Order Processes, and also Brillouin and Rayleigh Scattering*, vol. 41, no. 2, pp. 226–236, 2010.

[22] J. Kūrti, C. Magyar, A. Balázs, and P. Rajczy, "Vibrational analysis for short carbon chains with alternating and cumulenic structure," *Synthetic Metals*, vol. 71, no. 1-3, pp. 1865–1866, 1995.

[23] A. Lucotti, M. Tommasini, M. Del Zoppo, C. Castiglioni, G. Zerbi, F. Cataldo, C. S. Casari, A. L. Bassi, V. Russo, M. Bogana *et al.*, "Raman and sers investigation of isolated sp carbon chains," *Chemical physics letters*, vol. 417, no. 1-3, pp. 78–82, 2006.

[24] H. Tabata, M. Fujii, S. Hayashi, T. Doi, and T. Wakabayashi, "Raman and surface-enhanced raman scattering of a series of size-separated polyynes," *Carbon*, vol. 44, no. 15, pp. 3168–3176, 2006.

[25] A. Lucotti, C. S. Casari, M. Tommasini, A. L. Bassi, D. Fazzi, V. Russo, M. Del Zoppo, C. Castiglioni, F. Cataldo, C. E. Bottani *et al.*, "sp carbon chain interaction with silver nanoparticles probed by surface enhanced raman scattering," *Chemical Physics Letters*, vol. 478, no. 1-3, pp. 45–50, 2009.

[26] A. Milani, M. Tommasini, and G. Zerbi, "Connection among raman wavenumbers, bond length alternation and energy gap in polyynes," *Journal of Raman Spectroscopy: An International Journal for Original Work in all Aspects of Raman Spectroscopy, Including Higher Order Processes, and also Brillouin and Rayleigh Scattering*, vol. 40, no. 12, pp. 1931–1934, 2009.

[27] E. B. Wilson, J. C. Decius, and P. C. Cross, *Molecular vibrations: the theory of infrared and Raman vibrational spectra*. Courier Corporation, 1980.

[28] C. Mapelli, C. Castiglioni, G. Zerbi, and K. Müllen, "Common force field for graphite and polycyclic aromatic hydrocarbons," *Physical Review B*, vol. 60, no. 18, p. 12710, 1999.

[29] H. Tabata, M. Fujii, and S. Hayashi, "Surface-enhanced raman scattering from polyyne solutions," *Chemical physics letters*, vol. 420, no. 1-3, pp. 166–170, 2006.

[30] K. Hanamura, M. Fujii, T. Wakabayashi, and S. Hayashi, "Surface-enhanced raman scattering of size-selected polyynes (c8h2) adsorbed on silver colloidal nanoparticles," *Chemical Physics Letters*, vol. 503, no. 1-3, pp. 118–123, 2011.

[31] A. Milani, A. Lucotti, V. Russo, M. Tommasini, F. Cataldo, A. Li Bassi, and C. S. Casari, "Charge transfer and vibrational structure of sp-hybridized carbon atomic wires probed by surface enhanced raman spectroscopy," *The Journal of Physical Chemistry C*, vol. 115, no. 26, pp. 12 836–12 843, 2011.

[32] A. Milani, M. Tommasini, V. Russo, A. L. Bassi, A. Lucotti, F. Cataldo, and C. S. Casari, "Raman spectroscopy as a tool to investigate the structure and electronic properties of carbon-atom wires," *Beilstein journal of nanotechnology*, vol. 6, no. 1, pp. 480–491, 2015.

[33] A. Milani, V. Barbieri, A. Facibeni, V. Russo, A. L. Bassi, A. Lucotti, M. Tommasini, M. D. Tzirakis, F. Diederich, and C. S. Casari, "Structure modulated charge transfer in carbon atomic wires," *Scientific reports*, vol. 9, no. 1, pp. 1–10, 2019.

[34] F. Cataldo, "Stability of polyynes in air and their degradation by ozonolysis," *polymer degradation and stability*, vol. 91, no. 2, pp. 317–323, 2006.

[35] C. S. Casari, A. L. Bassi, L. Ravagnan, F. Siviero, C. Lenardi, P. Piseri, G. Bongiorno, C. E. Bottani, and P. Milani, "Chemical and thermal stability of carbyne-like structures in cluster-assembled carbon films," *Physical review B*, vol. 69, no. 7, p. 075422, 2004.

[36] W. A. Chalifoux and R. R. Tykwinski, "Synthesis of polyynes to model the sp-carbon allotrope carbyne," *Nature chemistry*, vol. 2, no. 11, pp. 967–971, 2010.

[37] L. Shi, P. Rohringer, K. Suenaga, Y. Niimi, J. Kotakoski, J. C. Meyer, H. Peterlik, M. Wanko, S. Cahangirov, A. Rubio *et al.*, "Confined linear carbon chains as a route to bulk carbyne," *Nature materials*, vol. 15, no. 6, pp. 634–639, 2016.

[38] L. D. Movsisyan, D. V. Kondratuk, M. Franz, A. L. Thompson, R. R. Tykwinski, and H. L. Anderson, "Synthesis of polyyne rotaxanes," *Organic letters*, vol. 14, no. 13, pp. 3424–3426, 2012.

[39] L. Ravagnan, P. Piseri, M. Bruzzi, S. Miglio, G. Bongiorno, A. Baserga, C. S. Casari, A. L. Bassi, C. Lenardi, Y. Yamaguchi *et al.*, "Influence of cumulenic chains on the vibrational and electronic properties of s p- s p 2 amorphous carbon," *Physical review letters*, vol. 98, no. 21, p. 216103, 2007.

[40] M. Bogana, L. Ravagnan, C. S. Casari, A. Zivelonghi, A. Baserga, A. L. Bassi, C. E. Bottani, S. Vinati, E. Salis, P. Piseri *et al.*, "Leaving the fullerene road: presence and stability of sp chains in sp2 carbon clusters and cluster-assembled solids," *New Journal of Physics*, vol. 7, no. 1, p. 81, 2005.

[41] F. Cataldo, "Simple generation and detection of polyynes in an arc discharge between graphite electrodes submerged in various solvents," *Carbon (New York, NY)*, vol. 41, no. 13, pp. 2671–2674, 2003.

[42] S. Peggiani, A. Senis, A. Facibeni, A. Milani, P. Serafini, G. Cerrato, A. Lucotti, M. Tommasini, D. Fazzi, C. Castiglioni *et al.*, "Size-selected polyynes synthesised by submerged arc discharge in water," *Chemical Physics Letters*, vol. 740, p. 137054, 2020.

[43] S. Peggiani, P. Marabotti, R. A. Lotti, A. Facibeni, P. Serafini, A. Milani, V. Russo, A. L. Bassi, and C. S. Casari, "Solvent-dependent termination, size and stability in polyynes synthesized via laser ablation in liquids," *Physical Chemistry Chemical Physics*, vol. 22, no. 45, pp. 26 312–26 321, 2020.

[44] L. Ravagnan, N. Manini, E. Cinquanta, G. Onida, D. Sangalli, C. Motta, M. Devetta, A. Bordoni, P. Piseri, and P. Milani, "Effect of axial torsion on s p carbon atomic wires," *Physical review letters*, vol. 102, no. 24, p. 245502, 2009.

[45] R. Eastmond, T. Johnson, and D. Walton, "Silylation as a protective method for terminal alkynes in oxidative couplings: A general synthesis of the parent polyynes h (c-c) nh (n= 4–10, 12)," *Tetrahedron*, vol. 28, no. 17, pp. 4601–4616, 1972.

[46] M. Tsuji, S. Kuboyama, T. Matsuzaki, and T. Tsuji, "Formation of hydrogen-capped polyynes by laser ablation of c60 particles suspended in solution," *Carbon*, vol. 41, no. 11, pp. 2141–2148, 2003.

[47] T. Johnson and D. Walton, "Silylation as a protective method in acetylene chemistry: Polyyne chain extensions using the reagents, et3si (c-c) mh (m= 1, 2, 4) in mixed oxidative couplings," *Tetrahedron*, vol. 28, no. 20, pp. 5221–5236, 1972.

[48] M. Nakagawa, S. Akiyama, K. Nakasuji, and K. Nishimoto, "Novel linear relation in the electronic spectra of α, ω-diarylpoly-ynes," *Tetrahedron*, vol. 27, no. 22, pp. 5401–5418, 1971.

[49] A. L. Shi Shun and R. R. Tykwinski, "Synthesis of naturally occurring polyynes," *Angewandte Chemie International Edition*, vol. 45, no. 7, pp. 1034–1057, 2006.

[50] M. Younus, A. Köhler, S. Cron, N. Chawdhury, M. R. Al-Mandhary, M. S. Khan, J. Lewis, N. J. Long, R. H. Friend, and P. R. Raithby, "Synthesis, electrochemistry, and spectroscopy of blue platinum (ii) polyynes and diynes," *Angewandte Chemie International Edition*, vol. 37, no. 21, pp. 3036–3039, 1998.

[51] W. A. Chalifoux and R. R. Tykwinski, "Synthesis of extended polyynes: Toward carbyne," *Comptes Rendus Chimie*, vol. 12, no. 3-4, pp. 341–358, 2009.

[52] Y. P. Kudryavtsev, R. Heimann, and S. Evsyukov, "Carbynes: Advances in the field of linear carbon chain compounds," *Journal of materials science*, vol. 31, no. 21, pp. 5557–5571, 1996.

[53] Y. P. Kudryavtsev, S. Evsyukov, M. Guseva, V. Babaev, and V. Khvostov, "Carbynethe third allotropic form of carbon," *Russian chemical bulletin*, vol. 42, no. 3, pp. 399–413, 1993.

[54] S. Szafert and J. Gladysz, "Carbon in one dimension: Structural analysis of the higher conjugated polyynes," *Chemical reviews*, vol. 103, no. 11, pp. 4175–4206, 2003.

[55] B. Larade, J. Taylor, H. Mehrez, and H. Guo, "Conductance, i- v curves, and negative differential resistance of carbon atomic wires," *Physical Review B*, vol. 64, no. 7, p. 075420, 2001.

[56] S. Tongay, R. Senger, S. Dag, and S. Ciraci, "A b-i n i t i o electron transport calculations of carbon based string structures," *Physical review letters*, vol. 93, no. 13, p. 136404, 2004.

[57] O. Cretu, A. R. Botello-Mendez, I. Janowska, C. Pham-Huu, J.-C. Charlier, and F. Banhart, "Electrical transport measured in atomic carbon chains," *Nano letters*, vol. 13, no. 8, pp. 3487–3493, 2013.

[58] A. D. Scaccabarozzi, A. Milani, S. Peggiani, S. Pecorario, B. Sun, R. R. Tykwinski, M. Caironi, and C. S. Casari, "A field-effect transistor based on cumulenic sp-carbon atomic wires," *The journal of physical chemistry letters*, vol. 11, no. 5, pp. 1970–1974, 2020.

[59] V. I. Artyukhov, M. Liu, and B. I. Yakobson, "Mechanically induced metal–insulator transition in carbyne," *Nano letters*, vol. 14, no. 8, pp. 4224–4229, 2014.

[60] M. Liu, V. I. Artyukhov, H. Lee, F. Xu, and B. I. Yakobson, "Carbyne from first principles: chain of c atoms, a nanorod or a nanorope," *ACS nano*, vol. 7, no. 11, pp. 10 075–10 082, 2013.

[61] F. Hu, C. Zeng, R. Long, Y. Miao, L. Wei, Q. Xu, and W. Min, "Supermultiplexed optical imaging and barcoding with engineered polyynes," *Nature methods*, vol. 15, no. 3, p. 194, 2018.

[62] A. Ivanovskii, "Graphynes and graphdyines," *Progress in Solid State Chemistry*, vol. 41, no. 1-2, pp. 1–19, 2013.

[63] A. Szabo and N. Ostlund, "Introduction to advanced electronic structure theory," *Modern Quantum Chemistry*, 1996.

[64] J. Labanowski, "Simplified and biased introduction to density functional approaches in chemistry," *Ohio Supercomputer Center, Ohio Supercomputer Center*, vol. 1224, pp. 43 221–1153, 1996.

[65] J. Kohanoff and N. Gidopoulos, "Density functional theory: basics, new trends and applications," *Handbook of molecular physics and quantum chemistry*, vol. 2, no. Part 5, pp. 532–568, 2003.

[66] R. G. Parr, "Density functional theory of atoms and molecules," in *Horizons of quantum chemistry*. Springer, 1980, pp. 5–15.

[67] J. P. Perdew and S. Kurth, "Density functionals for non-relativistic coulomb systems in the new century," in *A primer in density functional theory*. Springer, 2003, pp. 1–55.

[68] C. Adamo and V. Barone, "Toward reliable density functional methods without adjustable parameters: The pbe0 model," *The Journal of chemical physics*, vol. 110, no. 13, pp. 6158–6170, 1999.

[69] S. Grimme, J. Antony, S. Ehrlich, and H. Krieg, "A consistent and accurate ab initio parametrization of density functional dispersion correction (dft-d) for the 94 elements h-pu," *The Journal of chemical physics*, vol. 132, no. 15, p. 154104, 2010.

[70] K. Khamoushi, "Structure and properties of rare earth neodymium zinc titanate," *arXiv preprint arXiv:1502.07530*, 2015.

[71] M. Wanko, S. Cahangirov, L. Shi, P. Rohringer, Z. J. Lapin, L. Novotny, P. Ayala, T. Pichler, and A. Rubio, "Polyyne electronic and vibrational properties under environmental interactions," *Physical Review B*, vol. 94, no. 19, p. 195422, 2016.

[72] A. Milani, M. Tommasini, V. Barbieri, A. Lucotti, V. Russo, F. Cataldo, and C. S. Casari, "Semiconductor-to-metal transition in carbon-atom wires driven by sp2 conjugated end groups," *The Journal of Physical Chemistry C*, vol. 121, no. 19, pp. 10 562–10 570, 2017.

[73] M. Tommasini, A. Milani, D. Fazzi, A. Lucotti, C. Castiglioni, J. A. Januszewski, D. Wendinger, and R. R. Tykwinski, "π-conjugation and end group effects in long cumulenes: Raman spectroscopy and dft calculations," *The Journal of Physical Chemistry C*, vol. 118, no. 45, pp. 26 415–26 425, 2014.

[74] C. M. Breneman and K. B. Wiberg, "Determining atom-centered monopoles from molecular electrostatic potentials. the need for high sampling density in formamide conformational analysis," *Journal of Computational Chemistry*, vol. 11, no. 3, pp. 361–373, 1990.

[75] A. Milani, M. Tommasini, and C. Castiglioni, "Atomic charges from ir intensity parameters: theory, implementation and application," *Theoretical Chemistry Accounts*, vol. 131, no. 3, pp. 1–17, 2012.

[76] N. C. C. Comparison and B. Database. (2020) Nist standard reference database number 101. [Online]. Available: http://cccbdb.nist.gov/